

# Compression-induced factors influencing the damage of engineered skeletal muscle

**Citation for published version (APA):**

Gawlitta, D. (2007). *Compression-induced factors influencing the damage of engineered skeletal muscle*. [Phd Thesis 1 (Research TU/e / Graduation TU/e), Biomedical Engineering]. Technische Universiteit Eindhoven. <https://doi.org/10.6100/IR616387>

**DOI:**

[10.6100/IR616387](https://doi.org/10.6100/IR616387)

**Document status and date:**

Published: 01/01/2007

**Document Version:**

Publisher's PDF, also known as Version of Record (includes final page, issue and volume numbers)

**Please check the document version of this publication:**

- A submitted manuscript is the version of the article upon submission and before peer-review. There can be important differences between the submitted version and the official published version of record. People interested in the research are advised to contact the author for the final version of the publication, or visit the DOI to the publisher's website.
- The final author version and the galley proof are versions of the publication after peer review.
- The final published version features the final layout of the paper including the volume, issue and page numbers.

[Link to publication](#)

**General rights**

Copyright and moral rights for the publications made accessible in the public portal are retained by the authors and/or other copyright owners and it is a condition of accessing publications that users recognise and abide by the legal requirements associated with these rights.

- Users may download and print one copy of any publication from the public portal for the purpose of private study or research.
- You may not further distribute the material or use it for any profit-making activity or commercial gain
- You may freely distribute the URL identifying the publication in the public portal.

If the publication is distributed under the terms of Article 25fa of the Dutch Copyright Act, indicated by the "Taverne" license above, please follow below link for the End User Agreement:

[www.tue.nl/taverne](http://www.tue.nl/taverne)

**Take down policy**

If you believe that this document breaches copyright please contact us at:

[openaccess@tue.nl](mailto:openaccess@tue.nl)

providing details and we will investigate your claim.

# **Compression-induced factors influencing the damage of engineered skeletal muscle**

A catalogue record is available from the Library Eindhoven University of Technology

ISBN-10: 90-386-2589-8

ISBN-13: 978-90-386-2589-8

Copyright ©2006 by D. Gawlitta

All rights reserved. No part of this book may be reproduced, stored in a database or retrieval system, or published, in any form or in any way, electronically, mechanically, by print, photoprint, microfilm or any means without prior written permission of the author.

Cover design: Debby Gawlitta / Oranje Vormgevers

Printed by Universiteitsdrukkerij TU Eindhoven, Eindhoven, The Netherlands.

This research was supported by the Dutch Technology Foundation STW, applied science division of NWO, and the Technology Program of the Ministry of Economic Affairs.

# **Compression-induced factors influencing the damage of engineered skeletal muscle**

Proefschrift

ter verkrijging van de graad van doctor aan de Technische Universiteit Eindhoven, op gezag van de Rector Magnificus, prof.dr.ir. C.J. van Duijn, voor een commissie aangewezen door het College voor Promoties in het openbaar te verdedigen op donderdag 25 januari 2007 om 16.00 uur

door

**Debby Gawlitta**

geboren te Tegelen



Dit proefschrift is goedgekeurd door de promotor:

prof.dr.ir. F.P.T. Baaijens

Copromotoren:

dr. C.V.C. Bouten

en

dr.ir. C.W.J. Oomens

*A theory is something nobody believes, except the person who made it.  
An experiment is something everybody believes, except the person who made it.  
-Albert Einstein-*



# Contents

<b>Summary</b> .....	<b>1</b>
<b>1 Introduction</b> .....	<b>3</b>
1.1 Pressure ulcers.....	4
1.2 In vitro muscle model studies .....	6
1.2.1 Skeletal muscle.....	6
1.2.2 Single cell studies .....	8
1.2.3 Engineered muscle studies .....	8
1.3 Rationale and outline.....	12
<b>2 The influence of serum-free culturing on skeletal muscle development in a tissue-engineered model</b> .....	<b>15</b>
2.1 Introduction .....	16
2.2 Materials and methods .....	17
2.2.1 Cell and tissue culture .....	17
2.2.2 Experimental design .....	18
2.2.3 Creatine kinase activity .....	18
2.2.4 Total protein content.....	19
2.2.5 Immunofluorescence .....	19
2.2.6 Cell metabolism.....	19
2.2.7 Statistical analysis .....	19
2.3 Results .....	20
2.3.1 Creatine Kinase activity .....	20
2.3.2 Total protein content.....	20
2.3.3 Immunofluorescence .....	21
2.3.4 Cell metabolism.....	23
2.3.5 Monolayer cultures.....	23
2.4 Discussion .....	25
2.5 Acknowledgments.....	28
<b>3 Evaluation of a continuous quantification method of apoptosis and necrosis in tissue cultures</b> .....	<b>29</b>
3.1 Introduction .....	30
3.2 Materials and methods .....	31
3.2.1 Cell and tissue culture .....	31
3.2.2 Progression of cell death in 2D and 3D cultures .....	31

3.2.3 YO-PRO-1 and PI dual staining.....	32
3.2.4 Visualization .....	32
3.2.5 Probe performance .....	33
3.2.6 Quantification of cell death in time.....	33
3.2.7 Statistical analysis .....	34
3.3 Results.....	34
3.3.1 Progression of cell death in 2D and 3D cultures.....	35
3.3.2 Nuclear Morphology .....	36
3.3.3 Probe performance .....	38
3.4 Discussion.....	39
3.4.1 Induction of apoptosis in 2D and 3D cultures.....	39
3.4.2 Nuclear Morphology .....	39
3.4.3 Probe performance .....	40
3.5 Acknowledgments .....	41
<b>4 The relative contributions of compression and hypoxia to development of muscle tissue damage: an in vitro study .....</b>	<b>43</b>
4.1 Introduction.....	44
4.2 Materials and methods .....	45
4.2.1 Cell and tissue culture .....	45
4.2.2 Ischemia .....	45
4.2.3 Compression.....	47
4.2.4 Analysis of cell death.....	48
4.2.5 Experimental design.....	49
4.2.6 Statistical analysis .....	50
4.3 Results.....	50
4.3.1 Normoxia and compression.....	50
4.3.2 Hypoxia and compression.....	51
4.3.3 Temporal profile of cell death.....	52
4.4 Discussion.....	54
4.5 Acknowledgments .....	58
<b>5 Ischemic factors and deformation influence metabolism of engineered skeletal muscle .....</b>	<b>59</b>
5.1 Introduction.....	60
5.2 Materials and Methods.....	61
5.2.1 Cell and tissue culture .....	61
5.2.2 Experimental conditions.....	62
5.2.3 Analyses of metabolism and viability.....	63
5.2.4 Statistical analysis .....	64

5.3 Results .....	64
5.3.1 Acidification .....	64
5.3.2 Effects of glucose deprivation .....	65
5.3.3 Effects of lactic acidification .....	66
5.3.4 Effects of deformation and hypoxia .....	67
5.3.5 Effects of deformation and / or hypoxia combined with acidification .....	68
5.3.6 Tissue viability after 5 days (MTT) .....	69
5.4 Discussion .....	70
5.5 Acknowledgments .....	74
<b>6 General discussion .....</b>	<b>75</b>
6.1 Introductory remarks .....	76
6.2 Engineered skeletal muscle .....	76
6.3 Monitoring cell and tissue status .....	77
6.4 Imposing experimental compression and ischemia .....	78
6.5 Most important findings and implications .....	79
6.6 Future of pressure ulcer research .....	81
<b>References .....</b>	<b>85</b>
<b>Appendix A Diffusion of markers into and out of compressed tissues .....</b>	<b>96</b>
A.1 Background .....	97
A.2 Approach .....	97
A.3 Materials and methods .....	97
A.4 Results .....	99
A.5 Conclusions .....	102
A.6 Acknowledgments .....	103
<b>Samenvatting .....</b>	<b>104</b>
<b>Dankwoord .....</b>	<b>106</b>
<b>Curriculum vitae .....</b>	<b>108</b>

## *Contents*

# Compression-induced factors influencing the damage of engineered skeletal muscle

## Summary

Pressure ulcers are regions of damaged soft tissue, which develop following sustained mechanical loads. They often originate over stiff objects, such as bony prominences or external prostheses. Pressure ulcers represent both a serious health care issue, because they may increase the length of hospitalization of patients, and a potential threat to the patient's health and quality of life, which may already be compromised by an underlying pathology. In particular, subjects with decreased mobility or impaired sensations may not be able to relieve the sustained loading in time to prevent development of tissue damage. Pressure ulcer prevalence is still unacceptably high, between 10-24% in The Netherlands, depending on the nature of the institution examined.

Superficial pressure ulcers can develop in the skin layer, affecting the epidermis and/or dermis and are classified as stage I or II. These superficial ulcers can progress from the skin to underlying tissues and even to the bone. This process represents evolution to a stage III or IV pressure ulcer. In contrast to these ulcers, which advance from the skin layer to the deeper tissues, a pressure ulcer may also originate in the deeper tissues, where they are referred to as a 'deep tissue injury'. The skeletal muscles are particularly susceptible to damage development as a result of tissue compression. These deep ulcers progress under intact skin towards the surface. Due to their subcutaneous progression, they are difficult to identify and almost always result in a stage III or IV pressure ulcer, once they have punctured the skin. Consequently, because skeletal muscle tissue is very susceptible to compression-induced damage and because deep tissue injury may originate in this tissue, the present thesis focused on damage development in skeletal muscle tissue.

Although many prevention and treatment strategies have been developed, pressure ulcer etiology is not completely understood. This understanding, however, is essential to provide appropriate individual care, improve existing strategies and to be able to detect early stages of an ulcer. Current theories propose ischemia (insufficient blood perfusion), lymphatic occlusion, reperfusion, and cellular deformation as potential causes for the onset of pressure ulcer development. The present thesis was aimed at providing more insight into damage development in skeletal muscle as a result of ischemia and/or deformation.

To examine the effects of these individual factors an in vitro approach, involving an engineered skeletal muscle model, was chosen. The model was obtained by the differentiation of myoblasts (muscle cells) in a collagen gel towards mature muscle cells. Existing muscle models were adapted and optimized, followed by the characterization of their differential capacity towards mature muscle properties.



## *Summary*

In order to study the progression of cell death, both apoptotic and necrotic in nature, caused by both deformation of the engineered muscle tissue and ischemic factors, a new protocol was developed. This method enabled real time non-invasive monitoring of damage development inside the 3D tissue. Fluorescent identification of both apoptotic and necrotic cells was established for experimental periods up to 24 hours.

In addition, custom made experimental arrangements were designed to facilitate application of deformation and ischemic factors. The ischemic factors studied included hypoxia, in the form of lack of oxygen, glucose deprivation, and tissue acidification by the release of lactic acid. The influence of deformation and the ischemic factors on damage development in the tissue was examined by applying several cell death markers, but also indicators of metabolic changes.

Increases in tissue damage with time and with amount of compression were observed according to existing data from literature. Interestingly compression at levels of 20% and 40% strain, as opposed to hypoxia at oxygen concentrations of less than 6%, affected tissue viability within the first 24 hours of the experimental period. Hypoxia, however, caused an increased metabolic response in this time period compared to control tissues. After 24 hours, hypoxia had resulted in elevated glucose utilization as well as enhanced lactate production. This may imply a transition to anaerobic metabolism. However, this was not associated with an increasing degree of cell death.

The presence of lactate, and concomitant lower pH values, in the culture medium appeared to down-regulate tissue metabolism. However, if the concentration of lactate exceeded a certain threshold of approximately 25mM, cell metabolism was arrested resulting in an increased degree of cell death. This finding was comparable to the response of the tissue during glucose deprivation. Once glucose concentrations approached negligible values, metabolic activity ceased and the amount of cell death increased.

Considering the effects of all factors separately or in several combinations, it may be suggested that on a short term (within 24 hours) deformation, extreme acidification, and glucose deprivation caused increased cell death. By contrast, non-extreme acidification and hypoxia influenced tissue metabolism, but not the development of cell death. However, after a prolonged experimental period of 5 days, only hypoxia and extreme acidification resulted in death of the complete tissue, while deformation, glucose deprivation, and non-extreme acidification produced a lesser degree of cell death. Although deformation and non-extreme acidification did not cause cell death of the complete tissue, a combination of both factors did.

In conclusion, a model system has been developed to identify the effects of deformation and/or ischemic factors on engineered skeletal muscle tissue. Influences of the individual or combined factors were investigated. The findings of this thesis contribute to the understanding of pressure ulcer etiology. Eventually, they might contribute to the development of improved clinical guidelines and to more directed research on pressure ulcer detection and prevention.

# Chapter 1

## Introduction

Parts of this chapter are based on: D. Gawlitta, C.V.C. Bouten, *In-vitro muscle model studies*, in Pressure ulcer research: current and future perspectives; Editors: Bader, D.L., Bouten, C.V.C., Colin, D., Oomens, C.W.J., in press, Springer-Verlag, Book Chapter 16, ISBN 3-540-25030-1 (2005)

## 1.1 Pressure ulcers

Biological tissues are susceptible to developing damage due to mechanical compression. The compression leads to tissue deformation and may result in tissue damage depending on its magnitude and duration. Sustained loading can lead to a condition commonly known as pressure ulcers. In particular, subjects with limited mobility, because they are bedridden or wheelchair bound, experience prolonged loading and are at risk of pressure ulcer development. In addition, medical devices, such as plaster cast, prostheses, or tubing, that remain on the body for an extended period of time, can exert mechanical loading, potentially leading to pressure ulcer development.

Based on the severity of the ulcer, i.e. the amount and type of layers of soft tissue affected, several classification methods of pressure ulcers have been proposed (Shea, 1975; Yarkony et al., 1990; Harker, 2000). In general, ulcers involving the skin are classified as type I or II, the superficial pressure ulcers. More severe ulcers may extend from the skin into the fat and muscle layers, and even to the bone. These wounds are classified as types III and IV or deep pressure ulcers. The classification suggests a sequential 'top-bottom' development of the wounds, starting as type I in the skin, and subsequently evolving into type II, III, or IV wounds. However, also the 'bottom-top' theory for deep pressure ulcers has been postulated (Bliss, 1998; Bouten et al., 2003a), suggesting that the wounds can start within deeper tissue layers and progress towards the skin. The bottom-top hypothesis is supported by the fact that skeletal muscle tissue is highly susceptible to sustained deformation, eventually leading to tissue breakdown in the form of deep pressure ulcers (Nola and Vistnes, 1980; Daniel et al., 1981). Thus, deep pressure ulcers can originate within the skin or muscle tissue layers. This onset may be attributed to the nature of the surface loading and the tissue integrity and geometry. It should be noted that both theories of the origin and development of ulcers are not necessarily mutually exclusive.

The importance of distinguishing deep tissue injury (DTI) in addition to the other four types of pressure ulcers has recently been recognized by the NPUAP and EPUAP. They are defined as pressure-related injuries under intact skin (Ankrom et al. 2005). Their importance is illustrated by their progression. They may initially appear as a deep bruise, but develop into a stage III or IV pressure ulcer despite the most appropriate treatment.

The tissue breakdown starts at the cellular level with disintegration of contractile proteins and damage to the muscle cell membrane and nucleus, followed by inflammatory reactions. Although skeletal muscle tissues are very susceptible to damage development due to compression, deep pressure ulcers represent the smaller proportion of ulcers in the general patient population in hospitals and nursing homes (2.2-6.4% for grades III and IV only, as compared to 13.2-32.4% for all pressure ulcers (Bours et al., 2002)). However, among specific patient groups, such as spinal cord injured (SCI) individuals, a pressure ulcer prevalence of around 31% (Vidal and Sarrias, 1991; Fuhrer et al., 1993; New et al., 2004; Caliri, 2005; Chen et al., 2005) has been recorded with values for types III and IV together ranging from 13.6 to 21% (Vidal and Sarrias, 1991; Fuhrer et al., 1993; New et al., 2004). Indeed, as high as 50-

85% of spinal cord injured patients were estimated to develop a pressure ulcer at least once in their lives (Rodriguez and Garber, 1994; New et al., 2004). The high prevalence in SCI patients is, however, not only a result of the patient's immobility. Loss of muscle tone, in particular in those suffering from flaccid paralysis, changes in tissue mechanical properties and blood circulation also increase the risk of developing deep pressure ulcers (Scelsi, 2001). For example, decreases in mechanical integrity were demonstrated by Reger et al. (1990) who compared total tissue deformation between paraplegic and healthy female subjects in supine positions with MR-techniques. Full tissue thicknesses from bone to skin at the trochanter and ischial tuberosities were reduced by application of surface loads up to 60 mmHg (8.0 kPa). As a result, the compressive strains in the paraplegic group were estimated to be in the range of 42-67%, whereas the control group exhibited strains between 20 and 35%. The majority of the deformation was observed in the muscle tissue. Interestingly, Lin et al. (2004) applied ultrasound measurements to visualize tissue deformations in the buttock tissue of healthy subjects during sitting, subjected to pressure increments up to 75 mmHg. Their findings show a 66% decrease in the thickness of the muscular layer in healthy subjects.

Although it is known that both the duration and magnitude of compression affect muscle tissue viability, the etiological pathways whereby tissue compression leads to cell damage are not well understood. To date, theories have mainly focussed on the impairment of metabolite and oxygen transport through the tissue (Kosiak, 1959; Dinsdale, 1974; Daniel et al., 1981; Peirce et al., 2000). Tissue compression may occlude afferent blood vessels by narrowing their lumen, which then can no longer deliver enough oxygen to the tissue resulting in local ischemia. Due to the impaired tissue perfusion, transport of nutrients and waste products to and from the metabolically active muscle cells is affected. Occlusion of the lymphatic system may also result in impaired transport as the removal of waste products, excess fluids and proteins from the tissue will be prevented (Krouskop et al., 1978; Miller and Seale, 1981; Braden and Bergstrom, 1987; Reddy and Cochran, 1981). In addition, the restoration of transport during tissue *reperfusion* can be extremely harmful because of the presence of reactive oxygen species, which can accumulate in the tissue upon load removal (Ytrehus et al., 1995; Blaisdell, 2002; Tsuji et al., 2005).

The direct effect of cell deformation due to compressive straining has only recently been identified as a possible cause of deep pressure ulcer development (Landsman et al., 1995; Bouten et al., 2001; Wang et al., 2005). Cell deformation triggers a variety of effects such as altered membrane stresses, volume changes and cytoskeletal reorganisation, which may be involved in early cell damage. It has been shown that the response of muscle cells to deformation during tensile or shear straining is crucial to cellular degeneration or adaptation (Vandenburgh et al., 1991a; Cheng et al., 1995) and a comparable response was found for compressive straining (Breuls et al., 2003a; Wang et al., 2005).

In summary, the etiology of pressure ulcer formation is undoubtedly multifactorial in nature and several or all of the aforementioned processes can play a role.

**This thesis concentrates on providing insight into the underlying mechanisms of compression-induced skeletal muscle breakdown related to deep pressure ulcers, with special emphasis on ischemia and mechanical deformation as the causes of cell death.**

Before addressing the rationale of the thesis and presenting the experimental approach adopted to examine its aims, some background information on in vitro muscle models will be provided to illustrate their applicability in pressure ulcer-related research.

## **1.2 In vitro muscle model studies**

As it is difficult to distinguish between mechanical or ischemic induction of cell death in human subjects or in animal models, an alternative model system is required. Ideally, a hierarchy of model systems ranging from single cell in vitro models (Peeters et al., 2003), to tissue level models (Breuls et al., 2003a; Bronneberg et al., 2006), animal models (Bosboom et al., 2001; Stekelenburg et al., 2005b), and human studies, should provide information about the relative contributions of, for example, cell deformation, local ischemia, and reperfusion to the development of tissue damage. By studying the development of damage after mechanical loading at various levels of complexity (from cell to human) and relating their outcomes a systematic analysis of pressure ulcer etiology can be performed.

For studying the relative contributions of deformation and ischemia in damage development, an in vitro cultured muscle tissue equivalent was chosen. An important advantage of this approach is the ability to control all experimental input parameters and to study the response of the tissue to all factors separately. Moreover, in vitro models give rise to less ethical considerations than in vivo (animal or human) studies. Another benefit of in vitro cell culture is the fact that the same cell clone or cell line can be used in different studies and in different laboratories to improve reproducibility of results. Cell lines can be used to create muscle models applying the concept of tissue engineering. In tissue engineering, cells are cultured in or on a scaffold material and stimulated, using chemical, physical, or mechanical modalities. Stimulation may trigger the cells to proliferate, remodel their extracellular matrix or induce maturation of the culture, to obtain engineered tissue that resembles native tissue. The frequently applied and established cell line for engineering skeletal muscle has been the C2C12 murine myoblast cell line (Yaffe and Saxel, 1977).

Some general information on muscle anatomy and physiology is provided in the next section.

### **1.2.1 Skeletal muscle**

Anatomy Skeletal muscle, or striated muscle, in general contracts voluntarily after stimulation of a nerve. The muscle is divided into compartments by several sheets of connective tissue to enable force transmission. These compartments, the fascicles, are composed of the muscle fibers (the muscle cells). The muscle fibers provide the ability to contract. They contain myofibrils (figure 1.1) that are built up from sarcomeres, the

contractile units in the cells. Myosin and actin molecules compose the sarcomeres and are arranged such that a striated pattern is created.

Muscle cells are formed by fusion of myoblasts (muscle precursor cells) during myogenesis. In vitro, mononucleated myoblasts can be induced to fuse into myotubes (figure 1.2), an immature muscle fiber. Depending on the source of the myoblasts namely, primary isolated cells or foetal-derived cells, a stage of maturation beyond the myotube stage can be achieved.

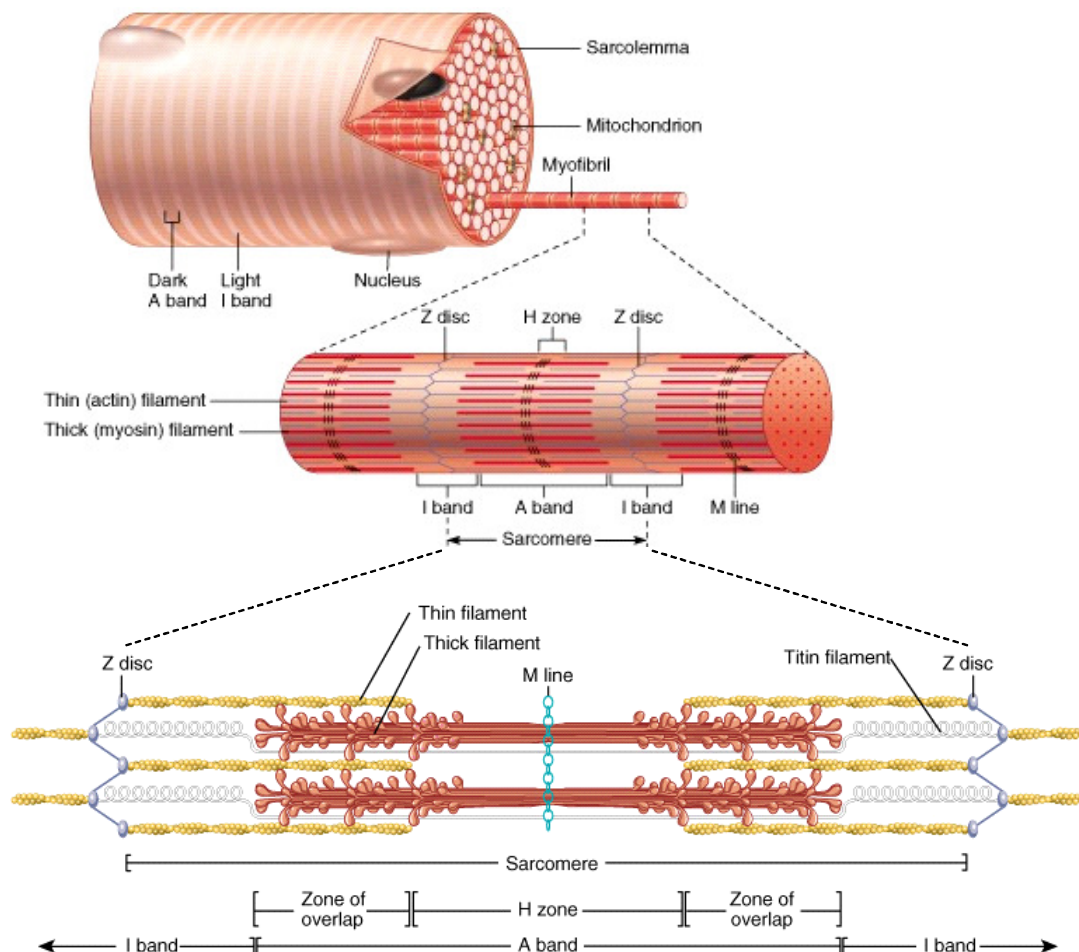


Figure 1.1: The anatomy of a muscle fiber is illustrated on top and in the center the composition of a myofibril is shown with its characteristic bands. On the bottom, a single sarcomere is depicted with a description of its components (the image was adapted from Benjamin Cummings 2001).

**Physiology** Following an action potential originating from the neuromuscular junction,  $\text{Ca}^{2+}$  is released into the cytosol of the muscle fibers. The ions subsequently bind to troponin. This uncovers attachment sites on the actin molecule in the sarcomere, to which the myosin heads can bind. The binding causes a release of inorganic phosphate and a conformational change of the myosin, which results in relative movement of actin and myosin filaments: the contraction.

The inorganic phosphate that is released during the contraction was dissociated from ATP (adenosine triphosphate). ATP is the molecule that provides the energy in the body. It also provides energy for many other processes besides muscle contractions.

ATP is obtained from glucose, preferably by aerobic metabolism. However, when muscle cells are deprived of oxygen and all available energy stores are depleted, anaerobic metabolism is used to produce ATP. The latter pathway results in a lactic acid build-up, which subsequently diffuses into the extracellular space. If anaerobic metabolism persists for an extended period of time without reperfusion, cellular acidification may occur.

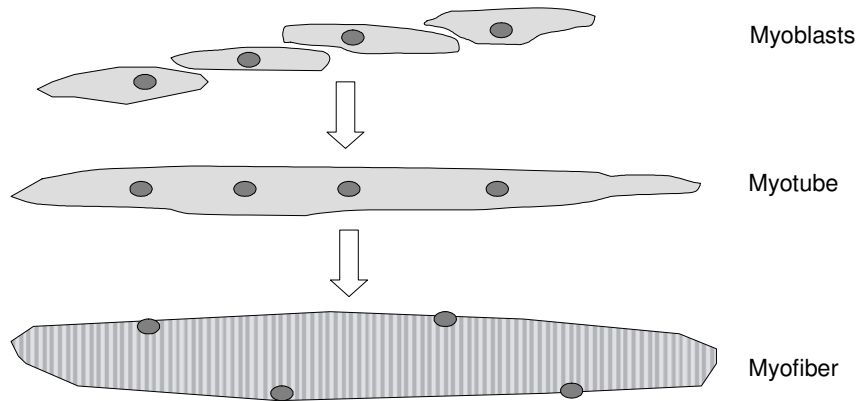


Figure 1.2: The formation of a muscle cell is schematically shown. Myoblasts fuse into multinucleated myotubes and if their maturation continues, this results in cross-striated myofibers with peripherally located nuclei.

### 1.2.2 Single cell studies

For determining the effect of compression on muscle tissue several studies were conducted on engineered skeletal muscle or single cells. Comprehensive studies on the compression of individual C2C12 myoblasts were performed in the host laboratory (Peeters et al., 2003; 2004; 2005a; 2005b). The single cell studies were performed using a custom made loading device that enabled monitoring of the morphological and biomechanical response of the cells to compression (Peeters et al., 2003). Major findings were that structural membrane changes were observed when compression started to exceed approximately 50% compression. When studied in more detail (Peeters et al., 2005a), the cells clearly started to demonstrate membrane bulges at about 60% compression. This bulging continued until the cell membrane burst at approximately 70% compressive strain. Experiments, in which the cells were dynamically loaded, showed a lowering of the damage threshold to strains exceeding 40%, and membrane rupture occurred at approximately 50%. With respect to the frequency of loading, cell membranes ruptured more easily at high frequencies of up to 10 Hz rather than at lower frequencies of 0.1-0.3 Hz. Although a single cell model is very distinct from a patient at risk of developing pressure ulcers, it can provide fundamental understanding of the response of the smallest units in the human body to compressive loading. Through a hierarchical approach, the cellular response may assist in explaining the tissue response to compressive loading (Bouten et al., 2003b).

### 1.2.3 Engineered muscle studies

The single cell studies yield important information on the response of individual myoblasts to compression. In a tissue, however, these cells are surrounded by other

cells and extracellular matrix in a three-dimensional architecture. In this configuration, compressive tissue loads may be transferred to the individual cells in a variety of ways, resulting in distinct relationships between compressive straining and cell damage or death. In addition, in muscle tissue the myoblasts have fused to form multinucleated myotubes, which may react differently to compressive straining. The most important advantages of studying damage development in 'in vitro' models of skeletal muscle are that the model can be reproducible and easily controlled and manipulated. Cells can be genetically modified (Vandenburgh et al., 1996; 1998a), or stained to visualize either the whole cell (in situ) or a cellular protein of interest. In vitro systems for muscle culture can consist of tissue explants or of tissues engineered from muscle-derived cells. The latter method was chosen in the present thesis for its higher reproducibility and ease of manipulation. An important difference between in vivo muscle and engineered muscle constructs is the lack of capillary vessels in the latter. In vitro, the transport of molecules is limited to the speed of diffusion. Another difference is the absence of neuronal stimulation in the tissue engineered muscle.

Bouten et al. (2001) studied compression of C2C12 cells fused into myotubes and seeded in a 3% low gelling temperature agarose gel. For this purpose myoblasts were allowed to grow for four days in agarose constructs supplemented with growth medium and subsequently transferred to differentiation medium for another 8 days. The resulting cell population in the agarose gel then consisted of three sub-populations: 50% spherical myoblasts, 35% spherical myotubes, and 15% elongated rod-shaped myotubes. Only deformations of the first two subpopulations were considered when studying the effects of construct compression on cell damage. With a custom-built compression rig mounted to the stage of a confocal microscope, the agarose constructs were loaded in unconfined compression up to 40% compressive strain. Cell deformation was monitored in time using the viable fluorescent cytoplasm probe Calcein-AM and the change in cell diameters parallel to the axis of compression was measured. Overall, the cells changed from their spherical appearance to a more UFO-shaped morphology during compression. Cell strains in the direction of compression were similar to the applied construct strain. On a smaller scale, the myoblast subpopulation showed membrane buckling at 30 to 40% strain, while myotubes already showed signs of buckling at 20% strain. In a second experiment the influence of prolonged compressive straining (0-24 h, at 0%, 10%, and 20% strain) was studied. Cell damage was quantified from histology to identify membrane damage and/or nuclear condensation and fragmentation. A significant increase in cell damage was observed after 2h of compression at 10% strain compared to unstrained constructs, although cell damage remained fairly constant after 4h of compression (figure 1.3).

At 20% strain the percentage cell damage increased from about 40% at 1 h to almost 100% at 24h compression. In the unstrained controls the percentage of damaged cells remained constant throughout the entire loading period.

It should be noted that the level of 20% construct strain corresponded to a compression of about 32 mmHg or 4.3 kPa. This level of compression has long been considered as a causal factor for pressure ulcers, since it is traditionally quoted as the capillary closing pressure (Landis, 1930; Dinsdale, 1974; Reswick and Rogers, 1976). Pressures



exceeding this value were assumed to result in ischemia-induced pressure ulcers. The described experiments, however, prove that in the absence of capillaries and blood perfusion, the mere deformation of cells can cause considerable damage with time.

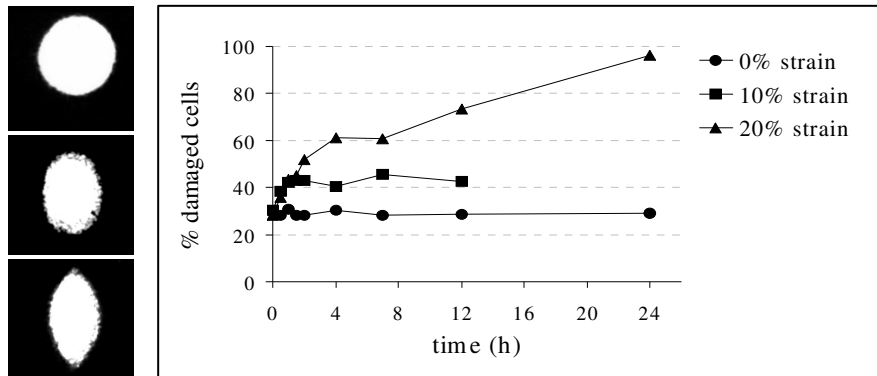


Figure 1.3: Percentage cell damage with time at 0%, 10% and 20% compressive straining (Bouten et al., 2001). The left images show gross cell deformation at 0% (top), 10% (middle), and 20% (bottom) strain.

Clinically relevant compression studies using the same muscle model of cell/agarose constructs were performed by Wang et al. (2005). Gross static strains of 10% and 20% were again applied for up to 12h, corresponding to pressures of 18 and 32 mmHg, respectively, although in this case cellular breakdown was categorised in terms of apoptosis, assessed by DNA Nick translation and necrosis (fluorescent probes and HE staining). The total amount of non-viable cells at 10% compression increased significantly after 4 h and a maximum percentage of 54% non-viable cells was found at 12 hours of straining. The DNA Nick translation revealed that the majority (70%) of the non-viable cells was undergoing apoptosis after 8 and 12 hours of compression.

A significantly different tendency was found for the 20% strained constructs. Here the percentage of non-viable cells was significantly higher than in unstrained controls even after 0.5 hours and reached a maximum value of 76% at 12 hours (control 30%). Again about 70% of these cells were undergoing apoptosis. The subpopulation of elongated myotubes seemed to be particularly sensitive to compression, as all of these cells had died within 1.5 hours.

The work of Wang et al. (2005) and Bouten et al. (2001) was based on an in vitro model of C2C12 cells in agarose gel. The percentage of cells actually fusing into elongated myotubes was rather small, about 15%, in these constructs. Furthermore, most cells remained spherical due to the lack of anchorage points in the gel. In actual skeletal muscle tissue the predominant cell population consists of elongated multinucleated myotubes. Therefore, Breuls et al. (2003a) attempted to provide a more physiological distribution of muscle cell morphology, using a modification of the cell-gel suspension protocol proposed by Vandenburg et al. (1998b).

C2C12 myoblasts were suspended in a collagen/matrigel mixture and differentiated into elongated myotubes. These constructs were disc-shaped with a diameter of approximately 10 mm. For the compression experiments a device was designed, containing an incubation chamber and glass indenters with a diameter of 5 mm. This

device was mounted onto the stage of a confocal microscope to compress the constructs, while visualizing cell morphologies and damage. Four levels of strain were

*Table 1.1: Summary of the major findings of selected 'in vitro' studies (Bouten et al., 2001; Breuls et al., 2003a; Peeters et al., 2003; Wang et al., 2005).*

Author	Model	Time scale compression	Main results
Peeters et al.	Single myoblasts	seconds	<ul style="list-style-type: none"> <li>• Stepwise strain &gt; 50%: structural cell damage</li> <li>• Strain &gt; 60%: membrane bulging</li> <li>• 72% strain: cells start to burst</li> <li>• Dynamic straining: bulging at 40%, bursting at 54%</li> <li>• Cells more sensitive to high frequency than low frequency</li> </ul>
Bouten et al.	Myoblasts and myotubes in agarose	1-24 hours	<ul style="list-style-type: none"> <li>• Strain &gt; 20%: buckling of myotubes</li> <li>• Strain &gt; 30-40%: buckling of myoblasts</li> <li>• Increase in damage in cell after 1 hour of straining</li> </ul>
Wang et al.	Myoblasts and myotubes in agarose	½ -12 hours	<ul style="list-style-type: none"> <li>• At 10% strain: increase in damage after 4h compression</li> <li>• At 20% strain: increase in damage after ½ hour compression</li> <li>• 60-70% of cell death due to apoptosis</li> <li>• Myotubes more sensitive to straining than myoblasts</li> </ul>
Breuls et al.	Myoblasts and myotubes in collagen/matrigel mix	1-8 hours	<ul style="list-style-type: none"> <li>• At 30% and 50% strain: immediate cell damage</li> <li>• At 30% strain: 50% damaged at 8 hours</li> <li>• At 50% strain: 80% damaged at 8 hours</li> </ul>

applied: 0%, 0+%, 30%, or 50%, where the 0% strain group represented unstrained (control) samples and the 0+% group represented constructs that were loaded with the tare strain of the resting indenter on the construct, in the absence of significant compression. This group served to study the effect of a non-porous indenter on diffusion of oxygen and nutrients from the culture medium into the construct. During the compression experiments, cells inside the constructs were monitored in real-time with viable fluorescent probes (Breuls et al., 2003b) to quantify cell viability after 0, 1, 2, 4, 6, and 8 hours.

The presence of strain invoked significant initial cell damage immediately after load application: approximately 8% in the 30% strain group and about 14% in the 50% group. At 30% strain a further increase in the percentage of cell death was observed between 2 and 6 hours, whereas at 50% additional cell death was found earlier, between 1 and 4 hours. After these periods the percentage of dead cells remained fairly constant. This is in agreement with the inverse relation between magnitude and duration of tissue compression and observed tissue damage in animal studies (Kosiak, 1959; 1961; Daniel et al., 1981). The plateau values for the percentage of damaged cells reached maximum values of just over 50% (at 30% strain) and above 80% (at 50% strain).

The combined results from the above studies can provide better insight into thresholds for muscle damage development in terms of magnitude and duration of applied strains. The most important observations are summarized in Table 1.1. The results may also be summarized as shown in figure 1.4, which represents a percentage of viable cells as a

function of magnitude and time of compression for all the selected studies. Clearly, the percentages of viable cells decreased with increasing strain magnitude. Furthermore, at constant strain magnitude, cell viability decreased with time of compression. It should

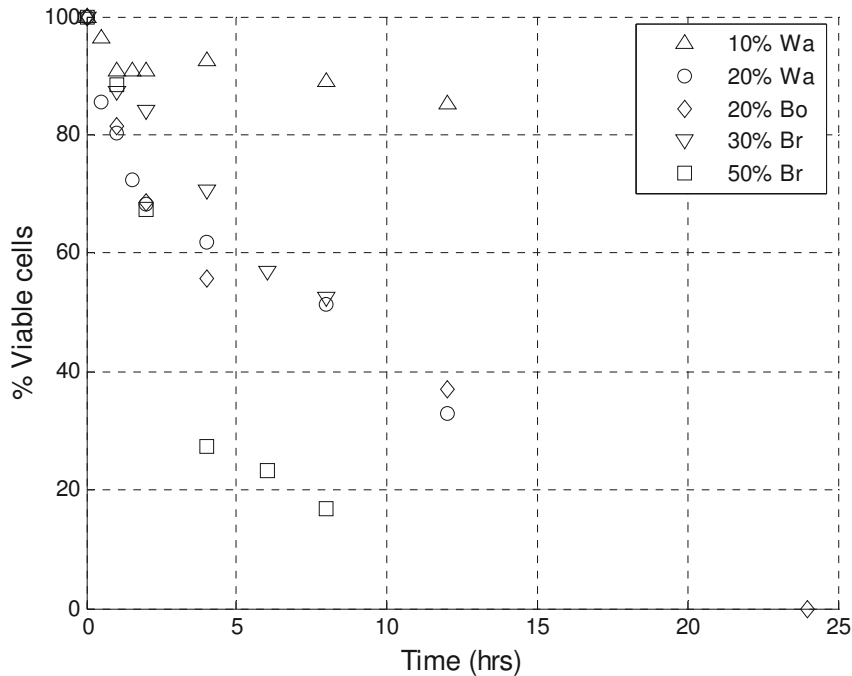


Figure 1.4: Combined percentages of viable cells in time from Bouten et al. (Bo, 2001), Breuls et al. (Br, 2003a), and Wang et al. (Wa, 2005). Percentages are normalised for the percentage cell death in unstrained controls. The legend indicates the results from the respective authors.

be noted that these inverse relationships between magnitude and time of compression were related to tissue deformation alone, rather than to impaired transport due to ischemia, lymphatic occlusion, or reperfusion, which were not incorporated in the in vitro models. The relative contribution of impaired oxygen transport to the observed cell damage, however, remains to be elucidated. So far, the effect of compression on the permeability of the tissue constructs for oxygen has not been quantified. Also, the effect of construct compression on the washout of waste products is not known. For example, in the work by Breuls et al. (2003a), constructs were compressed under a 5 mm diameter indenter and up to 50%, which could have limited the transport processes. If this effect is added to the possible removal of oxygen upon load application, hypoxia (oxygen deprivation) could have influenced the observed cell damage. Nevertheless, the distribution of cell death under the indenter was homogeneous (Breuls et al., 2003a) and not dependent of the distance of the cells to the edge of the indenter, as one might have predicted to occur in oxygen diffusion-related damage evolution.

### 1.3 Rationale and outline

Several hypotheses have been proposed to explain the onset of (deep) pressure ulcers. They involve all effects of externally applied load to the tissue. Compression may lead

to occlusion of lymphatic vessels and impairment of interstitial transport. It may cause collapse of the capillaries and thus an arrest of blood perfusion leading to tissue ischemia. Furthermore, the compression of the cells per se within the tissue can trigger damage development. Finally, upon load relief, tissue reperfusion can evoke free radical formation, which is harmful for the tissue.

In the present thesis an attempt was made to unravel the relative contributions of some of the factors underlying pressure ulcer development and to study their potentially combined contribution in muscle damage development. More specifically, the aim is to provide more insight in the relative contributions of deformation and ischemia to the development of muscle tissue damage. In order to attain this goal, several issues need to be addressed:

- ❖ Choice of a suitable model system to monitor development of tissue damage,
- ❖ Is lack of oxygen affecting viability in a different way than compression?
- ❖ What factor(s) involved in compression-induced ischemia is most damaging to the muscle model system?

Before addressing the latter two issues, the development of an appropriate model system is required. The intended model system consists of three components that are described in chapters 2 and 3. The first component was an engineered muscle model. The model established by Breuls et al. (2003a) was extended to contain aligned myotubes. Moreover, the degree of tissue differentiation towards mature muscle needed to be characterized and optimized. In association with the development of a convenient protocol for engineered muscle tissue formation, a comparison of the performance of several differentiation media in the tissue model is presented in chapter 2. A second essential component of the model system was the ability to enable real-time assessment of cell death in the tissue and discriminate both apoptotic and necrotic cell death in a non-invasive manner in culture. A vital staining technique was proposed and its applicability and its performance in marking apoptotic and necrotic cell death are summarized in chapter 3.

The last component involves the design of an experimental arrangement, which can both facilitate the control of normal culture conditions, such as temperature and humidity, and impose risk factors on the muscle model, such as clinically relevant compressive strains (20, 40%) and hypoxia (oxygen demand of the tissue exceeding oxygen availability). The relative contributions of compression and hypoxia on the viability of the engineered skeletal muscle constructs are described in chapter 4.

In chapter 5, the influence of more factors ischemic factors is examined, namely, . acidification and starvation of the tissue in terms of cell viability. The effects of the ischemic factors on metabolic parameters as well as cell damage are described. The last chapter discusses the most important findings of the thesis and their implications for clinical practice, as well as suggestions for future research will be discussed.



# Chapter 2

## The influence of serum-free culturing on skeletal muscle development in a tissue-engineered model

This chapter is based on: D. Gawlitta, K.J.M. Boonen, C.W.J. Oomens, F.P.T. Baaijens, C.V.C. Bouten, *The influence of serum-free culturing on skeletal muscle development in a tissue-engineered model*, Cells Tissues Organs, submitted, (2006)

## 2.1 Introduction

Primary cultures as well as different cell lines have been used to study myogenesis in vitro. They have been applied to increase our understanding of diseases, the development of damage and the possibilities of regeneration. A frequently used model to study skeletal muscle differentiation contains C2C12 murine myoblasts. C2C12 has been proved to be the designated cell line to use in these experiments, because it grows rather fast, culture conditions are relatively easy and it responds well to manipulations (Yaffe and Saxel, 1977; Blau et al., 1983; Kubo, 1991; Andres and Walsh, 1996; Shimokawa et al., 1998; Lawson and Purslow, 2000; Delgado et al., 2003; Shen et al., 2003; Burattini et al., 2004; Tannu et al., 2004). In addition, C2C12 cells have been used extensively for the production of 3D tissue engineered muscle (Okano and Matsuda, 1997, 1998a, 1998b; Dennis and Kosnik, 2000; Dennis et al., 2001; Srikakulam and Winkelmann, 2004), which is much more relevant for studying damage and disease and can also be used for studying the effects of chemical, electrical and mechanical stimulation on the differentiation of the cells.

C2C12 skeletal muscle myoblasts are typically differentiated in vitro by a nearly confluent density and serum reduction. After induction of differentiation, a series of events takes place in which the myoblasts elongate and fuse with each other to form myotubes (Furst et al., 1989; Andres and Walsh, 1996; Delgado et al., 2003; Shen et al., 2003). One of the most important events in this process is myofibrillogenesis when the sarcomere proteins assemble into a working contractile apparatus (Furst et al., 1989; Lin et al., 1994; Begum et al., 1998; Sanger et al., 2002).

The classical method for serum reduction in this cell line is switching from 10-20% FBS to 2-10% horse serum (Kubo, 1991; Lawson and Purslow, 2000; Portier et al., 1999). Recently however, attempts were undertaken to differentiate C2C12 myoblasts into myotubes by culturing in serum-free media (Portier et al., 1999; Lawson and Purslow, 2000). An advantage of this approach is that the presence of inconsistent and uncharacterized serum components is omitted. Also, murine cells no longer have to be cultured in sera from a different species. To replace the serum several growth factors and other components have been proposed. The insulin-like growth factors (IGFs) and insulin itself are known to promote both proliferation and differentiation of myoblasts (Ewton et al., 1994; Bach et al., 1995; Coolican et al., 1997; Conejo et al., 2001; Takahashi et al., 2002; Yang and Goldspink, 2002; Hill and Goldspink, 2003; Rabinovsky et al., 2003; Musaro et al., 2004; Cheema et al., 2005). In addition, a commercially available serum substitute, called Ultrosor G, was used to induce differentiation of myoblasts in monolayer cultures (Benders et al., 1991; Jacobs et al., 1992; van Kuppevelt et al., 1992; Portier et al., 1999; Sultan et al., 2006).

The influence of these serum-free media on differentiation has until now only been studied in monolayer cultures. In a three-dimensional organization cells behave differently as they are completely surrounded by extracellular matrix and other cells. Therefore, the goal of the present study was to characterize the influence of serum-free media on the differentiation of C2C12 in an engineered construct.

In general, three distinct approaches have been applied to create engineered skeletal muscle, or Bio-Artificial Muscle (BAM), with C2C12 cells in vitro. First, cells were

cultured in a collagen gel (Vandenburgh et al., 1996; Okano and Matsuda, 1997, 1998a; Breuls et al., 2003a, van Wachem, 1996), which can be molded into a desired shape. Another approach was cell culture on flexible substrates (Shansky et al., 1997; Vandenburgh et al., 1991b; Strohman et al., 1990), which stimulates the assembly of contractile proteins, in particular when the substrate's stiffness resembles the natural tissue stiffness (Engler et al., 2004; Griffin et al., 2004). Finally, cells were maintained in a monolayer culture, which rolled up between anchoring points (Dennis and Kosnik, 2000; Dennis et al., 2001; Swasdison and Mayne, 1992) directing the pre-stress that is created by the cells and thus producing cell alignment.

In the present study, existing protocols from literature were combined for assembly of engineered skeletal muscle from C2C12 murine myoblasts. Differentiation has been shown to have better results in the presence of a number of extracellular matrix proteins, especially laminin and collagen (Lawson and Purslow, 2000, Dennis et al., 2001). The gel suspension used in this study, which is composed of a collagen I / Matrigel<sup>®</sup> mixture (Vandenburgh et al., 1998b), contains both proteins. Especially Matrigel has been shown to significantly stimulate differentiation of primary muscle cells (Dusterhoft and Pette, 1993; Maley et al., 1995; Langen et al., 2003). The gel mixture was molded and cultured in modified culture dishes between two anchoring points (Dennis and Kosnik, 2000).

The influence of IGF-I and Ultrosor G, either separately or combined, are determined and compared to the maturation achieved by differentiating in 2% horse serum (the gold standard). Differentiation will be characterized by the expression of the proteins desmin, myosin, and actin, which are essential for the assembly of a functional contractile apparatus. Creatine Kinase (CK) activity was determined as a measure for myotube maturation because it appears in the cytoplasm of fused cells and not in single myoblasts (Yaffe and Saxel, 1977; Page et al., 1989; Shiesh et al., 1992; McArdle et al., 1999). The effects of the media on cell metabolism (assessed by MTT) were determined as well, to evaluate cell viability under the different differentiation media.

## **2.2 Materials and Methods**

### **2.2.1 Cell and tissue culture**

C2C12 murine skeletal myoblasts (ECACC, Salisbury, UK) were cultured in growth medium (GM) in an incubator at 37 °C and 5% CO<sub>2</sub>. GM consisted of 500 ml DMEM high glucose (Gibco, Breda, The Netherlands), with L-glutamine, 15% FBS (Biochrom AG, Berlin, Germany), 2% HEPES (Biochrom AG), 1% non-essential amino acids (Biochrom AG), and 0.5% gentamicin (Biochrom AG). At passage 14 they were harvested and seeded into gel constructs at  $4.9 \cdot 10^6$  cells/ml. The gel mixture consisted of collagen I gel and Matrigel (both BD Biosciences, Alphen a/d Rijn, The Netherlands) as previously described by Breuls et al. (2003a) and Vandenburgh et al. (1996). In short, cells were centrifuged and resuspended in a mixture (total 1 ml) of 0.39 ml GM, 0.5 ml collagen I (3.2 mg/ml), 27  $\mu$ l NaOH (0.25 M, Sigma, Zwijndrecht, The Netherlands), and 83  $\mu$ l Matrigel.



The cell/gel suspension was molded into shape in modified petri dishes between two Velcro anchoring points. The dishes were coated with 1.5 ml SYLGARD 184 elastomere (Mavom b.v., Alphen a/d Rijn, The Netherlands) and house-shaped pieces (appr. 5x7 mm) of Velcro with ‘rooftops’ facing each other (figure 2.1) were anchored to the dish with minute pins (26002-10, Fine Science Tools, Heidelberg, Germany), as described by Dennis et al. (2000, 2001). Dishes were filled with PBS and sterilized by exposure to UV for about 90 minutes. One hour after molding the BAMs into and between the anchoring points, 2.5 ml of growth medium was added to the culture. After 24 hours the medium was changed to differentiation medium (DM). This shift day (the growth medium was replaced by differentiation medium) is referred to as s0; subsequent culturing days are named accordingly. Differentiation medium was refreshed every 48 hours.

Five types of differentiation medium, DM, were tested in which FBS was replaced as summarized in table 2.1; Ultrosor G (BioSeptra, Cergy-Saint-Christophe, France), IGF-I (I8779, Sigma), and horse serum (Biochrom AG) were chosen as serum additive or substitute.

For comparison, also monolayer appearance of C2C12 myoblasts cultured in the presence of the five differentiation media was assessed in 12-well plates. At days s3, s5, s7, and s10 they were inspected with light microscopy.

Table 2.1: Listing of the abbreviations of the applied differentiation media (in DMEM) and their sera or substitutes.

Abbreviation of differentiation medium	Serum or serum replacement
HS (gold standard)	2% horse serum
HSI	2% horse serum + 32 ng/ml IGF-I
DMI	32 ng/ml IGF-I
DMU	0.4% Ultrosor G
DMUI	0.4% Ultrosor G + 32 ng/ml IGF-I

## 2.2.2 Experimental design

BAMs, differentiated with either of the differentiation media, were analyzed for protein quantities, metabolic activity, and examined histologically. They were sacrificed at days s0, s3, s6, and s10 of differentiation and subsequently blotting or immunofluorescence was performed or protein activities were measured as described in this section. They were cultured in batches for one of the end points, applying all the media types.

## 2.2.3 Creatine Kinase activity

After culture, BAMs were washed twice with PBS and incubated for 1 hour in 0.5% Triton X-100. Activity of CK was determined using a Granutest 2.5 CK NAC DGKCh kit (Merck, Darmstadt, Germany). The protocol’s incubation periods provided by the manufacturer were adjusted in our lab to enable measurement of small activities. 40 µl of sample was added to 1 ml CK reagent and absorbance was measured against a blank

at 340 nm at ten minute intervals after 50 minutes of reaction in an incubator. After 50 minutes the activity of the samples was found to have reached a plateau.

#### **2.2.4 Total protein content**

BAMs were created as described before, washed twice with PBS, cut loose from Velcro and sonicated in SET-buffer (0.25 M sucrose, 2 mM EDTA, 10mM Tris-HCl (pH 7.4)). Total protein measurements were performed using the bicinchoninic acid method (Sigma). Of each sample 5  $\mu$ l was added to 1 ml bicinchoninic acid solution supplemented with 1/50 4% copper sulphate. After 30 minutes at 37 °C, absorption was measured at 562 nm. As a control, the absorbance of a range of samples containing 0, 1, 3, 5, 10, 20, and 30  $\mu$ g of BSA in 5  $\mu$ l of SET-buffer was also measured.

#### **2.2.5 Immunofluorescence**

For qualitative immunohistochemistry, BAMs were washed with PBS, fixed with 10% formalin for 30 minutes, and permeabilized with 0.5% Triton-X-100 in PBS for another 30 minutes. Subsequently, BAMs were incubated twice for 20 minutes with 1% HS in PBS to block non-specific binding and incubated over night with an antibody against myosin heavy chain (1:250 MF20, developed by D. A. Fischman and obtained from the Developmental Studies Hybridoma Bank, maintained by The University of Iowa) in NET-gel (50mM Tris pH 7.4, 150 mM NaCl, 5mM EDTA, 0.05% NP40, 0.25% gelatin) with 10% horse serum. Then BAMs were washed 6 times 10 minutes in NET-gel and incubated with rhodamin-conjugated phalloidin (1:500, P1951, Sigma) and Alexa Fluor 488, goat anti-mouse IgG2b (1:1000, Invitrogen b.v., Breda, The Netherlands). Subsequently, BAMs were washed six times for 10 minutes with NET-gel, washed 4 times for 5 minutes in PBS and finally embedded in DABCO (Fluka). BAMs were viewed on a Zeiss confocal microscope (Axiovert 100M, Zeiss, Göttingen, Germany). Images were analyzed for protein structures indicative of myotube maturation.

#### **2.2.6 Cell metabolism**

The changes in metabolic activity in the BAMs were analyzed by application of an MTT assay (Sigma). The MTT assay involved a washing step in PBS before addition of 2.5 ml of the respective DM with 0.25 ml MTT (5 mg/ml in PBS) to each well. The cells were incubated for 30 minutes to allow crystal formation in metabolically active cells. Subsequently, the MTT mix was removed and the BAMs were washed three times with PBS. Every BAM was cut in half and weighed before the halves were placed in DMSO containing 10% Triton-X100 to dissolve the purple crystals. The samples were incubated on a shaking table for 1 hour (the blank reading was performed on the solubilization solution). Absorbance was measured on a plate reader at 570 nm, after transfer into a 96-well plate.

#### **2.2.7 Statistical analysis**

On all data, analyses of variance (ANOVA) were performed in the software package SPSS 12.0.1. Differences in total protein levels were posthoc tested applying

Bonferroni. Where variances were unequal (CK, MTT), Tamhane posthoc tests were performed to correct for this. Significance was set to  $p < 0.05$ . In the graphs means are depicted with error bars denoting standard deviations.

## 2.3 Results

### 2.3.1 Creatine Kinase activity

The macroscopic appearance of the BAMs is shown in figure 2.1. In these, creatine kinase was determined to evaluate myoblast fusion and differentiation. Under four of the five differentiation media applied, the myoblasts had successfully fused into myotubes as apparent from figure 2.2. They showed increases of creatine kinase activity with time, all exhibiting maximum activity at the final day of measurement, s10, though only significant under DMU, HSI, and DMUI. When compared, BAMs differentiated under HSI significantly exhibited the highest mean activity, followed by DMU and DMUI.

Maturation in DMI did not cause cell fusion or differentiation as no significant increase in CK activity was found when compared to control (s0).

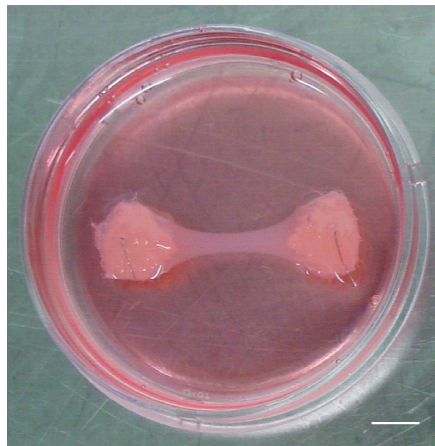


*Figure 2.1: Macroscopic appearance of a bio-artificial muscle, BAM, is shown with the gel between two pieces of Velcro and fixated by stainless steel pins. The bar indicates 5 mm.*

### 2.3.2 Total protein content

Total protein content of the BAMs was evaluated in time (figure 2.3). BAMs grown in all differentiation media had significantly decreased total protein content on all days after shifting the medium, except for DMU on s3. BAMs under DMI even continuously showed declined total protein content compared to earlier time points. The other media exhibited decreased levels of total protein but these did not reduce any further with time. On the final shift day, s10, BAMs differentiated under DMU and DMUI displayed the highest total protein contents.

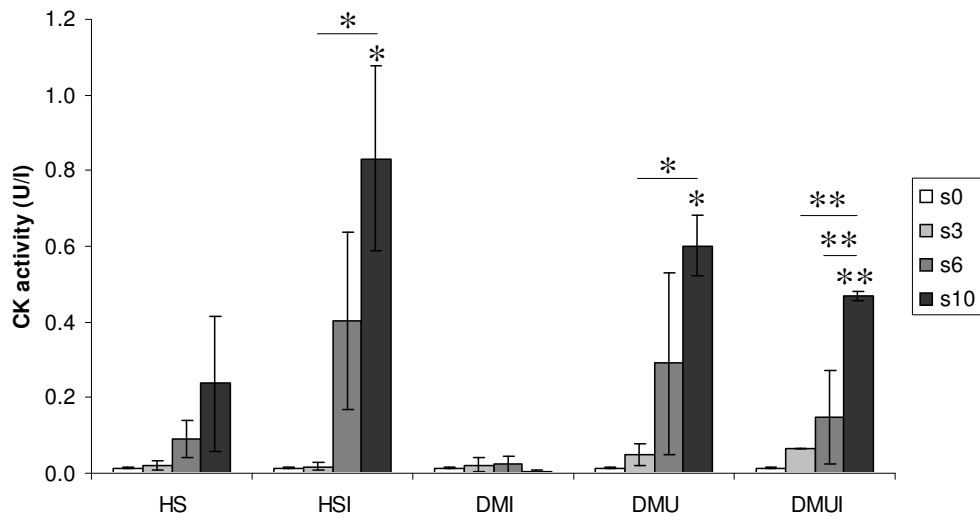


Figure 2.2: Effects of differentiation medium (HS, HSI, DMI, DMU, or DMUI) on CK activity in BAMs on days 0, 3, 6, and 10 after addition of DM. Stars with brackets denote significant difference between bars under brackets; stars denote significant difference as compared to s0, all  $p < 0.05$ .

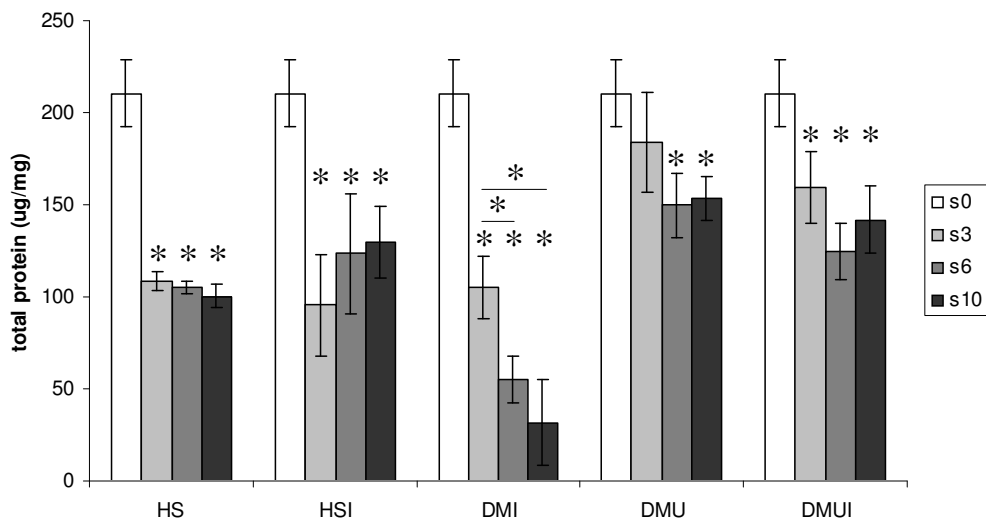


Figure 2.3: Effects of differentiation medium (HS, HSI, DMI, DMU, or DMUI) on total protein contents in BAMs on days 0, 3, 6, and 10 after addition of DM. Stars with brackets denote significant difference between bars under brackets; stars denote significant difference as compared to the control group (s0), all  $p < 0.05$ .

### 2.3.3 Immunofluorescence

Immunostained actin and myosin in the BAMs revealed structural differences among the differentiation media. Protein appearances on a tissue scale (figure 2.4A) and cellular scale (figure 2.4B) were evaluated. Differentiation of 3D constructs in the gold standard (HS) medium resulted in elongated as well as spherical cell structures. Here, myosin expression was predominantly observed in the rounded cells. Even less cell elongation was found in BAMs differentiated in DMI, but they did express myosin in the spherical cells. BAMs differentiated in the other three media contained mainly elongated cells. These cells exhibited myosin expression in punctuate patterns,



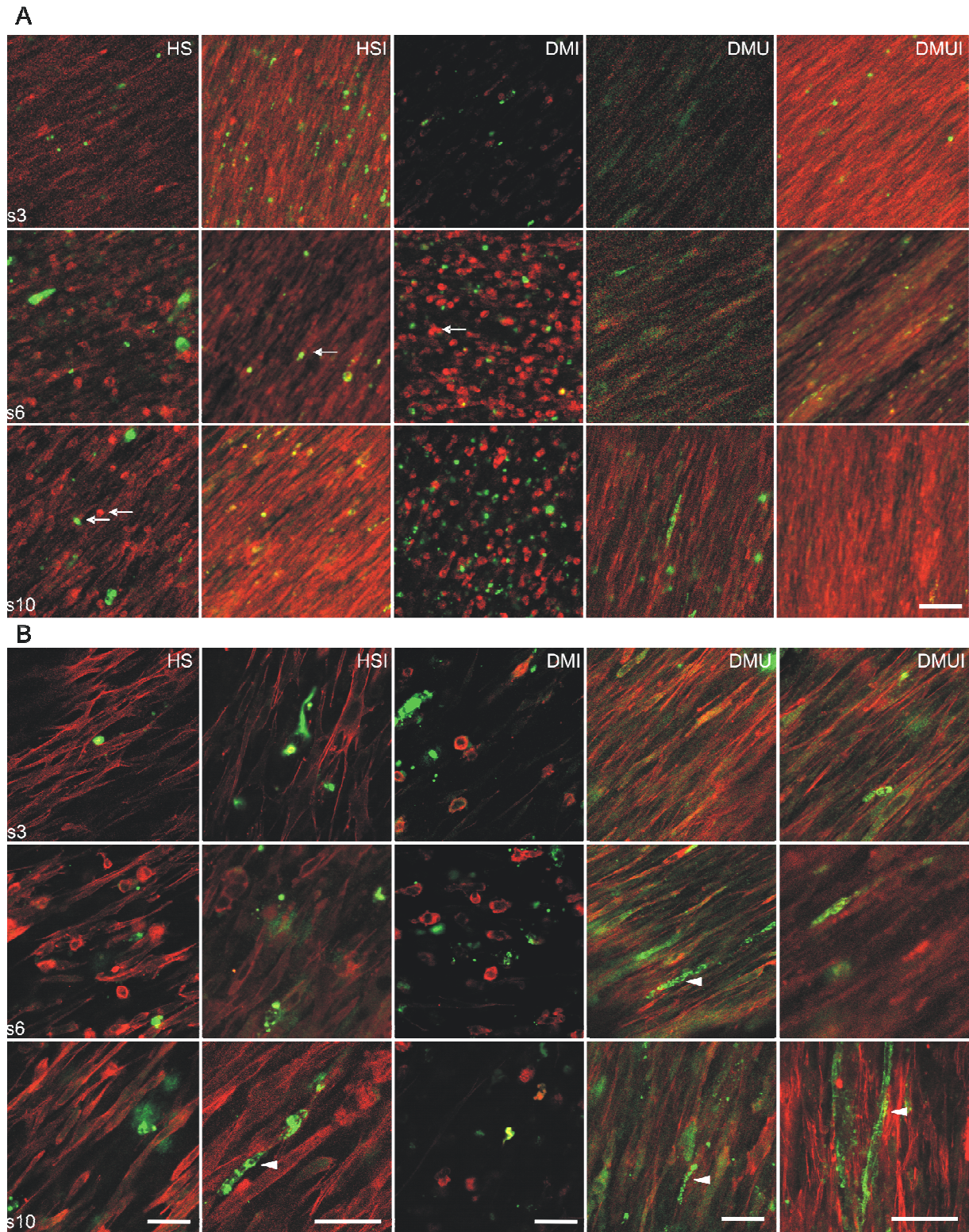


Figure 2.4: Immunofluorescent images of actin (red) and myosin (green) in BAMs treated in 5 different differentiation media (HS, HSI, DMI, DMU, and DMUI respectively). (A) Images are shown from 3 (top), 6 (middle), and 10 (bottom) days after medium change. Cells under HS and DMI show more spherical morphology (arrows), while the other differentiation media evoke more elongated structures. Magnification 200x, bar denotes 100  $\mu\text{m}$ . (B) Images are shown from 3 (top), 6 (middle), and 10 (bottom) days after medium change. Note the punctuate expression of myosin in HSI, DMU and DMUI-treated BAMs (arrowheads). Magnification 400x, bars denotes 50  $\mu\text{m}$ .

indicative of advancing maturation. Maturation also seemed to progress with time under influence of all five different media, as myosin heavy chain content increased. However, maturation did not reach the level of cross-striation in any of the cultures. In preliminary results of western blots, all media showed a tendency for desmin expression from day 6 onwards, independent of medium type. In BAMs, differentiated under DMI, no expression was found, apart from one case of desmin expression at s6.

### 2.3.4 Cell metabolism

Evaluation of cell viability in time was achieved by means of an MTT-assay. In figure 2.5, roughly two different tendencies were observed. BAMs differentiated in HS, HSI, or DMI showed decrements of metabolic activity in time ( $p < 0.05$ ). In contrast, BAMs under DMU and DMUI experienced just a slight decline in metabolic activity. In DMU no significant decrease in metabolism during the first three differentiation days was observed and differentiation in DMUI even slightly increased the metabolic activity within the first three days.

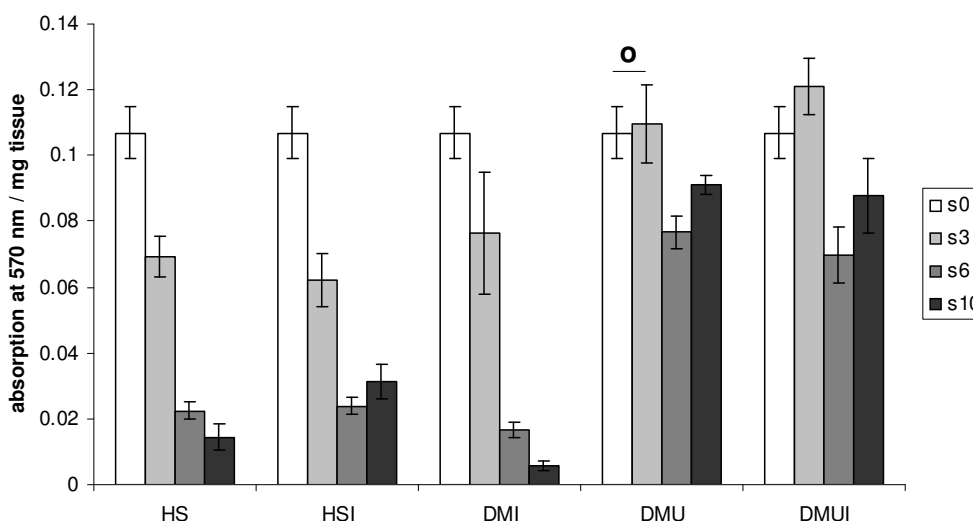


Figure 2.5: Effects of differentiation medium (HS, HSI, DMI, DMU, or DMUI) on metabolic activity (measured by MTT as absorption/ mg tissue) in BAMs on days 0, 3, 6, and 10 after addition of DM. All bars were found to be significantly different from the control bar (s0) and other bars in the same medium group, except from the difference indicated by the 'o' and bracket, all  $p < 0.05$ .

### 2.3.5 Monolayer cultures

Monolayer cultures of C2C12 were exposed to the five differentiation media for ten consecutive days (figure 2.6). Applying HS medium, it took over three days for the first myotubes to appear. At first, they had the appearance of myosacs (Lin et al., 1987, Yotov and St-Arnaud, 1996; Palmer et al., 2001) but by day 7 elongated myotubes were present in the culture. By the 10<sup>th</sup> day, some cell deterioration was evident (appearance of vacuoles). If IGF-I was added, the effects of HSI were similar to those of HS except that the myotubes started to develop at an earlier time point and at day 10 less deterioration was observed. In the DMI medium thin long myotubes had emerged



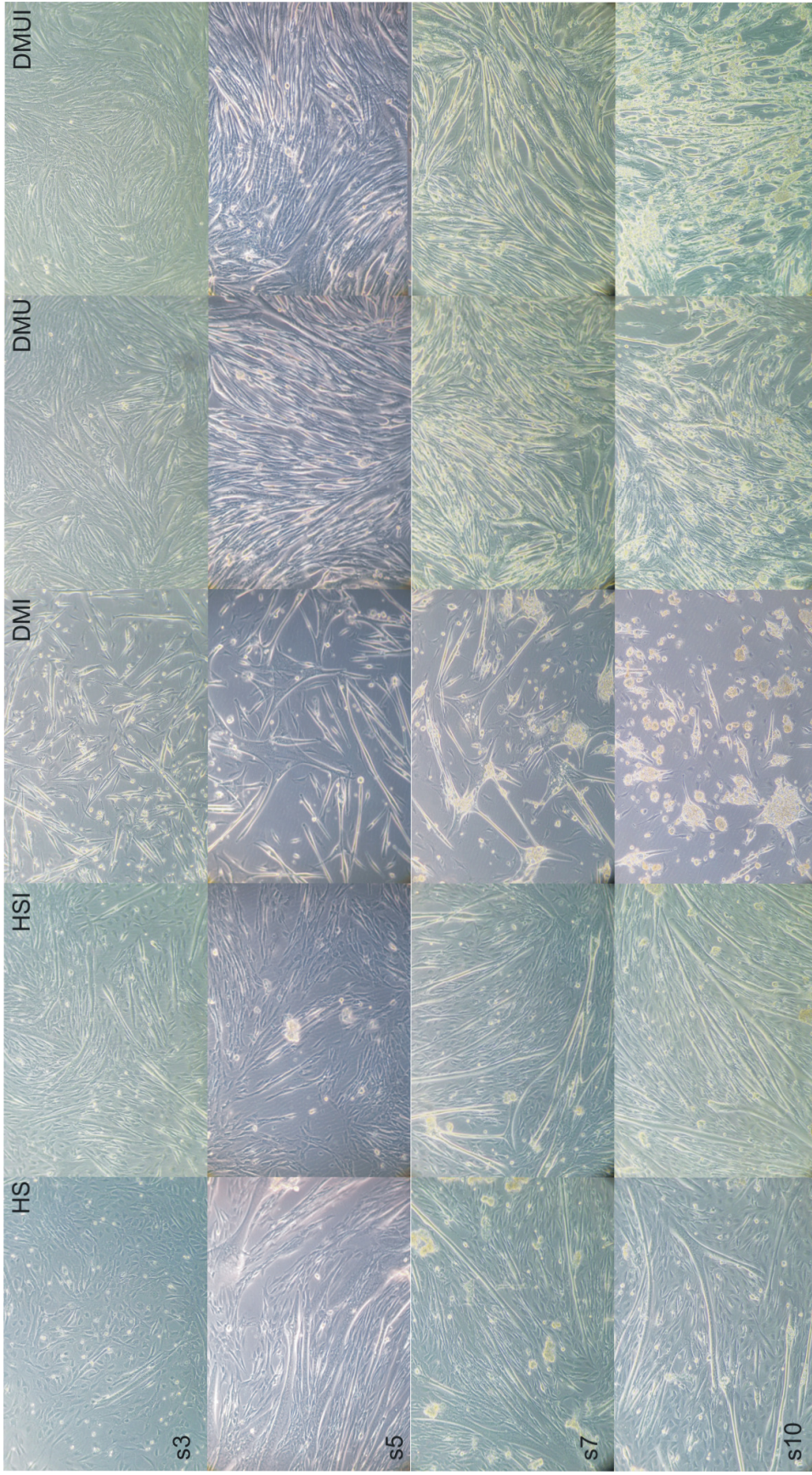


Figure 2.6: Light microscopic appearance of C2C12 myoblasts differentiated under HS, HSI, DMI, DMU, and DMUI, respectively. From the top to bottom images are shown for 3, 5, 7, and 10 days after shifting to differentiation medium.

by the third day and about 50% cell detachment was found, which progressed with time. From day 5 on, myosacs with 3-4 branches had developed and by day 7 already extended vacuolization was apparent. Progression of differentiation was much faster in DMU-treated cells. By day 3 thick myotubes had appeared that continued maturation until after the fifth day. Some myosac-like structures appeared as deterioration also started at day 7. The effects of DMUI were comparable to those of DMU.

Overall, differentiation in HS and HSI took 5-7 days and deterioration was observed soon thereafter (figure 2.7, left). The other three media, DMU, DMUI and DMI, strongly stimulated differentiation within 3 days with DMI resulting in thinner and less myotubes than the other two media.

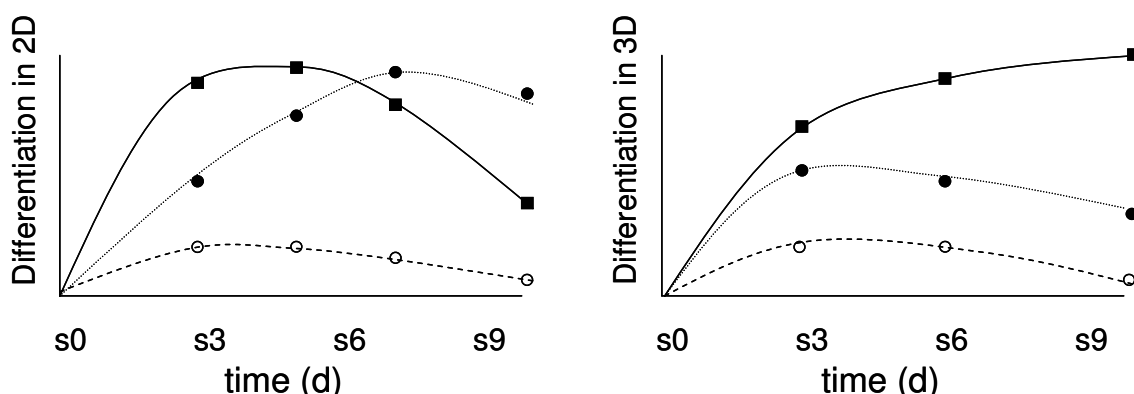


Figure 2.7: Graphical comparison of morphologically apparent myotube differentiation in monolayer (2D, left) and BAM (3D, right) cultures. In 2D (left) fast maturation is observed in DMU and DMUI (■), slower in HS and HSI (●) and only a little in DMI (○). In 3D (right) high comparable levels of maturation are achieved in DMU, DMUI, and HSI (■), less in HS (●), and again few in DMI (○).

## 2.4 Discussion

In the present study, an engineered skeletal muscle model containing C2C12 cells was applied to compare several serum-free differentiation media to the gold standard medium, containing 2% horse serum. Medium performance was assessed by several techniques varying from morphological examination, to protein expression, and metabolic activity.

Several studies have reported on the influence of differentiation media without serum on C2C12 monolayers, but to the authors' knowledge no report exists where the influence on three-dimensional C2C12 tissue cultures is investigated. The choice of serum-free differentiation media was based on most promising media reported in literature for two-dimensional culture. In addition to serum, all animal extracts applied in literature, such as chick embryo extract and rat brain extract, were omitted from the medium for their inconsistency of contents. Ultrosor G was chosen as a serum substitute for its content of a variety of substances that act pro-differentially in C2C12 (a.o. insulin, epidermal growth factor, fibroblast growth factor, transforming growth factor, insulin-like growth factor I, thyroxine, dexamethasone, and bovine serum albumin). Furthermore, insulin-like growth factors (IGFs) are more potent stimulators of myogenic differentiation than insulin (Florini et al., 1996) and were added for this



reason. All cell lines exhibit different sensitivity for IGF-I stimulation of differentiation due to their autocrine expression of the protein. Several concentrations of IGF-I imposed on C2C12 or other myoblasts have been reported in literature ranging from 200 ng/ml (26 nM, Takahashi et al., 2002), to 32 nM (Vandenburgh et al., 1991c), to 250 ng/ml (32.8 nM, Spangenburg et al., 2004; Semsarian et al., 1999). Therefore, the concentration of IGF-I that was applied in the present study was predetermined from monolayer cultures. Concentrations ranging from 32-100 ng/ml stimulated differentiation best.

Differentiation in 3D in the gold standard C2C12 differentiation medium containing 2% horse serum resulted in increased CK levels with time after medium shift. Maturation of the culture was further evidenced by elongated cell structures and some myosin and desmin expression. However, construct viability decreased as well as total protein contents, probably caused by cell death induced by starvation due to serum deprivation. Another explanation for the initially higher total protein content may be that some of the proteins from the bovine serum in the growth medium were not completely removed by the wash steps. However, it is not expected that this accounts for the complete declines from s0 to s3. Enrichment of the standard differentiation medium with IGF-I enhanced CK activity almost 4-fold by s10. The declined protein expression and loss of viability were comparable to those of constructs differentiated in HS. Nonetheless, addition of IGF-I on top of horse serum did positively affect the general cell morphology as less round cells were found and myosin was expressed in punctuate patterns, showing more advanced differentiation. Now, considering the serum-free media, the overall lowest level of differentiation was found if applying DMI. Not only no CK activity was present in those cells, protein contents also dramatically decreased, and cell viability had almost disappeared by s10. Desmin was not detected by s10. Immunostaining of those cultures showed only spherical cells instead of elongated fused cells, some of which contained myosin. In contrast, shifting to serum-free DMU or DMUI, both induced differentiation, as CK levels rose, and long myotubes appeared expressing punctuate myosin patterns. In addition, decrease in total protein levels were mild, as well as the decline in viability, suggesting a more protective role against starvation for DMU/DMUI than the other media.

These results suggest a role for IGF-I in differentiation that has to be supported by other pro-differential factors. Presence of just IGF-I (in DMI) stimulated increase in myosin but not desmin. When added to DMU, IGF-I did not increase differentiation, most probably due to its presence in Ultrosor G. It did stimulate differentiation in the presence of horse serum, which suggests that the amount present in the serum was not high enough to maximally stimulate differentiation of C2C12.

The overall effects of all media on 3D C2C12 differentiation are summarized in table 2.2. The serum-free alternatives DMU and DMUI did not only perform better than all other media that were tested but also even better than the gold standard differentiation medium with horse serum. Also, addition of both IGF-I and horse serum resulted in enhanced 3D differentiation as compared to just horse serum supplementation. When these findings are compared to differentiation in 2D some dissimilarities are striking (figure 2.7). Morphological appearance of myotubes created in 2D showed fast

maturation of cells in DMU, DMUI and DMI (within 3 days) while the other media stimulated more gradual differentiation (over 5 days). However, in 3D, maturation seemed to progress over a longer period of time. Interestingly, differentiation was not as greatly stimulated by HS in 3D as in 2D. In contrast in 2D, HSI induced differentiation comparable to that in DMU and DMUI. These inconsistencies between 2D and 3D for the media can be explained by several phenomena. First, a difference in cell densities may have had an effect on the cells. It is hard to compare monolayer confluence to 3D seeding density. The initial cell density was  $4.9 \times 10^6$  trypsinized cells per ml. Once the cells have attached to their 3D matrix they appear to be confluent, though it is hard to distinguish whether they are confluent in all three dimensions. Furthermore, the three-dimensional environment itself may affect cell behaviour, as cell-cell interactions, cell mechanics, and diffusion of nutrients and oxygen are influenced by 3D architecture. Obviously, the presence of the collagen/ Matrigel mixture in 3D will influence differentiation of the cells. After all, Matrigel contains several growth factors that enhance differentiation of the myoblasts. Finally, flexibility of the 3D gel may have influenced cell differentiation. During the remodelling phase of the cells after seeding in the gel, they gradually build up tension in the construct by compacting the matrix. This affects the stiffness of the tissue, which influences differentiation as shown by Engler et al. (2004). They have shown that myosin and actin striations emerge only on gels with stiffness typical of native muscle. For that reason, C2C12 hardly ever show cross-striations if cultured in a monolayer on rigid culture dish bottoms.

*Table 2.2: Summary of medium effects by assessment method and overall performance.*

	CK	Total protein	Histology	Metabolic activity
HS	+	+	-	-
HSI	++	+	+	-
DMI	-	-	-	-
DMU	+	++	+	+
DMUI	+	++	+	+

Recently, some studies reported the in-vitro engineering of vascularized muscle tissue (Levenberg et al., 2005; De Coppi et al., 2005). The lack of vasculature in engineered tissues restricts their size. Though the thickness of the BAMs cultured in the present study is limited, a non-viable core inside the tissue remained due to this restriction. However, this is not considered to intervene with optimization of differentiation medium in this model.

The developed model was not optimized for implantation or meat production (Benjaminson et al., 2002; Edelman et al., 2005), but intended for research purposes. The requirements for the muscle tissue cultures were high tissue viability, reproducibility, content of differentiated myotubes, ease of fabrication, and fast production in a tissue environment rather than a monolayer culture. The BAMs were

cultured to serve as model systems for studying the development of tissue damage after sustained mechanical loading; therefore contractility of the tissue is not essential. As we aim to real-time assess damage development by microscopic visualization, this is even an advantage.

## **2.5 Acknowledgments**

The authors are grateful to A. Oosterhof and Dr. T. van Kuppevelt (NCMLS, Radboud University Nijmegen, The Netherlands) for kindly sharing their experience with Ultroser G. Careful reading of the manuscript by Dr. R.P. Hesselink was greatly appreciated. The MF20 antibody was developed in Dr D.A. Fischman's lab and obtained from the Developmental Studies Hybridoma Bank developed under the auspices of the NICHD and maintained by the University of Iowa, Department of Biological Sciences, Iowa City, IA 52242. Financial support by The Dutch Technology Foundation (STW, grant EFB.6003) is gratefully acknowledged.

# Chapter 3

## Evaluation of a continuous quantification method of apoptosis and necrosis in tissue cultures

This chapter is based on: D. Gawlitta, C.W.J. Oomens, F.P.T. Baaijens, C.V.C. Bouten, *Evaluation of a continuous quantification method of apoptosis and necrosis in tissue cultures*, *Cytotechnology*, 46:139-150, (2004)

### 3.1 Introduction

Within the field of tissue engineering, monitoring viability or cell death during in-vitro culture is a valuable tool. Other research fields, such as developmental biology, cardiology and oncology, also benefit from such a method (Blankenberg et al., 2000). In those disciplines, such methods can give insight in processes of tissue damage and adaptation under in-vitro conditions (e.g. ischemia in heart explants, local (developmental) apoptosis in embryo culture). The ideal probe for evaluation of cell death in-vitro should give quantitative information on cell death in space and in time and should be non-destructive to the culture. The development of cell death should be assessable online for several days in the same ongoing culture. In addition, it should differentiate between apoptosis and necrosis to provide understanding of the pathways leading to cell death. Last, quantification should be easy and fast and applicable under in-vitro conditions in 2D and 3D cultures.

Several methods are available to assess cell death in engineered tissues and cell cultures but they are either destructive to the culture or unable to differentiate between apoptosis and necrosis in a spatio-temporal manner (see Park et al. (2000) for a review; Chung, 1983; Mosmann, 1983; Rieseberg et al., 2001; Stadelmann and Lassmann, 2000). Fluorescent cell staining, monitored by conventional fluorescence microscopy or by confocal microscopy, offers advantages over the aforementioned methods. Commercially available fluorescent probes (e.g. calcein / ethidium homodimer-1; Cell Tracker Green / propidium iodide) can be loaded to intact cell cultures and provide spatio-temporal information on cell death development without disrupting the culture (Wang et al., 2005; Breuls et al., 2003b). However, no differentiation between apoptosis and necrosis can be made. Another combination of fluorescent probes, fluorescently labeled annexin to indicate apoptosis and propidium iodide to label necrosis, is able to distinguish both types of cell death. A disadvantage of this method is that the apoptosis cannot easily be quantified, unless the culture is disrupted for flow cytometry.

Different cell death pathways can lead to necrosis and one of them is apoptosis, but necrosis can also occur 'spontaneously'. To be able to discriminate apoptosis and necrosis, an additional probe is required. If apoptosis can also be detected, it is possible to recognize adverse effects on cell viability earlier in the process and to determine if an apoptotic pathway preceded the onset of necrosis.

Until now, a combination of commercially available probes (Molecular Probes, V13243) has been applied to discriminate between both stages of cell death. This technique has been applied to fixated tissue sections (Suzuki et al., 1997), as microplate assay (Wronski et al., 2002), to flow cytometric measurements (Jerome et al., 2001; McGuire et al., 2001), and to 3D tissues (Boffa et al., 2005). One of the probes is a green fluorescent probe, YO-PRO-1 (YP), which can enter cells once their plasma membrane has reached a certain degree of permeability (Idziorek et al., 1995; Liu et al., 2004). The cell membrane becomes slightly permeable during apoptosis and YP can freely enter the cell and bind to its nucleic acids, which greatly enhances its fluorescence intensity. The other probe, propidium iodide (PI), is applied to stain for necrosis with its red fluorescence. This probe can only cross membranes of necrotic

cells and not those of apoptotic cells. PI fluorescence increases 20 to 30-fold once it binds to nucleic acids. The cell membrane of viable cells is impermeable to both YP and PI.

In the recent article by Boffa et al. (2005) the application of YP has been shown in 3D quantification of apoptosis at a certain point in time. The goal of the present study was to investigate the performance and effects of YO-PRO-1 and PI dual staining in continuous monitoring of development of apoptosis and necrosis in a tissue. As a model system C2C12 mouse myoblasts were used in the cultures. The agent, staurosporine, was applied in this cell line to induce apoptosis (McArdle et al., 1999). In this model system, more insight into the behavior of the dual staining method in ongoing cultures was obtained by monitoring the progression of apoptosis and necrosis after induction of cell death. The influence of time on probe intensity was evaluated, optimal probe concentrations were determined, and the influence of the probes on cell metabolism was quantified.

## **3.2 Materials and methods**

### **3.2.1 Cell and tissue culture**

C2C12 murine skeletal myoblasts (passages 10-15, ECACC, Salisbury, UK) were cultured in growth medium (GM) in an incubator at 37 °C and 5% CO<sub>2</sub>. Cells were differentiated from myoblasts into myotubes with differentiation medium (DM) at 80% confluency. GM consisted of 500 ml DMEM high glucose, with L-glutamine, 75 ml FBS, 10 ml HEPES, 5 ml non-essential amino acids, and 2.5 ml gentamicin; whereas DM contained 10 ml HS instead of 75 ml FBS.

C2C12 cells were seeded onto 12-well plates at a density of 20,000 cells/ml for the experiments involving monolayers. The monolayers were shifted from GM to DM as indicated in the respective experiments. For the 3D tissue culture, the cells were suspended in a rat-tail collagen I / matrigel mixture, as described previously by Breuls et al. (2003a) and Vandeburgh et al. (1996). In short,  $5 \cdot 10^6$  C2C12 myoblasts were suspended in 1 ml of gel mixture and molded between two anchoring points. Matrix remodeling during subsequent culturing resulted in a pre-stress that induced a unidirectional cell configuration between the anchoring points. After 1 day of culture, the cells were shifted to DM to induce the formation of myotubes (also described in chapter 2).

### **3.2.2 Progression of cell death in 2D and 3D cultures**

To evaluate the behavior of YP and PI as probes for monitoring apoptosis and necrosis in living cultures, positive control experiments, in which apoptosis was induced, were performed. Cell death in these experiments was quantified (by a MATLAB<sup>®</sup> computer program) and qualified (from nuclear morphology).

C2C12 myoblasts were differentiated with DM after 3 days of culture in GM in 12-well plates. At day 8 of culture 2 µl/ml staurosporine readymade (Sigma) was added to the cells to induce apoptosis (different concentrations were only applied, where

mentioned). This method was described by McArdle et al. (1999), who evaluated the effect of this agent on C2C12 cells by Annexin V staining and TUNEL labeling. They showed that apoptosis can be induced in C2C12 mouse myoblasts within 2 hours (phosphatidyl serine exposure) by addition of staurosporine (a protein kinase inhibitor). In the control group no staurosporine was added. In both groups, YP and PI were added to the cultures. The cells were placed in an incubator. After 0, 2, 3, 4, 5, 6, 7, 8, 9 and 10 hours they were transferred to a confocal laser scanning microscope for a short period of time, to monitor YP and PI fluorescence. Confocal images were taken at locations that were memorized by the microscope software. Scans were performed on 6 (first experiment) or 9 (second experiment) locations in 3 wells in each group. The above experiment was conducted twice to determine the reproducibility (reliability) of the procedure. During this experiment also higher magnification images were captured to check for changes in nuclear morphology (e.g. c-shape, nuclear fragmentation) that confirm development of apoptosis.

The above procedure was also carried out for evaluation of cell death progression in the 3D cultures. The 3D tissue was differentiated after 1 day of culture and the experiment was performed on day 4 of culture.

### 3.2.3 YP and PI dual staining

YP and PI were applied, respectively, for monitoring apoptosis and necrosis in the cell and tissue cultures. YO-PRO<sup>®</sup>-1 iodide (491/509 nm, Y3603, Molecular Probes) was dissolved in DMSO to a final concentration of 1mM. YP and PI (P3566, 1.0 mg/ml in water, Molecular Probes) were then diluted in DM. PI was diluted to a final concentration of 10 µg/ml, as described previously by Breuls et al. (2003b). The optimal concentration of YP was determined at 1 µM (see 'probe performance' sections).

### 3.2.4 Visualization

The progression of cell death was monitored every hour on a confocal laser scanning microscope (Axiovert 100M, Zeiss, Göttingen, Germany) with a 10x magnification objective. For the detection of YP fluorescence the probe was excited with a 25mW Argon laser at 488 nm. Emission was recorded above 510 nm. PI staining was measured by excitation with a 1 mW HeNe laser at 538 nm and emission was recorded above 570 nm. The microscope was equipped with a motorized stage. The LSM 510 (Zeiss) software enabled memorization of stage positions. In this way, cell death development could be monitored in time on fixed locations. For the 3D cultures, z-stacks were taken at each location in time (an example is shown in figure 3.2A). Before quantification, these were projected to render a 2D representation. In the 3D cultures applied here, the projection was allowed as nuclei hardly ever overlapped. The effects of photo bleaching on cell death appeared negligible as evidenced from regular comparison of cell death progression on locations that were not scanned before.

### 3.2.5 Probe performance

Probe performance was evaluated by determining the optimal concentration of YP that was intense enough for quantification and on the other hand as low as possible to avoid any interference with cell viability. The performance was further evaluated by determining the probe intensity over a three-day period. Finally, the probe should be non-toxic to the culture, so the influence of the probe presence in the culture medium was evaluated by an MTT assay.

*Optimal YP concentration and probe intensity in time* The optimal concentration of YP and the probe intensity were evaluated in one experiment. Several concentrations of YP in GM were added to wells after an attachment period of 24 hours: 0.01  $\mu\text{M}$ ; 0.1  $\mu\text{M}$ ; and 1.0  $\mu\text{M}$  together with 10  $\mu\text{M}$  PI. The performance of the probe could only be evaluated after induction of apoptosis. Therefore, staurosporine was added to the cells at 24, 48, and 72 hours (after adding the fluorescent probes). Cells were only taken out of the incubator for capturing confocal images. Probe intensity was measured at 6 randomly chosen locations for each concentration on the confocal laser scanning microscope, 7 hours after staurosporine addition, at 31, 55, and 79 hours. From the same experiment, the optimal YP concentration was determined.

*Cell metabolism* The effects of the dual staining on cell metabolism were studied by an MTT assay over a period of three days in GM. In short, four groups were formed ( $n=3$ ) in 12-well plates: control cells in GM, cells under 1  $\mu\text{M}$  YP in GM, cells in 10  $\mu\text{M}$  PI in GM, cells in both YP and PI in GM. After seeding, the cells were allowed to attach for 24 hours in GM. Thereafter, the respective groups were formed and metabolic activity was assessed after 24, 48, and 72 hours of exposure. The MTT assay involved a washing step in PBS before addition of 250  $\mu\text{l}$  GM and 20  $\mu\text{l}$  MTT (5 mg/ml in PBS) to each well. The cells were incubated in this MTT mixture for 30 minutes to allow crystal formation in metabolically active cells. Subsequently, the MTT mix was removed and replaced with isopropanol containing 10% Triton-X100 and HCl (Sigma, M-8910) to dissolve the purple crystals on a shaking table for 10-15 minutes (the blank reading was performed on the solubilization solution). After transfer into a 96-well plate, absorbance was measured at 570 nm.

### 3.2.6 Quantification of cell death in time

A custom-made program in Matlab was written for intensity threshold-based detection of pixels that either belonged to a green or red stained nucleus. First, background noise is removed by defining 95% of the first image of a series (time point 0) as noise. This noise can subsequently be removed from the successive images on the same location. Based on visually pre-determined threshold values, the program calculates the number of areas that have an intensity exceeding the threshold. The program can also separate overlapping nuclei. The program's results were verified by comparison with results from manual quantification. A small difference (maximum 5%) between results from both methods was found.



### 3.2.7 Statistical analysis

Differences in mean of the (raw) cell metabolism data were evaluated by one-way ANOVA. Post-hoc analysis was performed by applying Fisher's least significant difference (LSD) procedure. The numbers of apoptotic and necrotic nuclei, in the 2D and 3D cultures, were compared by their medians for each time point between the groups (with or without staurosporine). For this, Mann-Whitney (Wilcoxon) W tests were performed. All statistical calculations were carried out in STATGRAPHICS Plus 5.1.

### 3.3 Results

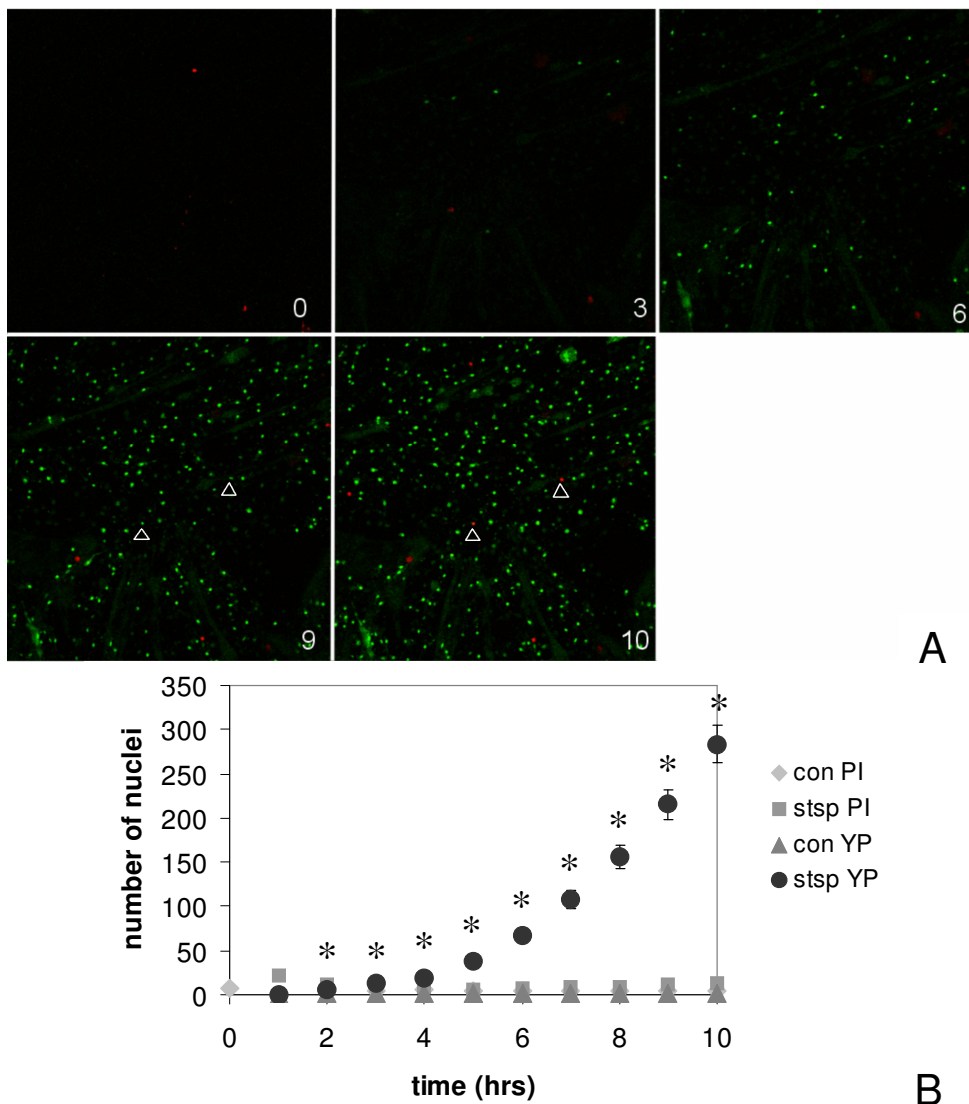
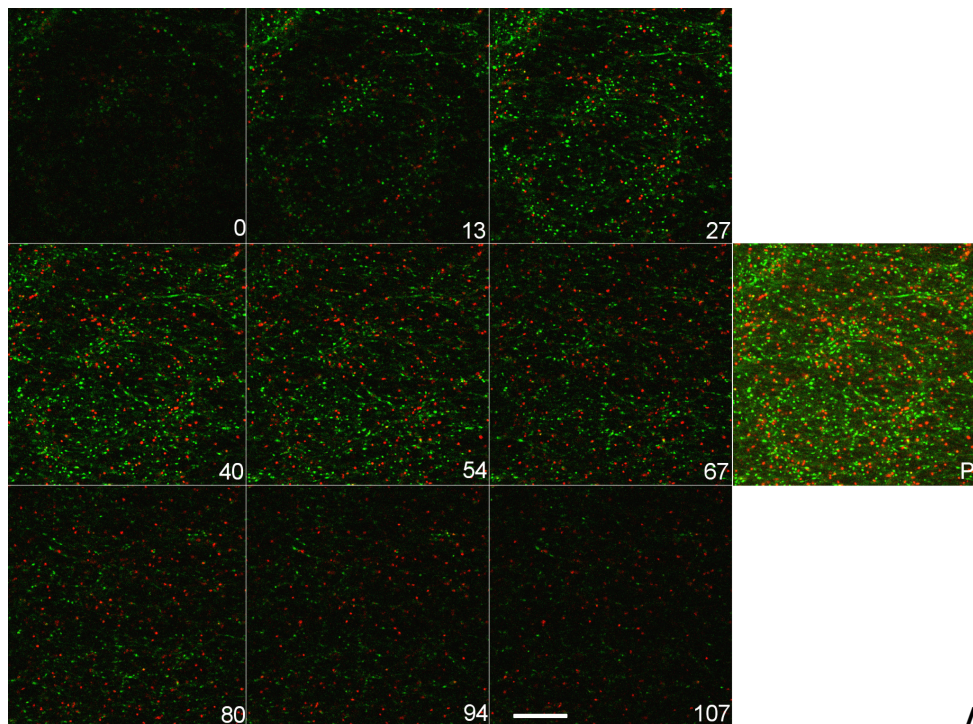


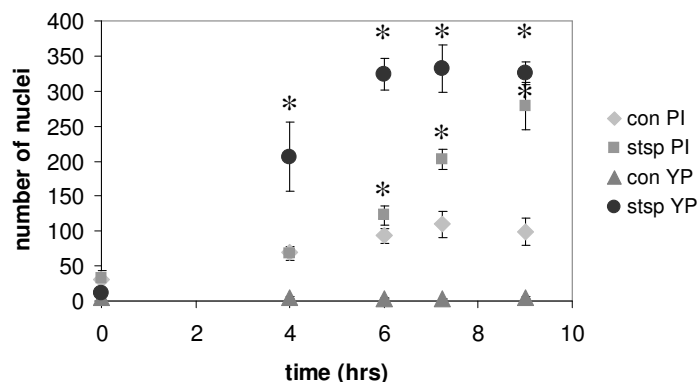
Figure 3.1: Development of apoptosis and necrosis after staurosporine addition to a C2C12 murine myoblast and myotube monolayer (differentiated for 5 days). (A) Time series showing apoptotic (green) and necrotic (red) nuclei in a monolayer culture at a fixed location in time, at 0, 3, 6, 9 and 10 hours after staurosporine addition to a C2C12 culture (100x magnification). Note the color shift of the nucleus at the arrowheads. (B) number of apoptotic (green, YP) and necrotic (red, PI) nuclei in time, for both control cells (con) and cells affected by staurosporine (stsp) (\*  $p < 0.05$ ).

### 3.3.1 Progression of cell death in 2D and 3D cultures

Images of the development of cell death in time as a result of staurosporine addition in a monolayer were recorded as presented in figure 3.1A. The amounts of YP-positive nuclei and PI-positive nuclei were quantified in time for both the control group (no staurosporine) and the experiment group (staurosporine added), as shown in figure 3.1B, by applying the Matlab program. The first signs of apoptosis as observed by YP staining of nuclei occurred between 2 and 3 hours after staurosporine addition. After eight hours, part of the nuclei that stained positive for apoptosis had become necrotic, as evidenced from a positive PI signal. A convenient property of the dual staining method was observed: the PI probe replaced the YP nuclear staining completely, once necrosis developed (figure 3.1A, arrowheads).



A



B

Figure 3.2: Projection of 3D data is demonstrated and results of the subsequent quantification. (A) A selection of slices through an engineered muscle construct is presented at 0, 13, 27, 40, 54, 67, 80, 94 and 107  $\mu\text{m}$  of height, respectively. On the right, P shows the projection of the complete dataset, which can be analyzed by a computer program. The bar denotes 200  $\mu\text{m}$ . (B) Progression of cell death in time in 3D muscle cultures after addition of staurosporine (stsp) or without staurosporine (con). PI nuclei represent the necrotic nuclei population, and YP shows numbers of apoptotic nuclei in time (\*  $p < 0.10$ ).

The reproducibility of the method was derived from the repeated experiments. In both experiments, elevated amounts of apoptotic nuclei (in the staurosporine treated cultures) were evident within 2-3 hours. The rates of increase in apoptotic nuclei and the maximum number after 10 hours were comparable as well.

In the 3D cultures, a comparable progression of cell death in time was observed (figure 3.2B). An increase in the number of apoptotic nuclei after 2-3 hours as observed in the 2D culture could not be confirmed (only after 4 hours), as no images were taken at these time points. After 6 hours, the number of apoptotic cells seemed to have reached a constant value. At this moment an increase in the number of necrotic cells commenced, as well as a slight increase in the number of necrotic cells in the control. The observed number of dead nuclei, up to 350, represented a considerable proportion of the total number of nuclei, approximately 900, present in a field of view.

### 3.3.2 Nuclear Morphology

Changes in nuclear morphology were monitored in time at fixed locations. Once cell permeability had increased by apoptosis, YP could enter the cell and stain the nucleus. In time, an increase in intensity of the green staining was observed. Upon completion of the apoptotic process, necrosis initiated and the green nuclear stain was

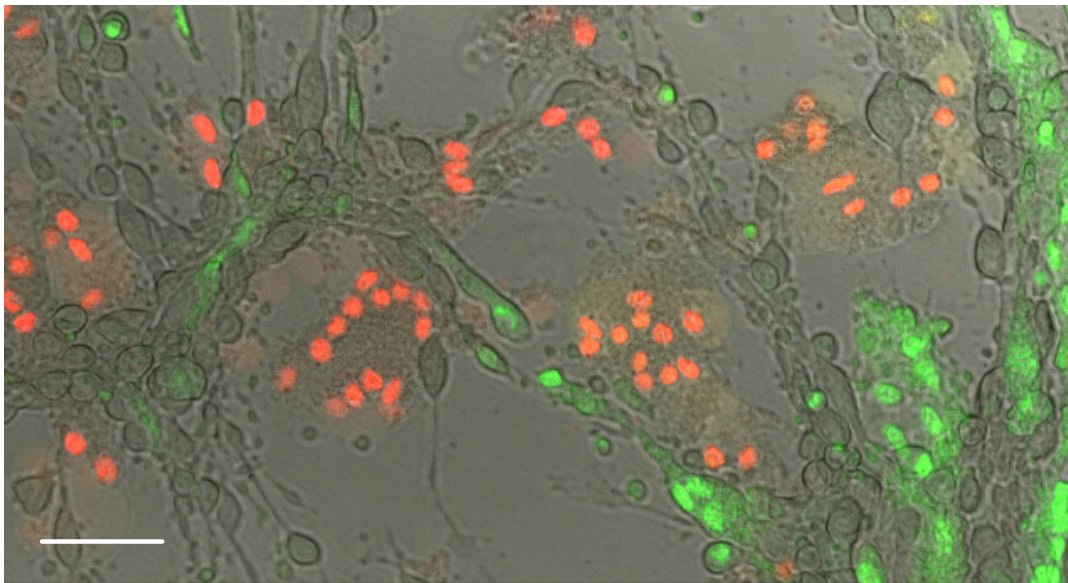


*Figure 3.3: This image shows the intact plasma membranes in viable and apoptotic cells (C2C12), whereas those of necrotic cells were hardly distinguishable. The image was captured 5 hours after induction of apoptosis (staurosporine 5  $\mu$ l/ml). Bar denotes 50  $\mu$ m.*

completely replaced by the red fluorescent PI, as mentioned before. The change from green fluorescent to red fluorescent labeling of the nuclei occurred within an hour. Therefore, the transitional period, the period in which the nucleus exhibited both green and red fluorescence, was rarely found in the images.

The increased cell membrane permeability was not only observed by influx of the fluorescent probes. Apoptotic cells had an intact cell membrane, whereas necrotic nuclei had no distinguishable membrane (figure 3.3). YP staining of the nuclei during



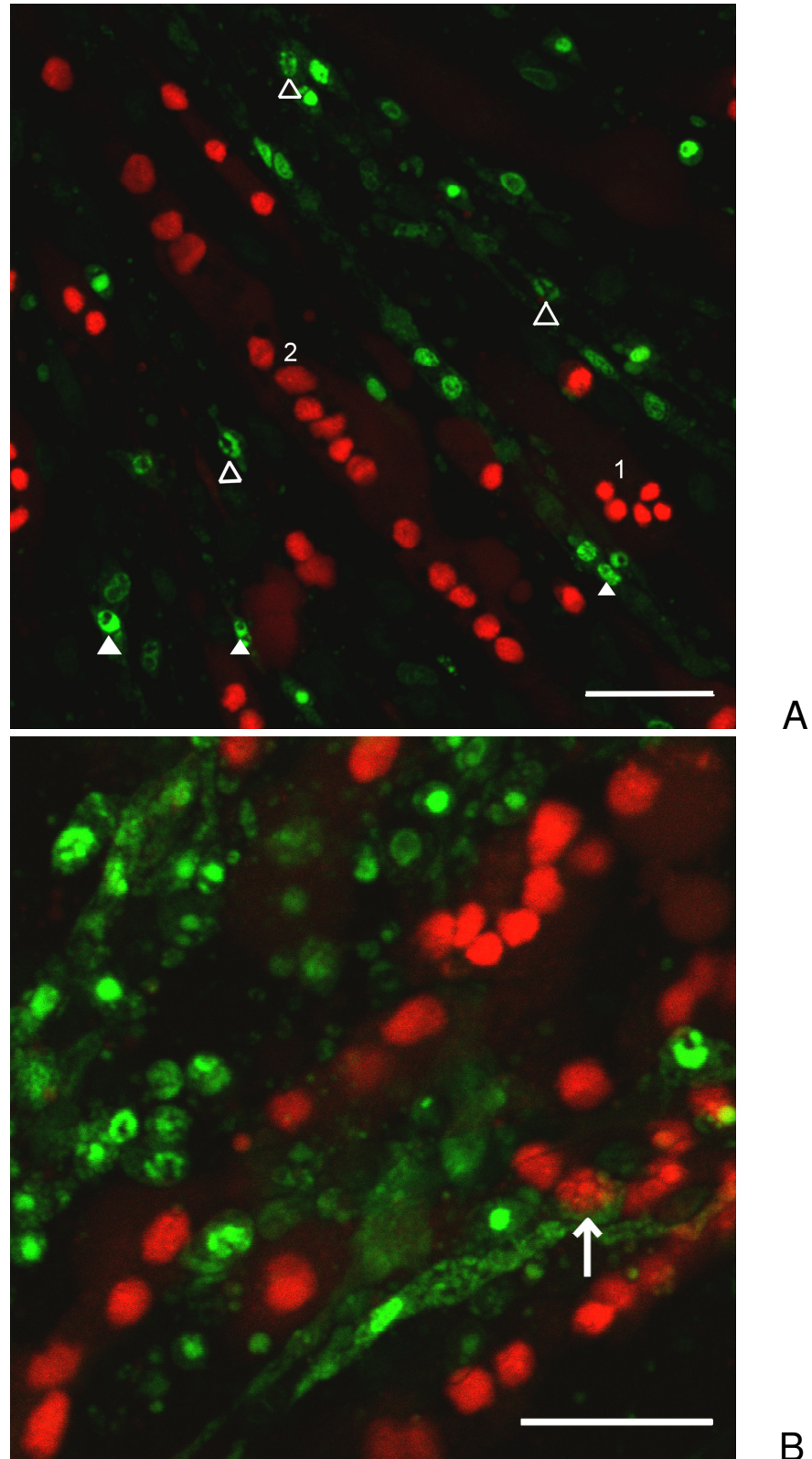


Figure 3.4: The effects on nuclear morphology of C2C12 cells after staurosporine addition, are shown. (A) Approximately 6.5 hours after addition of 2  $\mu\text{l/ml}$  staurosporine, nuclear fragmentation (open arrowheads) and crescent-shaped figures (closed arrowheads) were observed in C2C12 cells. Necrotic nuclei were marked by PI in red and showed no clear nuclear morphology in early (1) or late (2) necrosis. (B) The arrow shows a necrotic nucleus with apoptotic appearance. Bars denote 50  $\mu\text{m}$ .

development of apoptosis facilitated monitoring of nuclear morphology. Characteristics of apoptotic nuclei include chromatin condensation, fragmentation, and formation of c-shaped figures. In figure 3.4A, c-shaped figures and nuclear fragmentation are indicated by arrowheads. Early and late necrosis could be distinguished by an increasing size of the nucleus and decreasing intensity, caused by nuclear disintegration.

### 3.3.3 Probe performance

*Optimal YP concentration and probe intensity in time* The lowest concentration at which the probe still stained the nuclei of apoptotic cells was determined by incubation with staurosporine. Sufficient staining was seen at 1.0  $\mu\text{l/ml}$  and this concentration was applied in all other experiments. At this concentration, the probe was still capable of marking apoptotic cells after 3 days (79 hours). An increase in background signal was noticed with time. The difference in signal intensity between apoptotic nuclei and background staining was too low at 0.1  $\mu\text{l/ml}$  YP to distinguish them properly. At 0.01  $\mu\text{l/ml}$  of YP the probe concentration was found to be too low to distinguish apoptotic nuclei from the background even just after adding the probe to the cells (i.e. when the background staining is lowest).

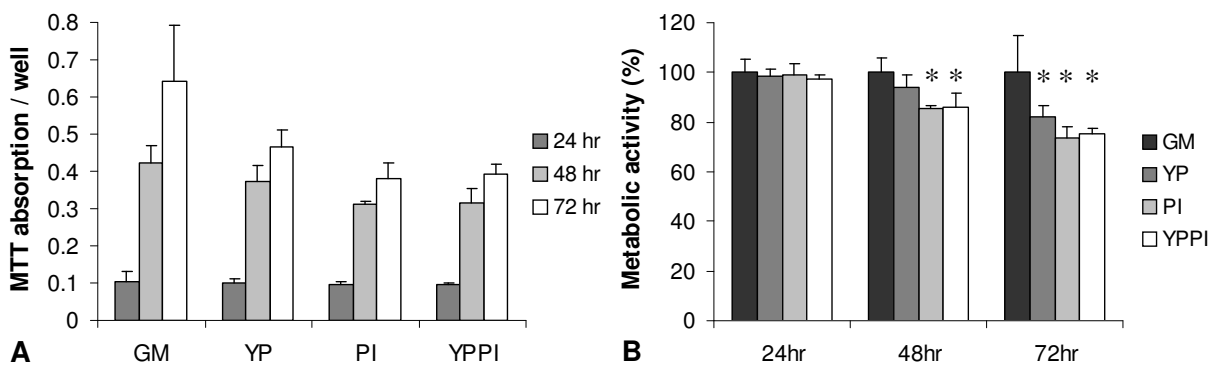


Figure 3.5: Absorption and metabolic activities of C2C12 cells for three days and three medium groups are shown. (A) Absorption values at 570 nm (corrected for blank value) are shown for the medium groups (GM, YP, PI, YP+PI) at 24, 48 and 72 hours. Within one medium group, all time groups are significantly different from both others. (B) Metabolic activity of all medium groups is shown, relative to the metabolic activity of the control group (GM) (\*  $p < 0.05$ ).

*Cell metabolism* The effects of YP, PI, and both YP and PI on cell metabolism are summarized in figure 3.5. The blank measurement was subtracted from the absorption values for the control group (GM) and the three experiment groups (figure 3.5A). In the control group a maximum increase in metabolic activity as a result of proliferation is observed. The experimental groups show a more moderate increase in metabolism. The absorption values were normalized to the control values from the cells in GM (figure 3.5B). Different effects were observed for the presence of YP and PI (or both) in the growth medium after 24, 48, or 72 hours of culture. Addition of YP to culture medium resulted in a significant decrease in activity after 3 days. Presence of PI in the medium resulted in declined metabolic activity of the cells after 48 hours. This

decrease was similar to the one observed for addition of both, YP and PI. So, the addition of both probes did not render a synergistic effect.

### **3.4 Discussion**

The present study shows the feasibility of YP /PI dual staining as a tool for spatial monitoring of apoptosis and necrosis in an ongoing culture. Apoptosis and necrosis can be quantified and distinguished in living cell cultures and engineered tissues in a non-destructive manner.

#### **3.4.1 Induction of apoptosis in 2D and 3D cultures**

From the results it can be concluded that C2C12 apoptosis, induced by staurosporine, can be monitored by YP staining, at least 5-6 hours before definite cell death (defined from PI labeling) commences. Thus, by applying the dual staining method presented in this study, it was possible to differentiate between two consecutive stages of cell death in both 2D and 3D cultures.

Previously, McArdle et al. (1999) induced apoptosis in C2C12 cultures by addition of 2  $\mu$ M staurosporine. They observed phosphatidyl exposure through annexin V binding from 2 hours after addition until 4 hours. From this, it can be assumed that YP stains apoptotic nuclei just after and concomitantly with early detectable events in apoptosis after staurosporine treatment. Also, labeling persisted during later apoptotic phenomena, such as cell shrinkage, nuclear condensation, and procaspase activation, and positive TUNEL labeling, as reported by McArdle's group as well. Twelve hours after induction, they found DNA laddering before cell detachment was completed (18 hours). After 24 hours the plasma membrane and nuclear membranes were fragmented, and the mitochondria were swollen and disrupted.

The development of apoptosis in the monolayer experiments started in both experiments 2-3 hours after addition of staurosporine. Thereafter, the number of nuclei undergoing apoptosis increased with time in a comparable, almost linear fashion. Also, the time point, at which the rise in the amount of necrotic nuclei occurs, is similar. The performance of the dual staining method was found to be reproducible.

The markedly different course of cell death development in the 3D culture could be explained by a different passage number of the cells and the extended culture time. Another factor influencing the culture's behavior was the 3D environment. Due to the collagen gel mixture, dead cells were trapped and shown on the initial cell death measurements as an increased number of necrotic cells. In monolayers, these dead cells normally detach from a culture substrate and float in the medium (out of the field of view) until washed away during medium replacement. Detached cells floated in the medium, above the focal plane of the confocal microscope and thus stayed 'undetected'.

#### **3.4.2 Nuclear Morphology**

YP-staining marked the presence of nuclear shapes characteristic of apoptosis. The shapes confirmed the execution of apoptosis in the cells exhibiting YP staining. Crescent c-shaped figures and condensed fragmented nuclei were observed. The study

by McArdle et al. (1999) confirmed the execution of apoptosis after addition of staurosporine to C2C12 cell culture. Compared to the annexin V staining applied in their work, YP staining exhibited a prolonged period of apoptotic cell identification. At the final stages of apoptosis, upon the influx of PI, the binding of YP to the nucleic acids was challenged, as the PI replaced the YP staining of the nucleus completely within a short time span. The nuclear morphology, characteristic of apoptosis, was no longer seen in this stage of cell death. Besides a distinction based on nuclear labels (green vs. red), the nuclear morphology can be applied to distinguish the type of cell death as well. Confusion may arise because the transition from apoptosis to necrosis may occur at any time point during the development of apoptosis. This is dependent on the energy level of the cell. In case of ATP (the cell's energy source) depletion, the process of apoptosis cannot be completed and necrosis will commence. This may result in nuclear morphology, typical for apoptosis with a necrotic (PI) staining (figure 3.4b).

### 3.4.3 Probe performance

Probe performance was evaluated by determining the optimal probe concentration, intensity of the probe in time, and probe toxicity.

*Optimal YP concentration and probe intensity in time* Since the best results were obtained with the maximum amount of YP in GM that was tested, one might expect that adding larger concentrations of the probe will further increase the distinguishing capability of the probe. However, in this study the minimally required amount of the probe for sufficiently marking apoptotic cells was determined. The intensity of the probe was sufficient up to 3 days after probe addition. In experiments exceeding this period, one might consider to reload YP/PI into the medium. However, the effects on cell metabolism need to be considered.

After 3-4 hours of incubating the cells with YP, an increased background staining of the cells was detected. This can be attributed to the presence of RNA in the cytoplasm of the cells (Suzuki et al., 1997). In online monitoring of cell viability it is not desirable to apply RNase for removal of this background staining. The background signal intensity of the RNA-bound YP was lower than that of DNA-bound YP. This might be caused by the more condensed structure of the DNA in the nucleus as compared to the more diffuse appearance of the RNA and DNA in the cytoplasm. In the presently used two-laser scanning system with YP and PI, in which no additional channel is available for e.g. cell monitoring, the RNA staining can be applied to track the cells in the culture by increasing the gain of the emission signal. In this way, no extra channel is required for detection of the cells. However, the use of YP for cell tracker purposes exclusively is not recommendable.

*Cell metabolism* The cell metabolism was clearly affected by addition of either YP or PI to the medium, or both. After 24 hours, the maximal decrease in metabolism was approximately 10%. However, this decrease was not found to be statistically significant. One might consider this as a tolerable influence on the culture. After 48 hours, the negative effect was significant as compared to the control group for addition of either PI alone, or YP and PI. Addition of YP still did not significantly influence the cell metabolism. Extension of the experiment duration rendered a maximal decrease in

metabolic activity of 40% after 72 hours. So, in experiments of periods exceeding 24 hours, involving both of the probes, these effects should be taken into account. The decrease in metabolism can be explained as decreased metabolic activity of the cells or a (partial) impairment of cell proliferation and therefore decreased total metabolic activity. Also, metabolic decrease can be caused by cell death. So, if an experiment exceeding 24 hours is performed, one might consider to more deeply study the effects on the cell culture to be able to differentiate the effects of the staining method or the experimental conditions on cell viability.

Despite the effects of YP and PI on cell metabolism during extended periods of time (> 1 day), the dual staining method is a convenient, non-destructive method for real-time quantification of apoptosis and necrosis on a local level in 2D and 3D cultures. The ability to distinguish, quantify and localize both kinds of cell death can contribute in elucidating cell death pathways in all research focusing on cell death development in monolayer cultures or (engineered) tissues. And finally, the dual staining facilitates online assessment of ultrastructural changes in the appearance of dying nuclei.

In future, the dual staining method will be applied in our lab to quantify the development of cell death in engineered muscle tissue. Cell death will be induced by tissue compression and ischemia to study the pathway of cell death development in (deep) pressure ulcers.

### **3.5 Acknowledgments**

Financial support by The Dutch Technology Foundation (STW, grant EFB.6003) is gratefully acknowledged.





# Chapter 4

## The relative contributions of compression and hypoxia to development of muscle tissue damage: *an in vitro study*

This chapter was based on: D. Gawlitta, W. Li, C.W.J. Oomens, F.P.T. Baaijens, D.L. Bader, C.V.C. Bouten, *The relative contributions of compression and hypoxia to development of muscle tissue damage: an in vitro study*, *Annals of Biomedical Engineering*, in press, (2006)

## 4.1 Introduction

Pressure ulcers develop under sustained mechanical loading. They can be conveniently categorized as superficial or deep pressure ulcers. Superficial ulceration is confined to skin tissues, whereas deep ulcers originate in the soft tissues adjacent to a bony prominence and may subsequently proceed towards the skin surface (Bliss, 1998; Bouten et al., 2003a). Indeed, skeletal muscle tissue has been shown to be particularly sensitive to prolonged compression (Nola and Vistnes, 1980; Daniel et al., 1981). Pressure ulcers involving muscle damage, denoted as grade III and IV ulcers, are typically observed in insensate patients with spinal cord injury (Byrne and Salzberg, 1996; Garber and Rintala, 2003). In addition, fiber morphology, contractile ability, and capillaries associated with muscle tissues are affected in this group of patients, which lead to an increased risk of deep ulcer development (Scelsi, 2001).

The deformation experienced by the tissue can result in cellular breakdown leading to tissue damage. Many studies have tried to explain the etiological pathways involved in this development of tissue damage, although precise understanding remains unclear. Most hypotheses are based on the impairment of molecular transport in the tissue, leading to a decreased or diminished flow in blood vessels or in the interstitium and lymph vessels (Kosiak, 1959; Dinsdale, 1974; Daniel et al., 1981; Miller and Seale, 1981; Reddy and Cochran, 1981; Barbenel, 1991). The impaired transport leads to ischemia, with associated oxygen deprivation, acidification and metabolite accumulation.

Recent studies have focused on the deformation of cells within tissues as an important inducer of cell damage following sustained compression (Bouten et al., 2003b; Breuls et al., 2003a). Nonetheless, the development of deep pressure ulcers (e.g. in the muscle tissue) is generally considered to be multifactorial in nature. To investigate the separate and combined effects of cellular deformation and oxygen deprivation, a tissue-engineered skeletal muscle model was selected. Such a tissue model offers great experimental control and ease of manipulation. In related studies by the authors, muscle cells were suspended in a gel matrix and compressed while development of cell necrosis and apoptosis was monitored with time (Bouten et al., 2001; Breuls et al., 2003a; Wang et al., 2005). However, none of these studies incorporate the effect of oxygen deprivation.

The present study tests the hypotheses that deformation and hypoxia influence cell viability on a different time scale and that the latter can aggravate the effect of deformation. In addition, it proposes that both factors will induce apoptosis in the tissue to various degrees. To achieve these aims, tissue-engineered muscle was exposed to different levels of compression (0%, 20%, and 40%) under normal tissue culture oxygen tension (20% oxygen) or hypoxic conditions (< 6%; Jiang et al., 1996). In this design, both the individual and combined effects of compression and hypoxia were investigated. During these insults, the development of cell death was monitored real-time in a specially designed experimental system. Viable fluorescent probes, YO-PRO-1 and propidium iodide, each based on increased membrane permeability, were used to distinguish apoptotic and necrotic cell death, respectively.

## **4.2 Materials and methods**

### **4.2.1 Cell and tissue culture**

C2C12 murine skeletal myoblasts (passages 10-15, ECACC, Salisbury, UK) were cultured in growth medium (GM) in an incubator at 37 °C and 5% CO<sub>2</sub>. GM consisted of 500 ml DMEM high glucose, with L-glutamine, 75 ml FBS, 10 ml HEPES, 5 ml non-essential amino acids, and 2.5 ml gentamicin. Cells were passaged every 2-3 days at 75% confluency.

Tissue engineered muscle was created by suspension of C2C12 cells in a rat-tail collagen I / matrigel mixture, as described previously in chapter 3 (Vandenburgh et al., 1996; Breuls et al., 2003a). To review briefly,  $5 \cdot 10^6$  C2C12 myoblasts were suspended in 1 ml of gel mixture and molded between two Velcro anchoring points. Matrix remodeling during subsequent culturing resulted in a pre-stress that induced a unidirectional cell configuration between the anchoring points within one day of culture. After this time, the cells were transferred to differentiation medium (DM) to induce the formation of multinucleated myotubes. DM contained 2 ml Ultrosor G (15950-017, Pall BioSepra S.A., France) as described previously (Portier et al., 1999). The first day of transfer to DM will be subsequently referred to as 's0' (shift day 0) and following days will be numbered in sequence. Experiments were performed on days s6 and s7.

The dimensions of the bio-artificial muscles (BAMs) were approximately 12 mm in length, 600 µm in height, and 2-3 mm in width. These dimensions exceeded the diffusion limit of between 100 and 200 µm inherent to dense engineered tissues (Brunelle and Chandel, 2002). Tissue formation commenced homogeneously throughout the gel, which allows for higher diffusion than actual tissue. However, with time cells at the outside started to form a dense layer with an associated increased hindrance to diffusion. As a consequence, insufficient oxygen and nutrients were supplied to the center of the construct, resulting in a shell of viable and differentiated cells, of approximately 200 µm thickness, over the complete length of the construct.

### **4.2.2 Ischemia**

A device (figure 4.1) was developed to impose ischemia and compression on the engineered tissue. The device consisted of an incubation chamber on a metal plate that was located on the stage of a confocal microscope. In the metal plate a window of 25 mm diameter was sealed by a 34 mm, round cover glass on a gasket (to facilitate monitoring of the cells). On top of the glass a further gasket was placed underneath a polycarbonate cylinder creating a culture bath. The tissue was maintained in the bath in DM at 37°C. The temperature was controlled by a thermocouple connected to a feedback system (West 6100+, TMC Instruments, Zeist, The Netherlands), which regulated heating by 6 small elements (24V, 1.3W) located in the cylinder wall. The complete chamber was continuously flushed, at a rate of approximately 5 ml/min, with a gas mixture containing 5% CO<sub>2</sub> to control the pH.

For normoxic experiments a 95% air and 5% CO<sub>2</sub> mixture was used, whereas hypoxic conditions were simulated by flushing the chamber with a 95% N<sub>2</sub> and 5% CO<sub>2</sub>

mixture. Evaporation of the medium was prevented by covering it with an approximate 2 mm layer of mineral oil (Sigma).

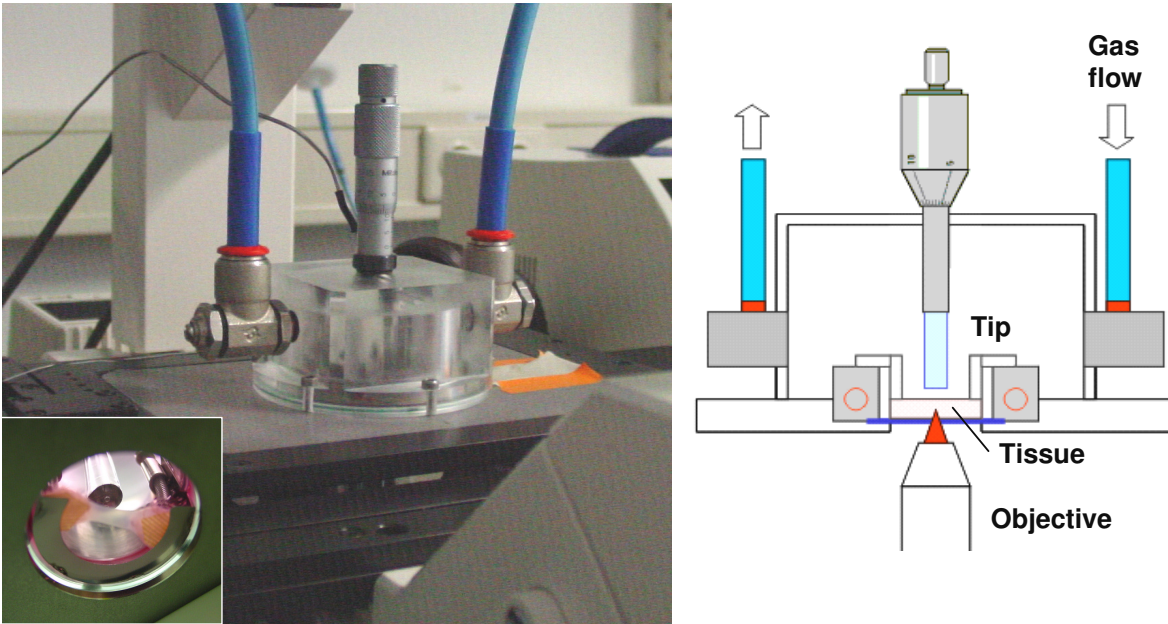


*Figure 4.1: A photographic (left) and a schematic (right) representation of the compression device. The micromanipulator connected to the glass tip is located above the tissue. The incubation chamber has controlled gas flow (containing 5% CO<sub>2</sub>) and the tissue is heated by elements (shown as red rings) in the cylinder surrounding the culture medium. The inset on the left shows the view of the set-up as seen from below with the indenter above the tissue.*

### Oxygen diffusion through oil layer

A separate experiment was performed to examine the ability of oxygen to diffuse through the oil layer as this has been previously questioned (Meldrum et al., 2001; Covington et al., 2005). Of special interest was the estimation of the time required for the oxygen concentration in the medium (below the oil layer) to attain hypoxic values. A custom-made combined electrode system containing a platinum working electrode inside a stainless steel reference electrode (separated by resin) was applied (unpublished data). The electrode was coated three times with Nafion (Sigma) to form a sealing membrane. Calibration of the electrode in culture medium was performed at 100% nitrogen and atmospheric oxygen tension after equilibration of medium with the gas. Linearity of electrode performance was assessed elsewhere (unpublished data). After equilibration of medium in open air, the medium was covered with mineral oil. Subsequently, the measurement of oxygen tension in the incubation chamber at 37°C was started simultaneously with the gas flow of the N<sub>2</sub>/CO<sub>2</sub> gas mixture. The data were corrected for temporal drift of the electrode that was measured in a separate experiment, where oxygen tension was monitored in medium that was in equilibrium with atmospheric oxygen tension.

### 4.2.3 Compression

A glass tip (5 mm diameter) for tissue compression was connected to a spindle-free micromanipulator (Mitutoyo, Veenendaal, The Netherlands) in the top of the chamber (figure 4.1). Tissue thickness (in z-direction) was determined by lowering the tip of the micromanipulator until it just made contact with the construct. At this point, the distance between the tip and the cover glass was assumed to be equal to the sample height. The distance was measured by confocal line stacks in reflection mode of the microscope (figure 4.2). From this uncompressed thickness, the displacement of the tip was calculated to render either 20 or 40% of global tissue compression.

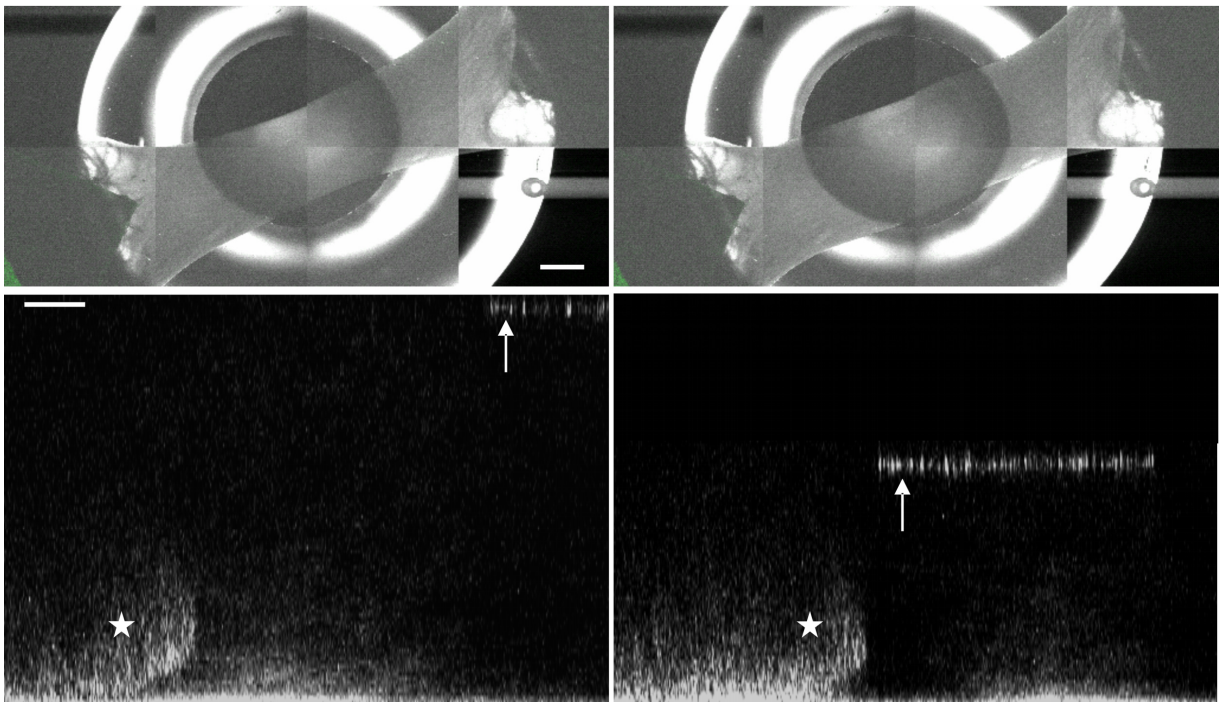


Figure 4.2: Top: An increase in sample thickness from before (left) to during (right) 40% compression (tile scan, bar denotes 1 mm). Bottom: Measurement of tissue thickness between the glass bottom and the glass tip (arrows) at the moment that the tip touches the sample (left) and after imposing 40% compression (right) (linestack, bar denotes 100  $\mu\text{m}$ ). Notice that only reflection from the bottom of the tissue (stars) can be seen.

In a series of experiments, the influence of compression on the total number of nuclei in a 3D field of view was evaluated applying a viable nuclear stain, SYTO-13 (Invitrogen, Breda, The Netherlands). The viable stain was restricted to these pilot experiments and was not applied in the experiments performed to measure viability in combination with YO-PRO-1 and propidium iodide. As a result of the unconfined compression in the z-direction, the BAMs were stretched in the xy-plane, causing a decreased number of nuclei in the field of view. Analysis of the resulting images indicated a linear relationship ( $r^2 = 0.9967$ ) between compression and disappearance of nuclei from the monitored volume, as indicated in figure 4.3. In addition, the images confirmed that no new nuclei appeared in the three-dimensional volume during the experiments. This finding may be due, in part, to the limited penetration depth in the z-direction of the confocal microscope into the tissue (150-200  $\mu\text{m}$ , depending on tissue

properties), which may further decrease during tissue compression. Alternatively, it may be due to the three-dimensional architecture of the tissue construct, involving cells located in a shell of approximately 150-200  $\mu\text{m}$  thickness of its complete length. Nonetheless this allows for a direct comparison of the number of nuclei in both control and compression experiments. Therefore, a correction was made for the number of nuclei in BAMs subjected to 20 or 40% global compression based on figure 4.3.

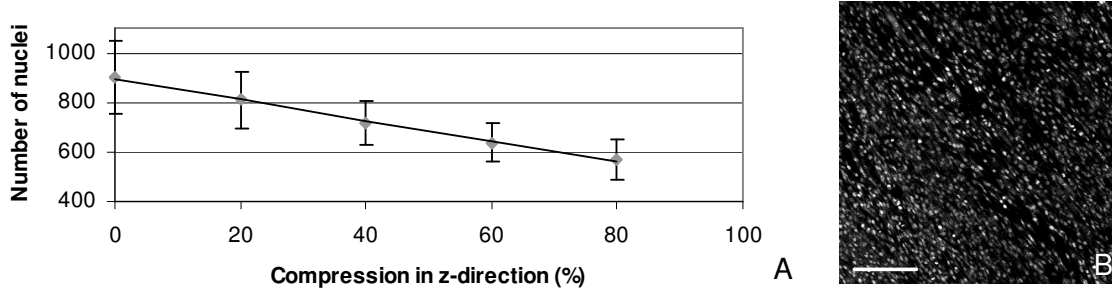


Figure 4.3: (A) Quantification of the number of nuclei in a field of view as a function of the amount of BAM compression ( $n=4$ ). A linear relationship was observed ( $R^2=0.9967$ ). This relationship was applied to correct for differing numbers of total nuclei in the experiment conditions. (B) The projected uncompressed field of view is shown with nuclei labeled by the viable stain SYTO-13 (bar denotes 200  $\mu\text{m}$ ).

#### 4.2.4 Analysis of cell death

A YO-PRO-1/ propidium iodide real time dual-staining method was applied to indicate apoptotic and necrotic nuclei of cells, respectively (Gawlitta et al., 2004). These probes can enter cells once their membrane is damaged. Their fluorescence is enhanced upon association with DNA or RNA, resulting in bright staining of the nuclei. During apoptosis YO-PRO-1 (YP) uptake is possible due to increased membrane permeability but propidium iodide (PI) is still excluded from the cell cytoplasm. Upon necrotic cell death, membrane permeability is increased further to permit PI diffusion into the cell. If a cell makes the transition from apoptosis to necrosis, the staining changes accordingly within an hour, resulting in a change from a green stain to a red fluorescence.

In all test conditions, YO-PRO<sup>®</sup>-1 iodide (Y3603, Invitrogen BV) and propidium iodide (P3566, Invitrogen BV) were diluted in DM to final concentrations of 1  $\mu\text{M}$  and 10  $\mu\text{M}$ , respectively. The progression of cell death was monitored every hour on a confocal laser-scanning microscope (Axiovert 100M, Zeiss, Göttingen, Germany) with a 10x magnification objective. The monitored locations were chosen below the indenter during experiments involving tissue compression. YO-PRO-1 was excited at 488 nm and its emission was recorded between 505 and 530 nm. Propidium iodide was detected by excitation at 543 nm and the emitted signal was read above 570 nm. A motorized stage and the LSM 510 (Zeiss) software enabled the temporal monitoring of death of individual cells. At each location stacks (<2 minutes) were created to measure cell death in 3D.

Propidium iodide-positive nuclei and YO-PRO-1 marked nuclei were counted by a custom-made program in MATLAB<sup>®</sup>. A threshold level of 0.2 was set to convert the original into black-and-white images for the PI signal. By contrast, a threshold for the

apoptotic signal was manually determined for each experiment because this value was influenced by slightly different intensity offsets dependent on the age of the probe. Nonetheless, the chosen thresholds were kept constant during the whole experiment. Unconnected pixels were bridged and holes were subsequently filled. Finally, single pixels (1.8 x 1.8  $\mu\text{m}$ ) were removed from the image. All positively detected pixel areas were labeled and their sizes were recorded in a histogram. Areas smaller than 3 pixels were assumed not to represent a nucleus and excluded from quantification of the total number of nuclei. The computed data were compared to manual estimations and a maximum random difference of 10% was observed between the results.

Cell death is converted into percentage cell viability (V), by using the following equation (1):

$$V = \frac{N - c(x - x_0)}{N} * 100\% \quad (1)$$

where N represents the total number of nuclei present in a field of view, as determined with the viable stain SYTO-13 in a separate experiment. The number of dead nuclei (x) was corrected for the initial amount of dead nuclei ( $x_0$ ); and c represents the factor correcting for disappearance of nuclei from the monitored volume.

#### 4.2.5 Experimental design

To distinguish the effects of compression and ischemia on cell death, the progression of 6 different experimental conditions (each with  $n=3$ ) were selected, as summarized in table 4.1. Two oxygen levels were chosen: <6% to simulate hypoxia and 20% to represent a normal oxygen tension. At both oxygen levels, the tissue was subjected to three levels of tissue compression, namely 0, 20, and 40%. BAMs at normoxia and 0% compression represented control tissue. Control samples were not in contact with the tip as previous research in the host laboratory (Breuls et al., 2003a; Bronneberg et al., 2006) has shown that the effect of the tip on the top surface of the construct, without compression, is negligible with respect to cell death development resulting from diffusional transport.

Table 4.1: Overview of the experimental conditions ( $n=3$  for each condition).

Compression level \ pO <sub>2</sub>	0%	20%	40%
20%	Normoxia *	Deformation	Deformation
<6%	Hypoxia	Hypoxia + deformation	Hypoxia + deformation

\* Controls are represented by the normoxic group.



### 4.2.6 Statistical analysis

Differences in viability of the BAMs between each of the experimental conditions were examined by a repeated measures test. They are depicted as mean  $\pm$  standard error of the mean (SEM). Post hoc determination of statistical significance was performed by multiple comparisons according to Tamhane accounting for unequal variances. All analyses were performed in SPSS 12.0.1, with  $p < 0.05$ .

## 4.3 Results

### 4.3.1 Normoxia and compression

The projections of the 3D scanned volumes with apoptotic (green) and necrotic (red) nuclei after 22 hours in the respective experiment conditions are shown in figure 4.4. In the control experiments (i.e. normoxia and no compression) the number of necrotic nuclei increased gradually with time. Initially, most of the dying nuclei appeared apoptotic (green) and changed within 2-4 hours into necrotic (red) nuclei. After 10 hours the cytoplasm of the cells started to exhibit green staining, although at a lighter shade of green than apoptotic nuclei, as indicated by the ellipses in figures 4.5A and B. The cytoplasmic staining by YP also rendered information on cellular shapes. Finally, after 22 hours some necrosis and apoptosis was present in the control BAMs (fig. 4.4A).

In the BAMs subjected to 20% compression under normoxia, again the gradual increase of green cytoplasmic fluorescence was observed, especially in the larger myotubes. Indeed the nuclei that became necrotic during tissue compression tended to be larger (over 2-fold increase) than nuclei that were necrotic at the beginning of the experiment. Also, their fluorescence was less intense. The transition time from apoptotic to necrotic nuclei was between 2-4 hours, a similar time period as for the control experiments. At 22 hours more necrotic cell death was evident after 20% compression (fig. 4.4B) when compared to control experiments.

In experiments with 40% of BAM compression large necrotic nuclei with low intensity staining were distinguished similar to those subjected to 20% compression. In the compression experiments more transitions from green to red nuclei were observed than in the controls. Another feature was that the entire cytoplasm of myotubes appeared to start emitting green fluorescence simultaneously. The majority of cells that had a green cytoplasm at first, contained apoptotic nuclei shortly thereafter, which eventually became necrotic. In general, all nuclei in a myotube appeared to stain for apoptosis or necrosis at the same time. It is interesting to note that, one of the locations monitored in all 40% normoxic experiments exhibited a wave of 'freshly' necrotic nuclei progressing inward in the field of view towards the end of the experiment (fig. 4.5C). All other locations resulted in necrotic nuclei as shown in figure 4.4C.

### 4.3.2 Hypoxia and compression

In the hypoxic state with no compression of BAMs an increase in the number of necrotic nuclei comparable to that in control experiments was found, as illustrated in fig. 4.4D. With the combined hypoxic and control experiments, modest cellular

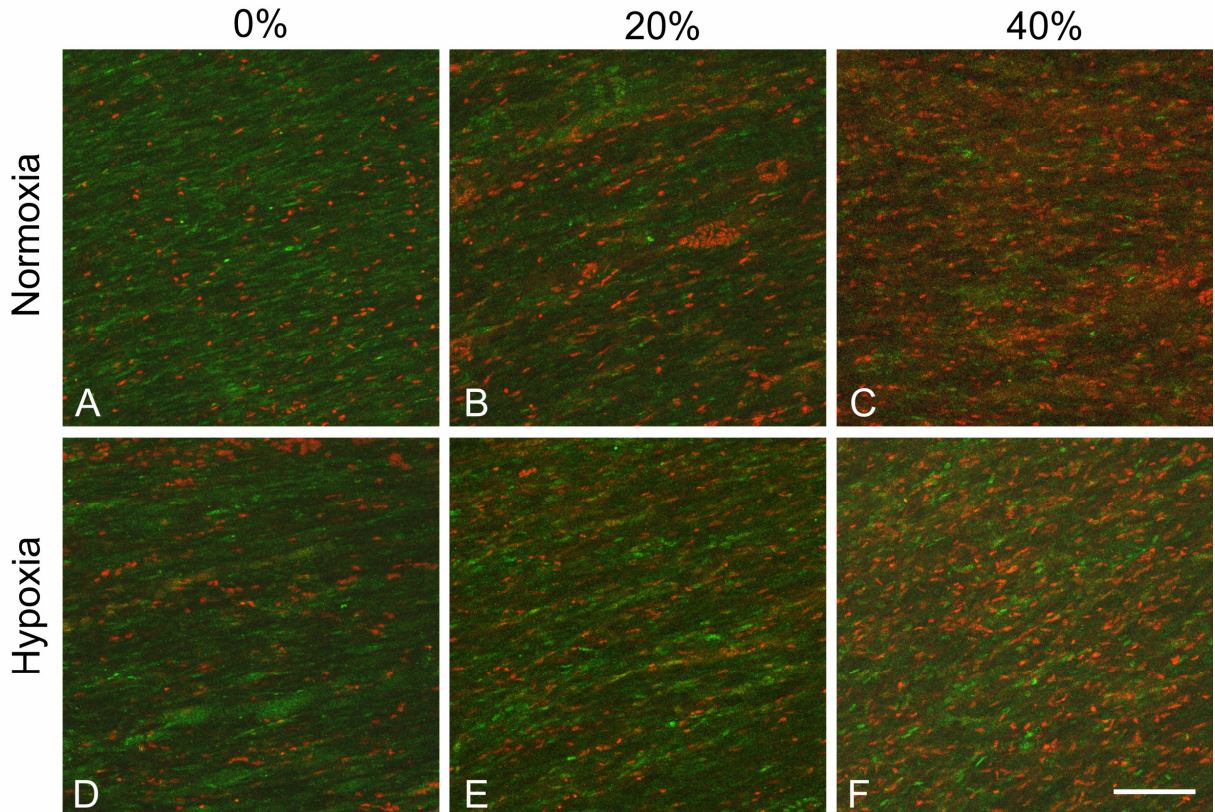


Figure 4.4: Z-projections of confocal stacks made after 22 hours from the BAMs of all six groups: at normoxia, with 0% (A), 20% (B) and 40% (C) compression; and at hypoxia, under 0% (D), 20% (E), and 40% (F) compression. Necrotic nuclei are shown in red and apoptotic nuclei in green. Note that the green probe illustrates not just nuclei but also the cytoplasm. The bar denotes 200  $\mu\text{m}$ .

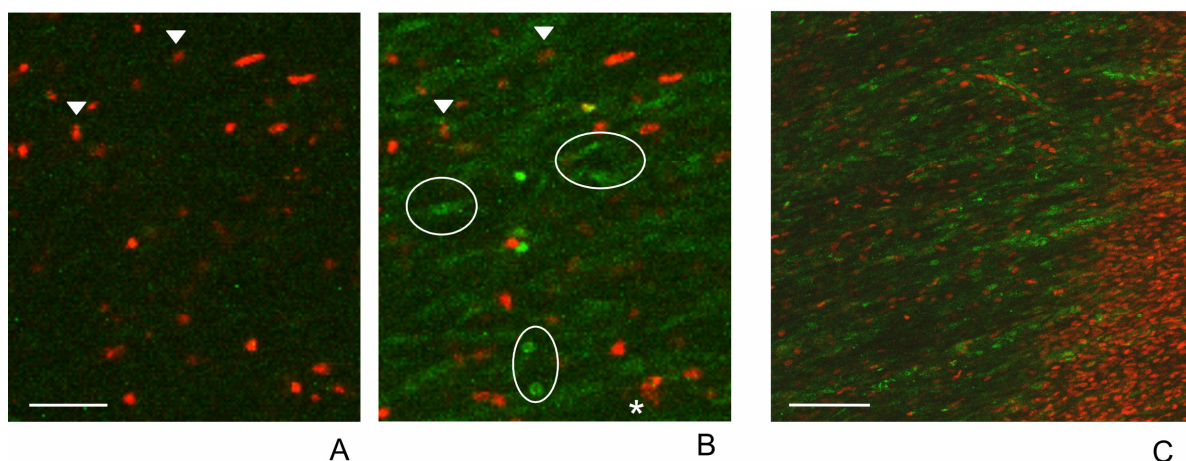


Figure 4.5: Images taken 1 hour (A) and 12 hours (B) after the start of a hypoxic experiment. Necrotic nuclei become less intense (arrowheads) and disintegrate with time (star). Apoptotic nuclei exhibit poor contrast with cytoplasmic staining (ellipses). The bar indicates 50  $\mu\text{m}$ . (C) From the right side a field of necrotic nuclei progressed into the field of view towards the end of a normoxic 40% compression experiment. This event was found in just one location of all experiments (bar denotes 200  $\mu\text{m}$ ).

compaction occurred as was deduced from the cytoplasmic YP staining. After 22 hours of 20% compression under hypoxia all nuclei were fluorescent, most of them exhibiting green fluorescence (fig. 4.4E). The YP-staining of the nuclei was not intense but transitions of these nuclei to a necrotic state were observed, suggesting that these nuclei, though not stained intensely, were apoptotic. The hypoxic, 40% compression experiments showed development of cell death resembling that in the normoxic series with the majority of nuclei being positive for propidium iodide after 22 hours (figure 4.4F).

Hypoxia in the medium was verified in a separate experiment, in which the culture chamber was continuously flushed with the 95% N<sub>2</sub> and 5% CO<sub>2</sub> mixture. Within a 90-minute time span, the oxygen tension in the medium below the layer of mineral oil decreased from 20% to below 6%, the value considered to represent the upper limit of hypoxia (Jiang et al., 1996), as illustrated in figure 4.6.

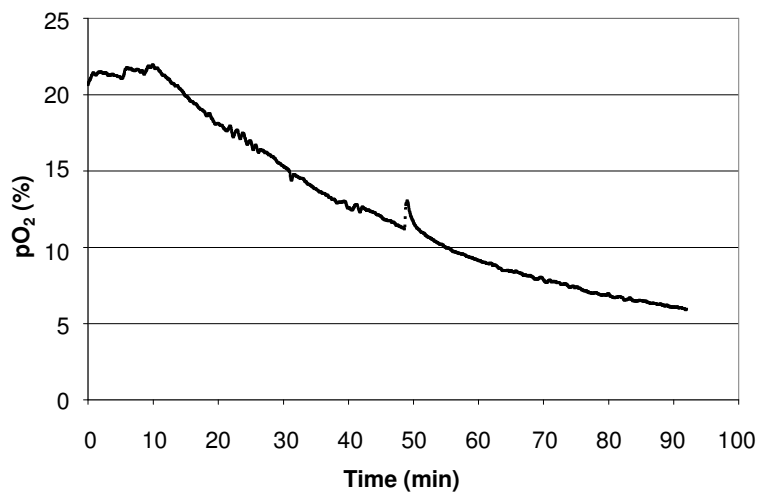


Figure 4.6: Curve showing the course of oxygen tension in time in culture medium covered with mineral oil, while the incubation chamber was continuously flushed with 95%N<sub>2</sub> and 5% CO<sub>2</sub>. The oxygen tension declined with time to hypoxic values (< 6%). The data were corrected for drift of the electrodes at atmospheric oxygen tension.

### 4.3.3 Temporal profile of cell death

Temporal profiles of viability due to necrotic cell death are presented in figure 4.7A. It reveals a significant reduction in viability due to immediate necrosis in up to 10% of the cells immediately following applied compression. Significant differences among the necrotic profiles for the six experimental conditions are summarized in table 4.2.

All compressed groups (except for the 20% compression, hypoxic group) exhibited significant decremental effects on tissue viability compared to the control group. Similar differences were found for these groups compared to the hypoxic group. However, no significant difference for the profiles was observed between the hypoxic and normoxic groups at any compression level within 22 hours. This may suggest that hypoxia had no additional effect on tissue viability due to necrosis, irrespective of the absence or presence of compression in the 22 hour time period.

Figure 4.7B illustrates the temporal profile of viable cells revealing little change in the first 7 hours due to apoptosis. Close examination of the six experimental conditions

revealed some discrimination based on the compression level. A significant effect of compression on apoptosis was found for all compressed groups compared to both the

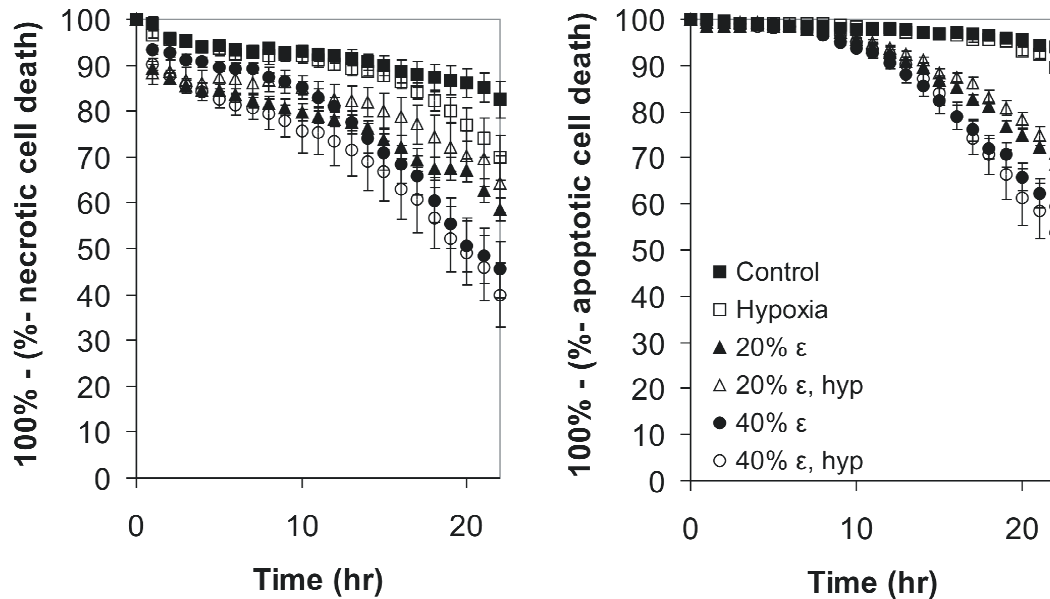


Figure 4.7: Percentages of viable cells (non-necrotic nuclei in (A), non-apoptotic in (B)) in time in control (■), 20% (▲) or 40% (●) compression, and hypoxic (□) conditions, with 20% (△) or 40% (○) compression. (A) The 20% compression (normoxia) group and both 40% compression groups were significantly different from both the control and hypoxic groups ( $p < 0.05$ ). (B) The 20% compression groups and the 40% compression groups were significantly different from both the control and hypoxic groups ( $p < 0.05$ ). The error bars represent standard errors of the mean.

control and hypoxic group (table 4.2). Deprivation of oxygen had no significant additional effect on the development of apoptosis, in either compressed or uncompressed BAMs.

The proportions of both apoptotic and necrotic cell death for the 40% compressed hypoxic group over the 22 hr time period is presented in figure 4.8. It can be seen that

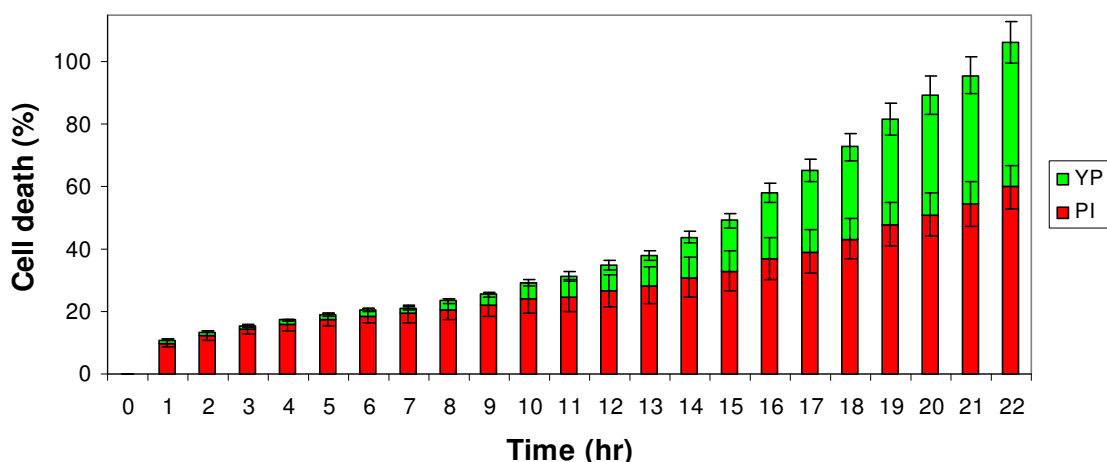


Figure 4.8: The mean percentages of necrotic (PI) and apoptotic (YP) cell death in time for the 40% compressed hypoxic group. The total number of affected nuclei was initially determined by the necrotic proportion. Note that cell death tends to exceed 100% at the final time point. This is caused by the minor variations in the total number of nuclei present in each field of view. Error bars represent standard errors of the mean.

the progression of cell death by the two processes increased monotonically to a value of approximately 100% by 22 hours.

The 40% compression, normoxic condition resulted in a comparable trend. Both 20% compressed groups exhibited a similar trend affecting approximately 70% of nuclei affected by 22 hours. In the absence of compression fewer cells were affected, between 30-40%, in both hypoxic and normoxic conditions.

Table 4.2: Comparison of significant differences in development of necrosis and apoptosis under the chosen test conditions (the percentages denote compression levels). 'A' and 'B' indicate which condition resulted in more necrotic or apoptotic cell death.

Comparison of test conditions		Necrosis	Apoptosis
Left: A	Right: B		
Normoxic, 0% versus Normoxic, 20%		*** B>A	*** B>A
Normoxic, 0% versus Normoxic, 40%		** B>A	*** B>A
Normoxic, 0% versus Hypoxic, 20%		n.s.	*** B>A
Normoxic, 0% versus Hypoxic, 40%		** B>A	*** B>A
Normoxic, 20% versus Hypoxic, 0%		*** A>B	*** A>B
Normoxic, 40% versus Hypoxic, 0%		** A>B	*** A>B
Normoxic, 40% versus Hypoxic, 20%		n.s.	* A>B
Hypoxic, 0% versus Hypoxic, 20%		n.s.	*** B>A
Hypoxic, 0% versus Hypoxic, 40%		* B>A	*** B>A

Comparisons of test combinations that are not shown were non-significant for both necrosis and apoptosis. Significance is indicated as n.s. (non-significant,  $p>0.05$ ),  $p<0.05$  (\*),  $p<0.01$  (\*\*), and  $p<0.001$  (\*\*\*). All other combinations were not statistically significant ( $p>0.05$ ).

#### 4.4 Discussion

The etiology of (deep) pressure ulcers has been addressed in selected studies (Bosboom et al., 2001; Breuls et al., 2003a; Gefen et al., 2005; Tsuji et al., 2005). Obstruction of the blood and lymphatic vessels have been suggested as causal factors for pressure ulcer development, as well as deformation of the tissue and the associated cells. A few studies have utilized in-vitro model systems with a controlled experimental input



(Breuls et al., 2003a; Wang et al., 2005). In the present study, such an in-vitro model was applied to study the relative contributions of hypoxia and compression to the progression of cell death in engineered skeletal muscle tissue. Hypoxia was considered to be the most important effect of ischemia in development of tissue damage.

Results indicated that hypoxia alone or superimposed on compression up to a level of 40% over a 22 hour period had only a minimal effect on cell death development, as assessed by either apoptotic or necrotic indices. In skeletal muscle tissue, the normal in-vivo oxygen tension is approximately 2.0-5.2% (15-40 mmHg; Prewitt and Johnson, 1976; Richmond et al., 1999). However, 20% oxygen in the gas phase was chosen to represent the normal oxygen tension as generally prescribed in cell culture studies in incubators. Hypoxia was considered to represent a state where oxygen availability does not meet oxygen demand. In the present study, hypoxia was defined as oxygen tensions below 6%. This threshold was based on an increase of HIF-1 (hypoxia inducible factor-1) DNA-binding activity with oxygen tension decreasing below 6% (Jiang et al., 1996). The actual oxygen tension applied during the hypoxic experiment conditions was below this threshold value. Although monitoring of oxygen tension only lasted 90 minutes, when values attained approximately 6% (fig. 6), an extrapolation of oxygen tension in a decreasing fashion could be predicted, as a result of both the continuous flushing and cellular consumption. This implies that the degree of hypoxia would have increased over the 22 hour experimental period.

Another explanation of the C2C12 cell's apparent insensitivity to hypoxia may be found in their oxygen conformance behavior. A study by Arthur et al. (2000) reported that as oxygen concentration declined, the cells tended to consume less oxygen without switching to anaerobic energy production. This adaptive response may delay the moment of actual hypoxia in the cells.

Table 4.3: Mean percentage of apoptotic nuclei as a proportion of total cell death (sum of apoptotic and necrotic cell death = 100%) for all experimental groups, in time.

Experiment duration (hr)	Mean percentage (%) of apoptotic cell death					
	Normoxia 0%	Normoxia 20%	Normoxia 40%	Hypoxia 0%	Hypoxia 20%	Hypoxia 40%
8	18	13	22	10	13	12
12	20	25	33	19	26	23
22	26	43	43	26	45	44

0%, 20%, and 40% in the experimental condition represent deformation of the tissue.

Although cell death development was also observed in control BAMs, cell death profiles in compressed BAMs were significantly different. The increase of cell death in the control BAMs may be explained by the natural turn-over of C2C12 cells in culture, which start to deteriorate after reaching their matured stage (authors' observations).

Tissue compression resulted in an immediate necrotic tissue response, which can not be explained by hypoxia over this time period. An apoptotic tissue response was also invoked by compression. A trend of increased cell death with both higher compression levels and time was found to be in agreement with previous experimental data on animal and human studies (Husain, 1953; Kosiak, 1959; Reswick and Rogers, 1976; Daniel et al., 1981). A previous cell-model study examining relative values of apoptotic and necrotic cell death revealed an increase in the apoptotic percentage of total cell death from 61% to 67% (10% increase) and 71% (16% increase) after 8 and 12 hours of 10% compression, respectively (Wang et al., 2005). In the present study, the apoptotic contribution was comparable, as summarized in table 4.3.

Thus, after 22 hours the percentages had increased to approximately 25% for uncompressed samples (both normoxic and hypoxic), whereas compressed samples incorporated 40-45% of apoptotic cell death. It should be noted that these proportions represented an underestimate, as those cells that had exhibited apoptosis were counted as being necrotic following the change in the fluorescent signals. Thus, no distinction was made in the present experimental protocol between necrotic cells originating from apoptosis or those directly exhibiting necrosis.

One experimental limitation involved the transfer of the tissue from its culture dish into the incubation device on the microscope, as indicated by the small increase in cell death during the control experiments. In addition, the BAMs proved to be sensitive to distortion in shape, i.e. torsion or impact shocks, which invoked an immediate necrotic response of the tissue during transfer. Samples that were exposed to such mechanical artifacts during transfer were discarded and excluded from subsequent group analysis.

Development of cell death under the tip was uniform for all randomly assigned locations, independent of positioning in the center or near the edge of the construct. The one exception that was observed with a necrotic 'wave' progressing into the field of view (fig. 5c), that may have been caused by either a sudden mechanical failure of the construct or by cellular release of signaling molecules.

The low intensity green fluorescence in the cytoplasm, as observed in the qualitative analysis after more than 10 hours may indicate the onset of apoptotic cell death. The staining coincided with low intensity staining of nuclei in most, but not all of the cells. The nuclei that exhibited the weak staining eventually became brighter and apoptotic before entering the necrotic phase. A possible explanation might be that the cytoplasmic signal was caused by a transient plasma membrane injury allowing a small amount of YP to enter the cell interior. This would explain the less distinctive nuclear staining. Once entering the apoptotic phase, the permeability of the plasma membrane increased enough to permit free diffusion of YP into the nuclei. Additionally, the cytoplasmic YP signal may be caused by endocytosis of the probe explaining the delayed time point at which enough dye had accumulated to generate a visible signal (fig. 7B).

The quantification method for the PI-stained nuclei was considered reproducible and objective as image thresholding was performed entirely without manual interference. However, the same method could not be applied to the apoptotic staining, as some manual threshold adjustment was necessary to compensate for the faint contrast

between apoptotic nuclei and cytoplasm with time. Each separate experiment required adjustment, as fluorescence intensities of apoptotic nuclei were not comparable between the experimental conditions.

The low intensity staining of apoptotic and necrotic nuclei during compression coincided with increased nuclear size. The increased size of nuclei was most probably a result of the compression per se. Indeed the larger nuclear dimensions may result in a decrease in dye density with an associated fading of the nuclear staining.

Determination of initial sample height was hindered by the fact that the tissue was thicker than could be established on the confocal microscope. In addition, the samples were not located on the cover glass but in a state of flotation above it. Therefore, the initial sample height was determined by gradually lowering the indenter until a small increase in tissue dimensions in the xy-plane was observed. This method may have influenced the reproducibility of the prescribed compression in four of the six experimental conditions. It should be noted, when interpreting the results, that all deformations were applied globally as the decrease in thickness of a complete tissue construct. The deformation at a local cell level might have been different. The mechanical properties of the gel and of the cells differ and both will exhibit viscoelastic behavior. This also applies in tissues when, for example, the globally applied compression levels do not represent the local deformation experienced by the cells (Oomens et al., 2003). The globally imposed deformations are large, though representative of tissue deformations during sitting and supine postures. Indeed, it has been previously shown that in-vivo deformation of muscle tissue deformation ranges from between 20-35% in lying human (healthy) subjects to 40-65% in paraplegic individuals (Reger et al., 1990). It should be recognized, however, that the present findings were obtained from murine 3D-cultured muscle samples and cannot be extrapolated directly into clinical practice. Recently, an elegant attempt was made to unravel the relative contributions of ischemia and deformation to development of deep pressure ulcers in a rat model (Stekelenburg, 2005b). The effects of muscle tissue compression and concomitant ischemia were compared to the effects of ischemia alone. A 2-hour loading protocol resulted in irreversible damage, whereas ischemia invoked reversible tissue alterations. However, this in-vivo study incorporated the imposition of complete ischemia whereas, in the present work, only hypoxia was implemented in the in-vitro model. Nonetheless, despite the use of different time periods, both studies revealed that ischemia per se did not invoke definite damage, whereas deformation did. These findings suggest an even more important role for tissue deformation in the development of deep pressure ulcers than has been previously assumed.

In future, other factors associated with ischemia, such as acidosis, need to be examined. This will enable a further understanding of pathways leading to pressure ulcer development, which is a critical stage in adjusting clinical guidelines in both treatment and prevention.



### **4.5 Acknowledgments**

The authors thank Rob van den Berg and Harrie van de Loo for their contribution to the design and manufacturing of the experimental system. This research was supported by the Dutch Technology Foundation STW, applied science division of NWO, and the Technology Program of the Ministry of Economic Affairs.

# Chapter 5

Ischemic factors and deformation  
influence metabolism of engineered  
skeletal muscle

## 5.1 Introduction

Pressure ulcers may develop after prolonged periods of tissue deformation (Daniel et al., 1981; Bliss, 1998; Bouten et al., 2003a). The deformation may lead to reduced blood flow due to collapse of vessels with the associated ischemia of localized tissues. Such a sequence of events can occur in spinal cord injured (SCI) subjects who exhibit such inherent risk factors as immobility, desensitization, and tissues whose properties change with time such that they become less tolerant to external loading (Castro et al., 1999; Scelsi, 2001). Indeed SCI induces not only muscle atrophy and changes in the myofibrillar apparatus, but also changes in the microcirculation (Scelsi, 2001). The pressure ulcers that develop in this specific patient group often involve deep tissues, particularly skeletal muscle tissues. The ulcers may affect several tissue layers, starting at the skin and progressing towards the bone or in reversed order starting in the deep tissues and growing towards the surface.

When the ulcer is located in the subcutaneous layers underneath an intact skin, it is called deep tissue injury (DTI, Donnelly, 2005). When DTI proceeds to the skin, the result may be a stage III or IV open pressure ulcer (Ankrom et al., 2005). As it is known that skeletal muscle is in particular sensitive to compressive loading, this will be the focus tissue of this chapter.

Ischemia, reperfusion, lymphatic blockage and cellular deformation are each considered to play some role in pressure ulcer development (Kosiak, 1959; Dinsdale, 1974; Daniel et al., 1981; Reddy and Cochran, 1981; Miller and Seale, 1981). Most probably, the onset of damage development is multi-factorial in nature and requires the contribution of several of these factors (Bouten et al., 2003a; Stekelenburg, 2005b; Gawlitta et al., 2006). The various factors may also contribute to a different degree to the development of damage associated with different tissue layers, such as skin, fat or muscle.

Despite its potential multifactorial origin, the most established hypothesis for tissue damage development so far is mechanically induced capillary occlusion resulting in tissue ischemia and thus hypoxia (oxygen deprivation). However, previous studies on skeletal muscle might suggest a lesser role for oxygen deprivation in this tissue than has been previously assumed. Indeed, Stekelenburg et al. (2005b) showed that highly deformed regions of rat muscle correlated with areas of tissue damage as opposed to the ischemic regions resulting from tissue deformation. The ischemic period in this study was 2 hours, which is below the threshold of 4-5 hours for the onset of skeletal muscle necrosis (Labbe et al., 1987). A similar result was reported for in vitro, in engineered skeletal muscle constructs that developed tissue damage due to compression rather than oxygen deprivation (Gawlitta et al., 2006, chapter 4). During a 22-hour compression period the tissue viability was affected by imposed global deformations of 20% and 40%, but not by hypoxia. This may be explained by the oxygen conformance behavior of the cells, in that they consume less oxygen under oxygen deprivation, which may extend to 22 hours. In addition, they may adjust by switching to anaerobic metabolism. However, at some point in time the cells must respond to oxygen deprivation. Therefore, experiments for longer periods of time are

required. Also, the results may imply that ischemia with its associated hypoxia played a less important role in damage development than tissue deformation. However, hypoxia can not be considered to be the only adverse environmental event occurring during ischemia. In addition, other factors, such as acidosis, hyperkalemia, hypercapnia, lactate build-up, and glucose depletion will take place in ischemic tissues (Ferrier and Howlett, 2005; Louch et al., 2005).

The objective of the present study was to provide an improved understanding of the relative contributions of the events occurring during tissue compression, i.e. deformation and ischemia, to the development of muscle damage. Effects of deformation, tissue hypoxia, glucose depletion, and acidification due to lactate presence were determined in an in vitro muscle model. It was hypothesized that hypoxia would stimulate the tissue to switch to anaerobic metabolism. This implies that glucose is degraded into lactate, generating energy without the necessity for oxygen consumption. Thus, the employment of anaerobic metabolism will create more lactate and thus a more acidic environment, which may compromise cell activity and tissue viability. Furthermore, compression of the cells within the tissue is thought to affect the cells on a shorter term than ischemic factors.

Thus the objectives of this chapter are to examine the separate and combined effects of these ischemia-related factors on engineered muscle, using techniques modified from the previous chapters.

## **5.2 Materials and Methods**

### **5.2.1 Cell and tissue culture**

C2C12 murine myoblasts (ECACC, Salisbury, UK) were kept below 80% confluency in growth medium, containing high glucose DMEM (Gibco, Breda, The Netherlands), 15% FBS, 2% hepes, 1% non-essential amino acids and 0.5% gentamicin (all purchased from Biochrom AG, Berlin, Germany). Cells were harvested between passages 11 and 18 and resuspended in a gel mixture as described previously (chapter 2). Briefly, approximately 4 million cells were suspended in 1 ml of collagen I/ Matrigel mixture (both BD Biosciences, Alphen a/d Rijn, The Netherlands) and molded into shape between two Velcro anchoring points in 6-well plates. The 6-well plates were precoated with 1.5 ml SYLGARD 184 elastomere (Mavom b.v., Alphen a/d Rijn, The Netherlands). To this surface, house-shaped pieces of Velcro (5x7 mm) were glued approximately 10 mm apart with their 'rooftops' facing each other (figure 2.1, chapter 2).

The gel/cell mixture was molded between the Velcro anchoring points and placed into an incubator. Subsequently, after 1-2 hours the constructs were covered with growth medium. After 24 hours the growth medium was replaced by differentiation medium, which had the same formulation as growth medium, except that 0.4% Ultrosor G (BioSeptra, Cergy-Saint-Christophe, France) was used instead of FBS. Differentiation medium was refreshed every other day. The engineered muscle constructs were allowed to mature for a further 7-9 days before experiments were performed.

## 5.2.2 Experimental conditions

Several experimental conditions were imposed on the constructs for a period of five days, as indicated in table 5.1. It can be seen that in some cases two or more factors were imposed simultaneously, for example, hypoxia and deformation. Sampling of the medium was performed at time point 0 and repeated every 24 hours for 5 consecutive days without refreshing the medium in all groups. Every medium sampling of 100  $\mu$ l was withdrawn from a total of 3 ml.

*Tissue deformation* For experimental conditions involving tissue compression the mean undeformed height of the samples was determined as  $530 \pm 69 \mu\text{m}$  ( $n=16$ ). A tissue compression of  $34 \pm 8\%$  was achieved by placing rectangular stainless steel weights on top of the constructs on day 0, with spacers of  $350 \mu\text{m}$  at their four corners (figure 5.1A). These weights remained in place until day 5.

Table 5.1: Overview of experimental conditions imposed on engineered muscle for 5 days.

Experimental condition	Deformation (%)	Oxygen level (%)	Initial pH	Initial conc. glucose (g/l)
(a) Control	0	20	7.4	4.5
(b) Low glucose	0	20	7.4	<b>1</b>
(c) Hypoxic	0	<6	7.4	4.5
(d) Deformed	<b>34</b>	20	7.4	4.5
(e) Hypoxic, deformed	<b>34</b>	<6	7.4	4.5
(f) pH 6.5	0	20	<b>6.5</b>	4.5
(g) pH 6.5, hypoxic	0	<6	<b>6.5</b>	4.5
(h) pH 6.5, deformed	<b>34</b>	20	<b>6.5</b>	4.5
(i) pH 6.5, hypoxic, deformed	<b>34</b>	<6	<b>6.5</b>	4.5
(j) pH 6.0	0	20	<b>6.0</b>	4.5
(k) pH 5.3	0	20	<b>5.3</b>	4.5

Sample size,  $N$ , equaled 17 for comparisons of a, c, d, e and  $N$  was 6 for comparisons of a, b, f, g, h, i, j, k.

*Hypoxia* Samples were deprived of oxygen by incubation in an air-tight box (figure 5.1B), which was continuously flushed with a 95%  $\text{N}_2$  and 5%  $\text{CO}_2$  gas mixture over the 5 day period. Evaporation was prevented by overlaying the medium with mineral oil (Sigma). This layer of oil was also placed on medium of the normoxic (20% oxygen) samples that were kept in the incubator. In contrast, the air-tight box was heated in a warm water bath to  $37^\circ\text{C}$ . Sampling of the medium was performed with negligible disturbance of the hypoxic environment inside the box. Rubber sheets on top of the box were pierced with a needle but retained their air-tight property after repetitive puncturing (figure 5.1B).

Effects of the air-tight box in a warm water bath on tissue metabolism and viability were determined in a separate experiment in which the box was continuously flushed with an atmosphere of 95% air and 5%  $\text{CO}_2$ . There were no differences in either the

tissue viability or the tissue metabolism over a 5 day culture samples in the box compared to those in an incubator (data not shown).

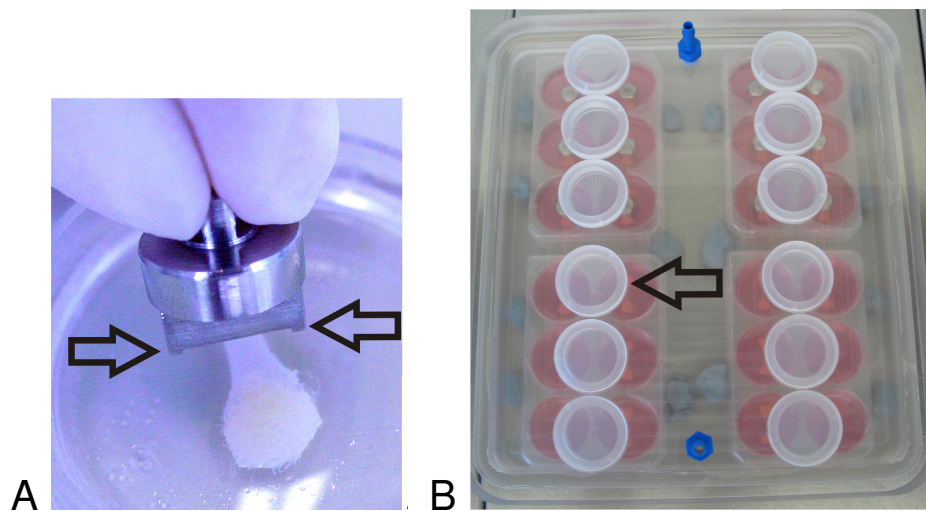


*Figure 5.1: Photographs of the experimental set-up. (A) One of the stainless steel loads is shown with the arrows indicating 350  $\mu\text{m}$  spacers on one side of the load. (B) Top view of the air-tight box is shown with four 6-well plates inside. One of the rubber sheets for medium sampling of two wells is pointed out by the arrow.*

**Acid** The influence of acidic pH values on sample viability was established by the addition of L-(+)-lactic acid (L1875, Sigma) to the culture medium, to achieve final pH values of 5.3, 5.8, 6.1, 6.4, 6.7, 7.4 (control) at day 0. A broad range of pH values was chosen, as the values reported in literature to be the lower threshold compatible with living cells also greatly varied (Taylor, 1962 (pH 6.5); Burnell, 1968 (pH 7.1); Webster et al., 2005; Willam et al., 2005 (pH 7.0)). Based on effects of these pH values in 24 hours (assessed by MTT), a pH value was chosen for the 5 day experiment. The medium pH was not adjusted after time point 0.

**Glucose concentrations** To assess the influence of glucose deprivation on the engineered muscle samples, two different concentrations of glucose were chosen. Tissue survival was assessed in high glucose (4.5 g/l) and low glucose (1 g/l) differentiation media without refreshment.

### **5.2.3 Analyses of metabolism and viability**

To assess the metabolic activity of the cells, glucose, lactate, pH and MTT assays were performed on the daily extracted medium samples. It should be recognized that changes in MTT could indicate either differences in cell number, caused by growth or death, differences in the metabolic activity of the cells per se, or a combination of both. Therefore, the viability of cultures was additionally determined from the release of LDH (lactate dehydrogenase).

**Glucose assay** Medium samples were diluted 40x in water. Assay reagent was prepared according to the manufacturer's protocol. Briefly, 2% v/v o-dianisidine (D2679, Sigma) was mixed with 98% v/v glucose oxidase/peroxidase reagent (G3660, Sigma). One part of diluted sample was mixed with 2 parts of assay reagent in 96-well plates. After 30 minutes of incubation, the reaction was stopped by the addition of 6M

sulphuric acid. Absorbance was measured at 540 nm against a background signal recorded at 650 nm on a plate reader. Calibration with a glucose standard was performed for each plate.

*Lactate assay* Medium samples were diluted 20x and one part was mixed with 10 parts of lactate reagent (TB 735-10, Kordia Life Sciences, Leiden, The Netherlands), prepared according to the manufacturer's recommendations. After 10 minutes, absorbance was read on a plate reader at 540 nm against background at 650 nm. Calibration curves were obtained using a range of L-(+)-lactic acid (L1875, Sigma) dilutions for each measurement.

*pH* Measurement of pH was performed by the application of pH indicator paper (Merck) ranging pH 6.4-8.0 and pH 5.4-7.0 with 0.2-0.3 unit intervals. Paper readings were confirmed with a glass tip electrode (SP10T, Consort, Turnhout, Belgium) and pH meter (P501, Consort).

*MTT assay* Metabolic activity of cells was detected by measuring the reduction of MTT to the purple formazan crystal. After incubation in MTT-medium mixture for 30 minutes, the samples were rinsed with PBS and the wet weight of 5 mm pieces that were cut from the tissue between the Velcro was determined. The 5 mm width of the excised tissue was based on the dimensions of the loaded tissue. Formazan crystal was extracted and dissolved in a 90% DMSO/ 10% Triton-X mixture. Absorbance was read at 570 nm.

*LDH assay* LDH release of the cells was assessed by an in vitro toxicology assay kit, LDH based (TOX7, Sigma). Samples were diluted 5x in water to a total volume of 30  $\mu$ l prior to the addition of the reagent. The reaction was terminated at 20 minutes with 10  $\mu$ l 1N hydrochloric acid. Absorbance was read on a platereader at 490 nm and corrected for background at 650 nm.

#### **5.2.4 Statistical analysis**

All data are presented as mean  $\pm$  standard error of the mean. The engineered samples were considered to be very reproducible in that they all contained an equal amount of cells. Therefore, no normalization was carried out. Differences over time and between groups were assessed using an analysis of variance (ANOVA) performed with SPSS software, version 12.0.1. A Bonferroni posthoc test was then applied and statistical significance was prescribed at the 5 per cent level (\* $p < 0.05$ ; \*\* $p < 0.01$ ; \*\*\* $p < 0.001$ ).

### **5.3 Results**

#### **5.3.1 Acidification**

The effects of medium pH on the viability of both myoblast monolayers and differentiated muscle tissue were examined after 24 hours. Changes in the metabolic activity of the monolayer culture, as assessed by MTT absorption, are illustrated in figure 5.2A. There was a clear decrease in metabolic activity with decreasing values down to pH 5.8, although no subsequent decrease at pH 5.3 was observed. By contrast, the metabolism of muscle tissues revealed no differences between the pH range 5.8-

7.4, but a significant decrease at pH 5.3 (figure 5.2B). Based on this finding, a lowest pH of 5.3 was applied in further experiments.

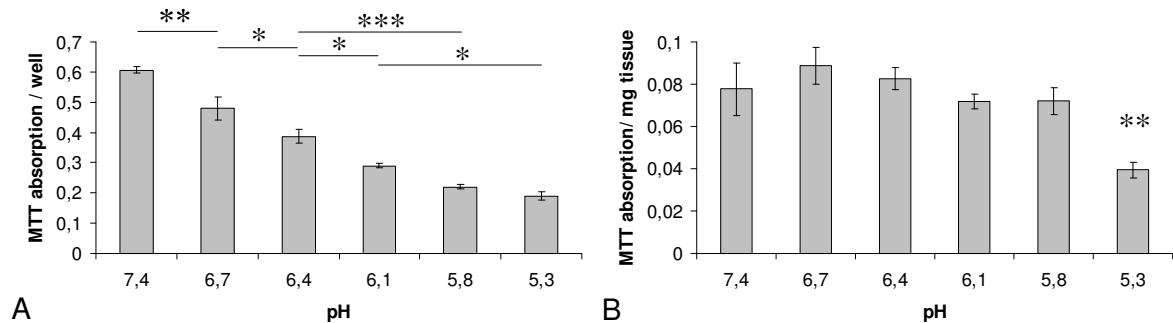


Figure 5.2: Effect of pH on cell viability assessed by MTT absorption for monolayer (A) and muscle tissue cultures (B) after 24 hours. Significant differences by the bars in figure A, while in figure B the difference against all other groups is shown (\*\* $p < 0.01$ ; \*\*\* $p < 0.001$ ; \* $p < 0.05$ ).

### 5.3.2 Effects of glucose deprivation

The effect of glucose deprivation during a 5 day period in the absence of medium refreshment was significant from 24 hours onwards (figure 5.3).

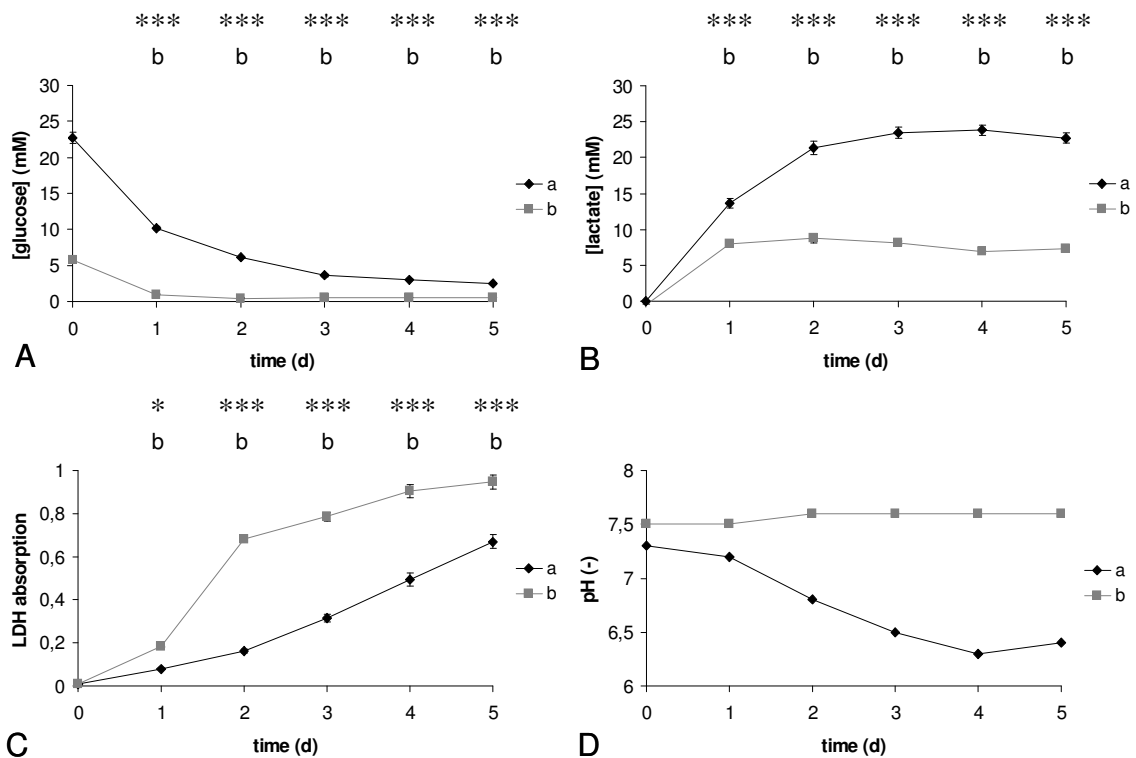


Figure 5.3: Effects of glucose deprivation on temporal profiles for (A) glucose utilization, (B) lactate production, (C) LDH release, and (D) medium pH, for experimental conditions (a) control and (b) low glucose (table 5.1). Significant differences of group b compared to control are indicated above the graphs (\*\* $p < 0.01$ ; \*\*\* $p < 0.001$ ; \* $p < 0.05$ ). Other inter-group differences were not statistically significant.

With reference to glucose utilization (figure 5.3A), it was evident that by day 1 there was no further glucose available to the cells in the low glucose medium. Accordingly,



metabolism was limited in the low glucose medium with lactate production reaching a maximum at day 1 and thereafter remaining constant (figure 5.3B). The control group, associated with a culture medium containing 4.5 g/l glucose, revealed an increase in lactate production up to day 3, thereafter remaining constant. As a result of limited glucose-derived energy production cell death was consistently higher in the low glucose group compared to the control group (figure 5.3C). It should be noted, however, that the latter group still revealed a monotonic increase in LDH release over the 5 day culture period. The differences between the control and low glucose group were also evident from pH profiles (figure 5.3D). The pH of the control medium decreased with time until day 3, thereafter remaining fairly constant. By contrast, the pH of the low glucose medium did not change over the culture period.

### 5.3.3 Effects of lactic acidification

Three separate experimental conditions with initial pH values of 6.5 (condition f), 6.0 (j), and 5.3 (k) were compared to the control group at pH 7.4 (a). The results for glucose concentration, as presented in figure 5.4A, reveal that the groups with an initial

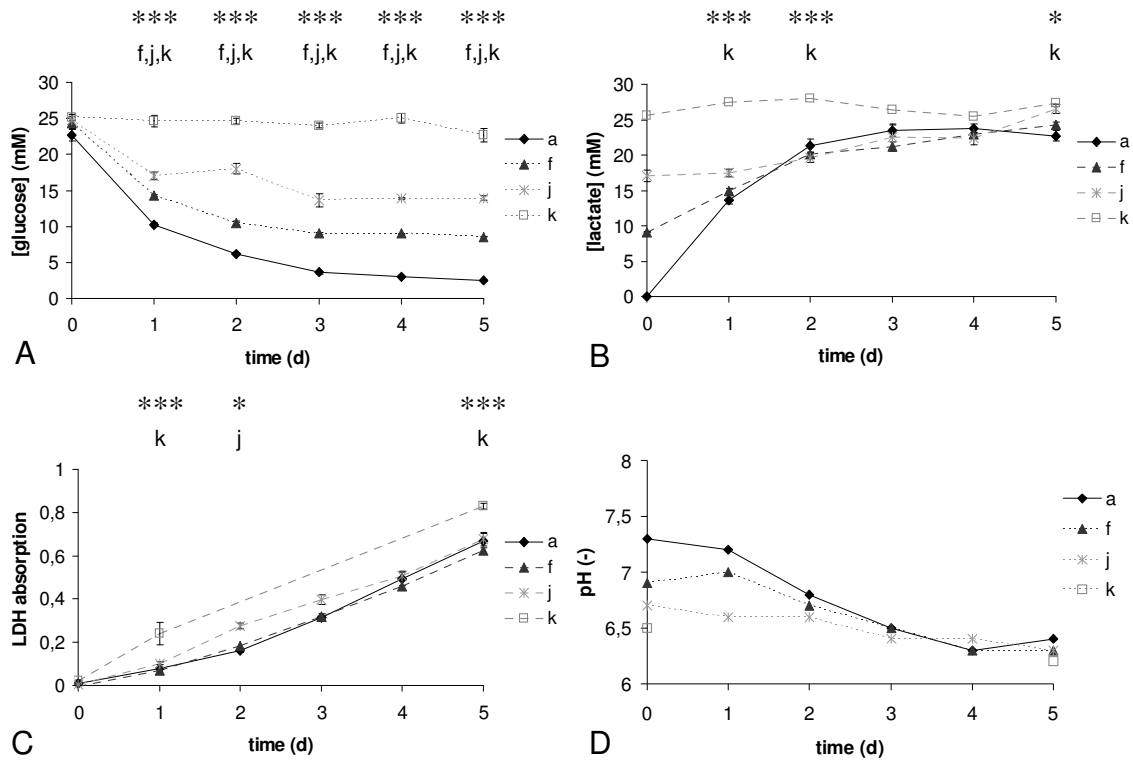


Figure 5.4: Effects of lactic acidification on temporal profiles for (A) glucose utilization, (B) lactate production, (C) LDH release, and (D) medium pH, for experimental conditions (control (a), pH 6.5 (f), pH 6.0 (j), pH 5.3 (k)). Significant differences between the groups f, j, k and the control group are indicated above the graphs (\*\*\*)  $p < 0.001$ ; \*)  $p < 0.05$ .

pH of 6.5 and 6.0 utilized increasing amounts of glucose until day 3, although corresponding utilization was always less than in the corresponding control groups. By contrast, the group starting with the most acidic value (pH 5.3) utilized very little glucose throughout the culture period. The corresponding lactate values were clearly higher in the three experimental conditions at the start of the culture period (figure

5.4B). However, by day 2 there was little difference in the concentration for two experiment groups f and j, and the control group (a). In a similar manner to its glucose utilization behavior, the experimental group (k) did not produce a change in the lactate concentration over the 5 day culture period. The LDH release profiles for all four groups increased monotonically with culture period (figure 5.4C). The highest LDH values corresponded to the experimental group (k) with the lowest initial pH value.

### 5.3.4 Effects of deformation and hypoxia

The effects of deformation (d) or hypoxia (c) per se or both simultaneously (e) were assessed for the 5 day culture period in a separate set of experiments (figure 5.5). The deformed tissue samples did not significantly change their glucose utilization (figure 5.5A), lactate production (figure 5.5B) or LDH release (figure 5.5C) compared to control tissues. By contrast, groups involving hypoxia in the absence or presence of deformation, consumed significantly more glucose than the control group on days 1

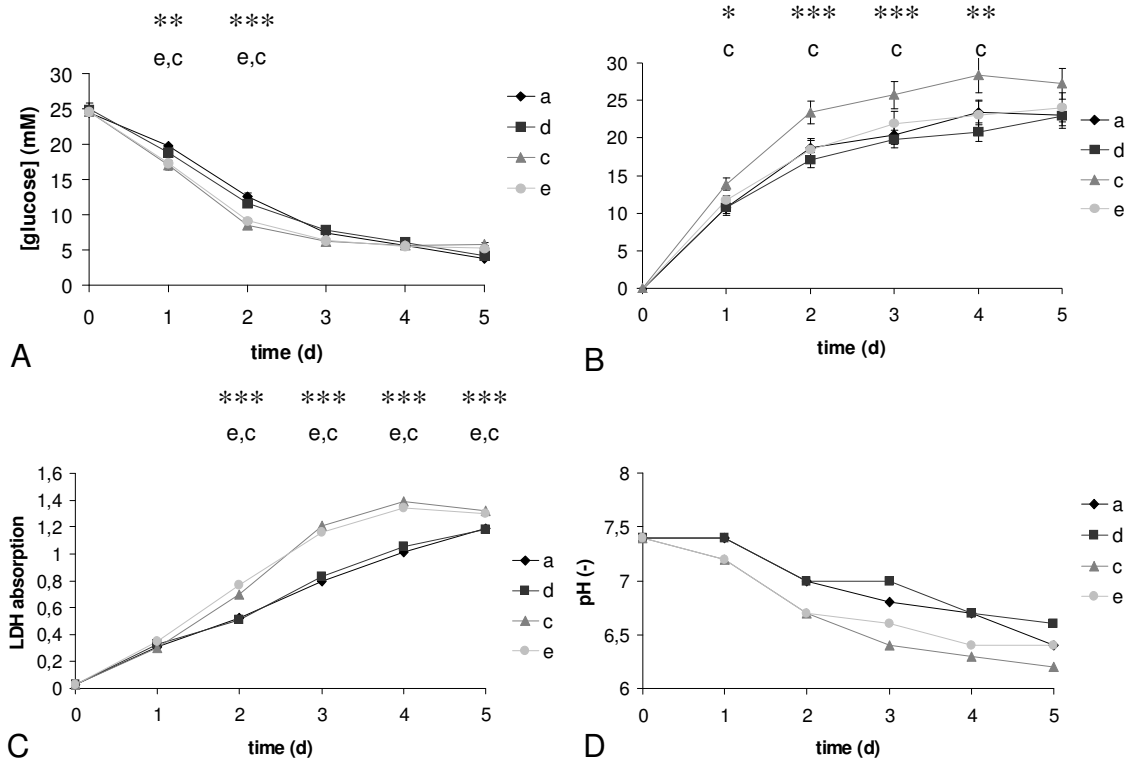


Figure 5.5: Effects of deformation and hypoxia on temporal profiles for (A) glucose utilization, (B) lactate production, (C) LDH release, and (D) medium pH, for experimental conditions (control (a), deformed (d), hypoxic (c), hypoxic, deformed (e)). Significant differences between groups d, c, e and the control are indicated above the graphs (\*\* $p < 0.01$ ; \*\*\* $p < 0.001$ ; \* $p < 0.05$ ).

and 2. There was a general increase in lactate release with culture time for the three experimental groups. However, the hypoxic group (c) was the only one which demonstrated a statistically significant increase in lactate release compared to control values at corresponding time points. The LDH release for both hypoxic groups was significantly increased from day 2 until day 5 compared to the other two groups as evident from figure 5.5C. Changes in pH were similar in the deformed and the control groups, while the pH of the media from both hypoxic groups was more acidic in

nature, although the differences were not statistically significant. The hypoxic group exhibited the lowest pH from day 3 onward (figure 5.5D). It is interesting to note that the results from the control group in this set of experiments differed from those in other experiments.

### 5.3.5 Effects of deformation and / or hypoxia combined with acidification

The effects of lactic acid, deformation, and hypoxia imposed on tissue either separately or in different combinations were analyzed. Figure 5.6A reveals that glucose utilization for all 4 experimental groups (f, g, h, i) followed a similar trend. Indeed, glucose utilization for each group was significantly impeded compared to the control samples

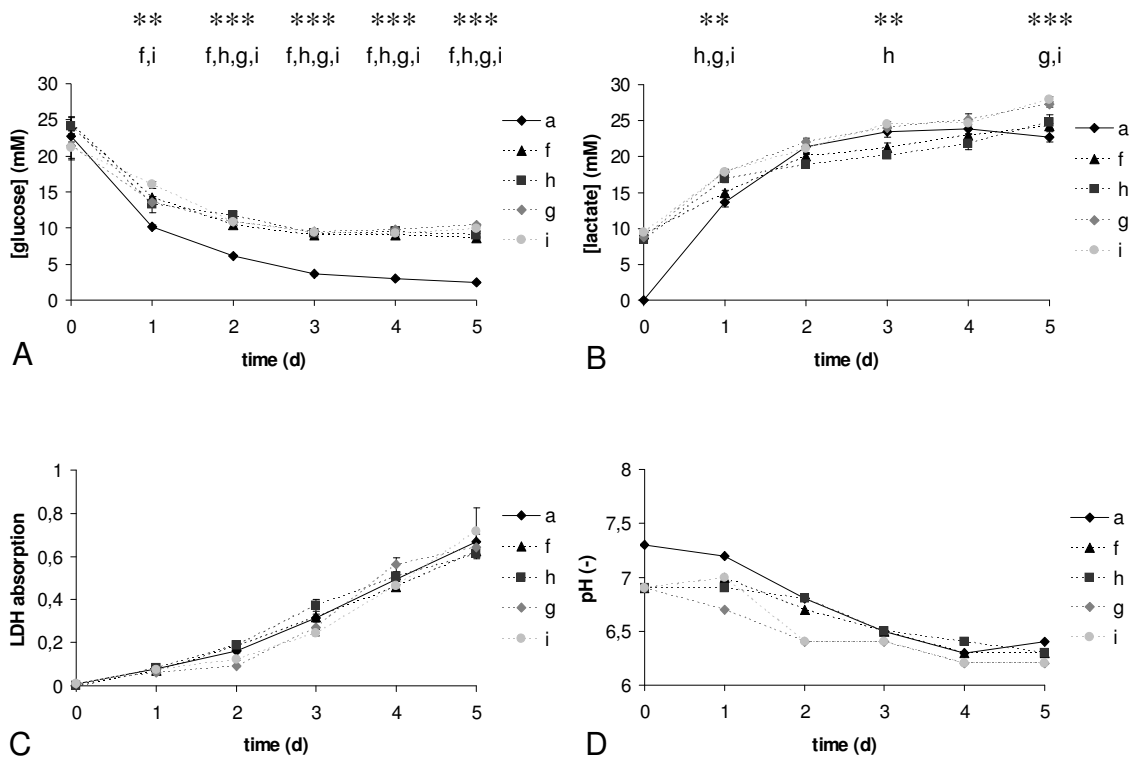


Figure 5.6: Effects of deformation and hypoxia during acidification on temporal profiles for (A) glucose utilization, (B) lactate production, (C) LDH release, and (D) medium pH, for experimental conditions (control (a), pH 6.5 (f), pH 6.5, deformed (h), pH 6.5, hypoxic (g), pH 6.5, hypoxic, deformed (i)). Significant differences between groups f, h, g, i and the control are indicated above the graphs (\*\*\*  $p < 0.001$ ; \*\*  $p < 0.01$ ; \*  $p < 0.05$ ).

( $p < 0.01$  for days 1-5). These data suggest that the acidification to pH value of 6.5 was the dominant influence on glucose utilization. With respect to lactate production, the levels for both the experimental groups and the control group were similar between days 2 and 4 (figure 5.6B). However, after 5 days in culture, significantly elevated levels of lactate were detected in the presence of both hypoxia and tissue deformation (g and i, figure 5.6B).

Despite the metabolic effects observed, LDH release was unaffected by all experimental conditions when compared to the control group. The temporal changes in pH largely reflected the levels of lactate concentrations. Thus a minimum pH value of

6.2 (figure 5.6D) is associated with lactate values of approximately 25 mM (figure 5.6B).

### 5.3.6 Tissue viability after 5 days (MTT)

Tissue viability of all experimental groups was assessed after the 5 day culturing period by an MTT assay (figure 5.7). Surprisingly, the low glucose group showed the highest overall metabolic activity though this group (b) exhibited the maximum LDH release as well (figure 5.7A).

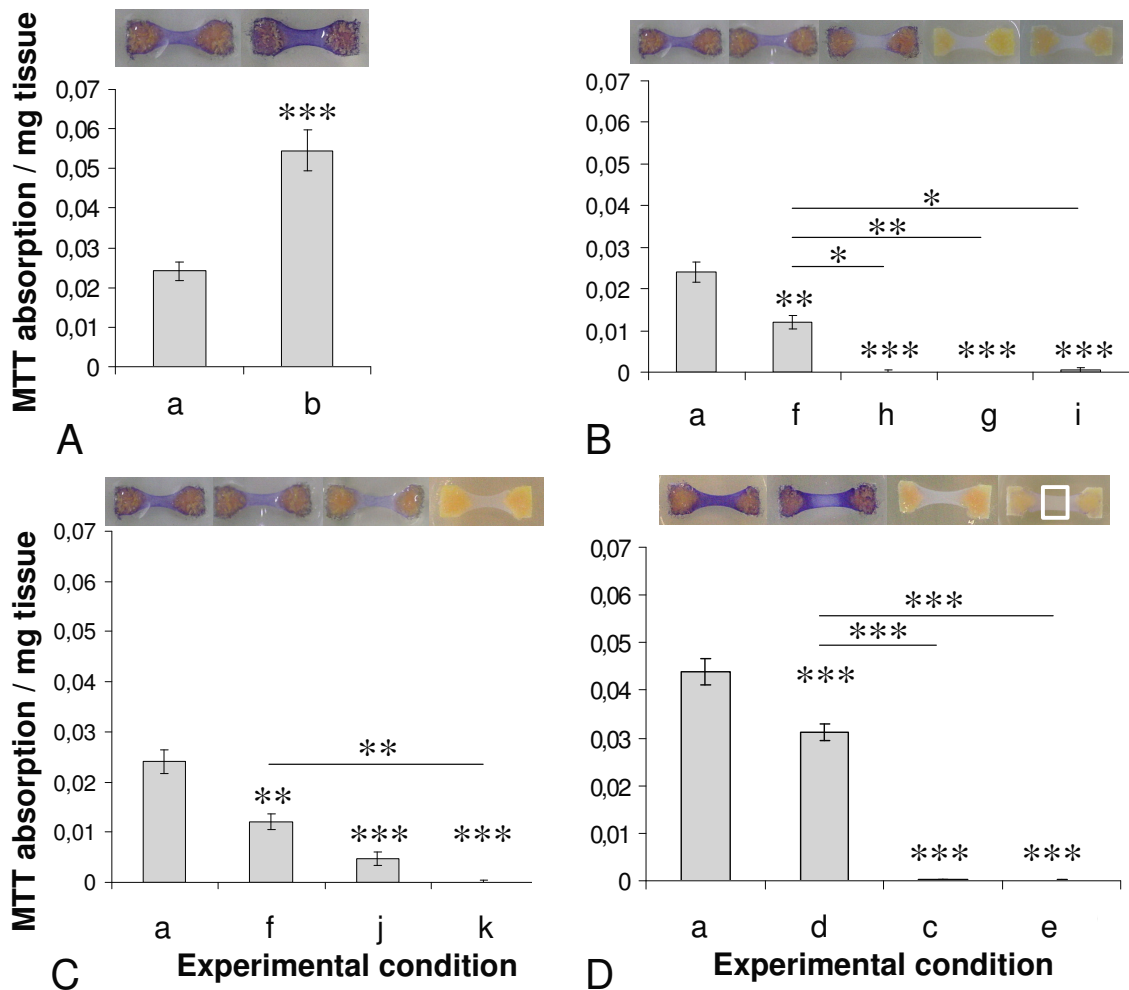


Figure 5.7: MTT absorptions per mg tissue are shown as assessed at day 5. (5.7A) Effects on MTT conversion for 'low glucose' (b); (5.7B) for 'pH 6.5' (f), 'pH 6.5, deformed' (h), 'pH 6.5, hypoxic' (g), and 'pH 6.5, hypoxic, deformed' (i); (5.7C) for 'pH 6.5' (f), 'pH 6.0' (j), and 'pH 5.3' (k); (5.7D) and for 'deformed' (d), 'hypoxic' (c), and 'hypoxic, deformed' (e) are depicted compared to the control group (a). Significant differences from control values are indicated by a star; or between groups by bars and a star (\*  $p < 0.05$ ; \*\*  $p < 0.01$ ; \*\*\*  $p < 0.001$ ). Images above the graphs show tissue MTT staining; in the lower right image a rectangle shows the tissue area from which MTT absorption values were determined.

At day 5, significant effects of the addition of lactic acid were observed (figure 5.7C), that were not found after 1 day of culturing (figure 5.2B, page 65). Tissue viability was not only affected by time, but also gradually decreased with increasing acidity, such that at a pH of 5.3 (k) there was a zero value for the MTT absorption.

From figure 5.7D it was clear that hypoxia in the absence (c) or the presence of deformation (e) resulted in a dramatic reduction in tissue viability, whereas the effect of deformation alone (d) was significant but not as dramatic as that involving hypoxia. The effect of deformation on tissue viability on day 5 as assessed by MTT was comparable to the one found after 24 hours of compression in pilot experiments (see appendix A).

The effect of acidification per se (f) or combined with hypoxia (g) and deformation (h) on MTT conversion revealed that by day 5, only activity in the acidic group (f) was present although about 50% of that observed in the control group (figure 5.7B). If, however, hypoxia (g) or deformation (h) or both (i) were imposed on top of lactic acid, metabolic (MTT) activity was reduced to 0. Comparing the effects by the separate factors of deformation (d), hypoxia (c) or acidification (f) on MTT absorption the reduction in metabolic activity was most dominant in the hypoxic group. However, combining the other two factors, deformation and acidification (h), resulted in a stronger effect than one of them per se.

## **5.4 Discussion**

Deep tissue injury (DTI) has gained increasing interest in recent years (Ankrom et al., 2005; Donnelly, 2005). DTI will develop under intact skin in the subcutaneous layers as a result of compression. It may progressively deteriorate towards the skin surface resulting in a type III or IV ulcer. However, little is known about its etiology and currently these ulcers under intact skin are classified as ‘unstageable’ pressure ulcers (Ankrom et al., 2005). Understanding development of muscle tissue damage may contribute in understanding the etiology of the onset of DTI and its rapid progression.

The present study addressed some factors that are thought to be involved in the onset of muscle tissue damage in pressure ulcer development. The influence of ischemic factors and deformation were assessed in an engineered muscle model. The advantage of the *ex vivo* situation is the ability to vary several etiological factors independently of each other and to monitor the tissue response in real time.

Comparison of engineered muscle culturing in high versus low glucose medium for 5 days showed that within a day after glucose depletion, lactate production and acidification of the medium were arrested and an increase in cell death, or LDH release, followed (figure 5.3). In apparent contrast to these findings, which suggest a cell death response after glucose depletion, metabolic activity as assessed by MTT conversion exceeded the response of all other groups (figure 5.7). This reaction of the tissue may be false positive, caused by the high glucose content of the MTT/medium mixture. At day 5, all tissue groups were incubated in the same MTT/medium mixture containing high glucose levels for comparative analysis. However, the transfer of the low glucose samples may have evoked an excessive metabolic response of the cells to the sudden increase in glucose concentration of the medium. Therefore, addition of MTT to the depleted medium instead may have resulted in a different outcome. The still viable cells after prolonged glucose starvation may in the mean time have utilized

other fuel resources such as glycogen stores, fatty acids, and possibly amino acids. Still, in conclusion, glucose deprivation resulted in a rapid increase of cell death.

Several concentrations of lactic acid were added to produce a range of pHs measured at room temperature and atmospheric CO<sub>2</sub> levels. It should be noted, however, that the initial pH values do not always correspond to the actually preset pH (figure 5.4D). This is due to the buffering capacity of the medium under 5% CO<sub>2</sub> and the temperature of 37 °C.

After addition of acidified medium to monolayer or tissue cultures, the influence on tissue viability was more pronounced in the 2D cultures than in 3D. This may be caused by the differential status of the cells, i.e. myoblasts in 2D as opposed to myotubes in 3D. It may additionally be explained by a protective effect of the extracellular gel environment associated with the 3D cultures.

From the metabolic data obtained during the 5-day culturing period of tissue in acidic media it was clear that increasing amounts of initially introduced lactic acid resulted in a decrease of glucose utilization of the cells and thus the equilibrium levels were at a higher glucose concentration (figure 5.4A). A pH of 5.3 appeared to have impeded tissue metabolism because no glucose was consumed, nor additional lactate was produced. This may suggest that a threshold value for lactic acidity between pH 6.0 (17 mM) and pH 5.3 (25 mM) exists for a transition from diminishing glucose metabolism to a metabolic arrest within a 5 day period. The presence of different initial concentrations of lactic acid, however, did not result in different lactate or plateau levels of pH, but rather caused convergence of the levels to approximately 23 mM and pH 6.2, respectively. These values may be considered threshold values for tissue death. The MTT data obtained at day 5 (figure 5.7C), showed that pH values of 6.5, 6.0, and 5.3 had affected viability, whereas after one day only a pH of 5.3 had decreased viability (figure 5.2B). This may be either caused by minimally increased cell death as assessed by LDH release, which accumulates to a measurable effect after 5 days, or by its effect on cellular metabolism as assessed by different amounts of glucose utilization. Nevertheless, presence of elevated levels of lactic acid decreased glucose metabolism with time, but had only effect on cell death if the acidic threshold was exceeded, which was the case for the most acidic 'pH 5.3' group.

The plateau level of extracellular lactate concentration is within the range of 20-30 mM that was applied to simulate lactic acidosis (Hansen et al., 2005). A concentration of 30 mM was also reported to build up during anaerobic exercise (Usher-Smith et al., 2006). The apparent threshold value for pH of 6.2, observed in the present chapter, was comparable to the values shown to provoke death in various cell types (Taylor, 1962; Webster et al., 1999). The effect of pH lowering in their monolayer cultures was observed within 24 hours in concert with our observations in the 2D cultures.

An increase in extracellular lactate reduced glucose utilization but only induced cell death for high concentrations of extracellular lactate. The depression of metabolism under declined extracellular pH was described before as an 'energy-saving' mechanism (Reipschläger and Pörtner, 1996; Vezzoli et al., 2004).

The effects of deformation and hypoxia on cell death have previously been described in chapter 4. In the present study, the experimental period was extended and the resulting changes in metabolism were determined. Hypoxia and combined hypoxia and deformation led to an increased glucose utilization, increased LDH release and decreased pH values (figure 5.5). However, only the hypoxic tissues in the absence of deformation had increased their lactate formation, which is indicative of a transition to anaerobic metabolism. In the present study, metabolic activity was only measured on the fifth day, when no significant activity had remained in both hypoxic groups to possibly explain this difference in metabolism. Nonetheless, though no changes in glucose, lactate, or LDH concentrations were observed for the deformed versus the control tissue, a significant decrease in metabolic activity (MTT) of the deformed tissue was found. The effect of compression on metabolic activity of the tissue (MTT) was also apparent within 24 hours (data shown in appendix A). The compression was expected to significantly affect LDH release compared to the control. This was not the case, which may be explained by the relatively large size of the LDH molecule that, in addition, may have been hindered by the compressed collagen network in the deformed portion of the tissue.

The following may explain the metabolic effects observed in the deformed tissues. Glucose, lactate, and LDH levels were assessed from medium samples rendering information on the complete construct. MTT data, however, were obtained more locally from the excised central (and thus deformed) portion of the sample (figure 5.7D (d)). The local effects of deformation may therefore be 'lost' in comparison to the metabolism of the remaining tissue if determined from the medium. On the contrary, hypoxia affected all of the tissue and resulted in significant changes of medium composition. Combined hypoxia and deformation did lead to a more acidic pH, but not more lactic acid. This may be caused by formation of other acids than lactic acid by these cells or by the death of the cells.

Concisely, deformation affected tissue viability at the short term and to a lesser extent, whereas hypoxia initiated an anaerobic adaptive response before killing the cells. The effect of deformation and hypoxia combined were dominated by the presence of hypoxia as established by the applied methods.

Upon tissue compression, development of cell death within 24 hours was observed by MTT staining and in chapter 4 by propidium iodide influx. In native muscle tissue the compression will not only lead to muscle cell deformation but also to minimized blood flow causing tissue ischemia. Tissue ischemia comprises hypoxia or even anoxia, which will cause the muscle cells to adapt by downregulating their energy demand (Hochachka and Lutz, 2001). This response of skeletal muscle is its oxygen conformance behavior (Arthur et al., 2000; Boutilier, 2001) and it is therefore considered one of the most hypoxia tolerant tissues (Boutilier, 2001; Vezzoli et al., 2004). Hypoxia or anoxia will also stimulate anaerobic glycolysis with concomitant lactate formation.

Finally, the factors acidification, deformation, and hypoxia were combined to obtain information on possible interaction. Glucose utilization appeared to be predominantly influenced by the presence of lactic acid as compared to the control. In contrast, in lactate production a significant trend for elevated lactate concentration (and more acidic pH) in both hypoxic acidic groups was found as compared to the non-hypoxic acidic groups. Though effects on metabolism were noticed, no difference in LDH release among the groups or compared to control was detected. The MTT metabolic assay, however, did reveal a significant difference in metabolic activity of the acidic group compared to the acidic, deformed and hypoxic groups. Taken together, these data suggest that medium acidity influenced tissue metabolism, but hypoxia and deformation aggravated these effects.

The effect of ischemic hypoxia has been studied extensively in cardiac myocytes (Webster and Bishopric, 1992; Webster et al., 1999; Kubasiak et al., 2002, and reviewed by Graham et al., 2004). The basic finding was that hypoxia alone did not cause apoptosis but that acidosis, reoxygenation, and reperfusion did. Their hypoxic cultures (without medium refreshment) became apoptotic after 2-3 days, a time point at which LDH release was observed in our cultures. Moreover, they confirmed that addition of lactic acid to pH 6.8 caused apoptosis independently of hypoxia in their myocytes.

Stekelenburg (2005b) performed indentation experiments on rat hind limb muscle. Results showed that tissue damage areas correlated with regions of maximum shear strain as opposed to tissue areas which were ischemic alone. This was based on observations during and after load application of 2 hours. The chosen time period was well below the 4-5 hours of ischemia known to cause ischemic tissue damage (Labbe et al., 1987). In the present study, partial ischemia and deformation were imposed for extended periods of time. Acidosis, hypoxia, and deformation all contributed to the development of damage in engineered muscle tissue. Deformation decreased viability (MTT, chapter 4) after the onset of compression within 24 hours. However, thereafter deformation did not result in a further increase in cell death to 100% by day 5. The effect of hypoxia was apparent after 24 hours, but only resulted in increased cell death after 48 hours. Although the effect of imposed lactic acidosis appeared to be instantaneous, the time to produce damaging amounts by hypoxic cells was considerably more extended. These findings support the hypothesis presented by Stekelenburg (2005b) that initially cell damage is dominated by deformation, but it is aggravated by ischemia at later time points.

The present study did not simulate ischemia completely as hyperkalemia and hypercapnia were not included. Apart from ischemia and deformation, reperfusion is another potential source of damage development in compressed tissues. The influence of this factor may be reduced by gradual reperfusion of ischemic tissues, which has been shown to significantly reduce tissue reperfusion damage (Unal et al., 2001; Durrani et al., 2006).

Interstitial and lymphatic transport may be significantly hindered during tissue compression. This factor was not directly examined in the study and, in addition, the



transport of waste products to other organs for elimination was also not possible in the engineered tissues. Nonetheless, even in the absence of these factors, the multifactorial base of pressure ulcer development in deep tissues from compression and ischemic factors has been confirmed.

In conclusion, within muscle tissues, both deformation and ischemia can play a role in damaging tissue. However, deformation affected tissue viability over a short time period, whereas the tissue model was better equipped to withstand ischemic factors and thus could survive ischemia alone for longer periods. It should be noted that the applied deformation was 34% and that higher deformations may occur, resulting in increased amounts of cell death. The ischemic factors tended to initiate cellular survival processes before cell death. During hypoxia, anaerobic metabolism was adopted resulting in lactic acid accumulation and acidification of the medium. In order to maintain anaerobic metabolism, the tissue consumed more glucose. Thus, this process may continue as long as sufficient glucose is available. In addition, lactic acidification should not exceed threshold values. Moreover, metabolism was downregulated by oxygen conformance behavior together with an energy-saving mechanism induced by acidification. When these factors were all combined and imposed for 5 days, the deformation had damaged the tissue initially. Subsequently, the hypoxia induced elevated lactic acid production, eventually exceeding the acid threshold, as there was ample glucose present to continue metabolism. Thus, as long as no deformation or ischemic thresholds are exceeded, the tissue may survive compression.

## **5.5 Acknowledgments**

The authors thank Rob van den Berg for his contribution to the design and manufacturing of the experimental system. This research was supported by the Dutch Technology Foundation STW, applied science division of NWO, and the Technology Program of the Ministry of Economic Affairs.

# Chapter 6

## General discussion

## **6.1 Introductory remarks**

Pressure ulcer prevalence figures are unacceptably high. In the Netherlands, they range from 10% in home healthcare to 24% in nursing homes (Halfens et al., 2006). The ulcers are not only very painful and increase length of hospitalization; they may also compromise quality of life and even lead to death. However, the etiology, or more correctly etiologies, of pressure ulcers is still largely unknown. The ulceration may start at superficial skin layers or from within the deep tissues, such as the skeletal muscle. Indeed ulcers affecting the deep tissue layers can originate from superficial layers with progression towards underlying tissue, or the origin of tissue breakdown can be located inside the deep tissue itself.

In general, risk factors for pressure ulcer development are associated with duration and amount of tissue compression, and tissue mechanical properties: e.g. immobility (duration), age (properties), nutritional status (properties), and underlying pathology (all). Patient subgroups such as the spinal cord injured are particularly susceptible to the development of these ulcers, as they are both immobile, insensate and exhibit altered mechanical tissue properties. Another subgroup consists of patients that are kept on emergency room stretchers or operating tables for more than three hours.

The present thesis focused on the development of deep pressure ulcers affecting skeletal muscle tissue. To elucidate on pressure ulcer etiology, first, a model system was required to enable separation of factors proposed to contribute to damage development. For this purpose, an existing engineered in vitro model of skeletal muscle was rigorously adapted and characterized. In addition, to facilitate real time monitoring of cell death, a dual staining technique was developed and extensively studied. The in vitro approach allowed for a high degree of control over environmental factors. An experimental arrangement was built, which permitted variation of the degree of deformation, oxygenation, and acidification. Finally, the model system was employed to investigate the influences of deformation and ischemic factors on tissue viability.

This chapter will discuss the methods applied and their limitations. The most important findings will be summarized and their implications for future research and applicability to clinical practice will be addressed.

## **6.2 Engineered skeletal muscle**

The procedures for the preparation of the engineered muscle constructs that was presented in chapter 2 was adapted from a combination of existing protocols (Vandenburgh et al., 1996; Okano and Matsuda, 1997, 1998a; Breuls et al., 2003). Suspension of C2C12 cells in collagen gels was a more consistent method for preparing engineered muscle than one depending on a co-culture with fibroblasts to provide for extracellular matrix components (Dennis and Kosnik, 2000; Dennis et al., 2001). In the latter approach the fine-tuning of all parameters for obtaining a reproducible construct with sufficient integrity, such as ratio of myoblasts/fibroblasts and medium additives, is a time-consuming process.

All attempts to generate engineered muscle presented in the literature had one common limitation, namely, the construct dimensions. As a result of limited oxygen and nutrient transport through a dense cellular layer in the absence of vascularization, the maximum distance of viable cells from a surface exposed to medium is between 100 and 200  $\mu\text{m}$  (Radisic et al., 2006).

Several attempts have been made to produce vascularized muscle in an *in vivo* setting (Okano and Matsuda, 1998b; Bach et al., 2006; Borschel et al., 2006). Recently, however, progress was made with *in vitro* engineering of vascularized muscle tissue from myoblasts, fibroblasts, and endothelial cells (Levenberg et al., 2005). In future, this technique may be improved to assist in creating larger engineered tissues.

The majority of literature available on production of engineered muscle tissue is aimed at creating tissue for implantation purposes; either for restoring lost tissue with a functional contractile equivalent (Fauza et al., 2001; Kosnik et al., 2001; Bach et al., 2004; Beier et al., 2006; Kamochi et al., 2006) or for protein delivery purposes (Powell et al., 1999; Payumo et al., 2002; Lu et al., 2003). Recently, a new application of engineered muscle was proposed in meat production (Benjaminson et al., 2002; Edelman et al., 2005).

By contrast, the muscle model used in the present thesis was optimized for reproducibility and ease of production and within these boundaries a maximum resemblance with native tissue. The model did not contain any artificial or natural vascularization, which necessarily restricted the degree of cellular viability, but simplified mechanical loading profiles. Cellular differentiation towards mature muscle fibers was incomplete as no cross-striations or contractions were observed. However, improvements were made compared to the muscle model previously developed in the host lab (Breuls et al., 2003a). Cellular alignment was introduced and the model was made more robust and reproducible. Additionally, the tissue was characterized and contained proteins that indicated differentiation beyond the myoblast stage.

Differentiation might be enhanced by adjusting substrate stiffness and by the application of mechanical (Vandenburgh et al., 1989; Powell et al., 2002) and electrical (Dusterhoft and Pette, 1990; De Deyne, 2000) stimuli. Also, stimulation by different growth factors may further improve differentiation (Bach et al., 1995; Conejo et al., 2001). With respect to differentiation capacities, neonatal myoblasts or muscle-derived stem cells may present a more potent cell source for muscle tissue engineering than the applied C2C12 cell line (Kosnik et al., 2001; Peng and Huard, 2004).

### **6.3 Monitoring cell and tissue status**

Tissue damage can be observed from its morphology, expression of proteins and/or release of proteins. Both the observation of tissue status without disruption of the culture and imaging muscle constructs which are essentially opaque limits the range of applicable techniques and, thus, fluorescence microscopy and analysis of small

volumes of the medium were the preferred methods. In chapter 4, global development of tissue damage was established from local cell death patterns. Subsequently, apoptosis and necrosis were distinguished in the development of cell death. Both probes were based on the permeability of cell membranes. Upon entering an apoptotic pathway, membrane permeability is compromised allowing certain molecules, such as YO-PRO-1, to enter the cytoplasm. After completion of apoptosis, the state of necrosis is reached and membrane integrity is further compromised, which permits the entry of the larger marker for necrosis, propidium iodide. Both markers stain for cellular DNA. However, apoptosis may also be indicated by other markers that interact with apoptosis-specific events. For example, JC-1, is applied to detect mitochondrial depolarization (Salvioli et al., 1997) and annexin V is used to label phosphatidyl serine exposure (Vermes et al., 1995). Even more specific labeling is possible to eventually identify the apoptosis pathways that are activated by, for example, cellular deformation or ischemia.

Tissue status can additionally be derived by the analysis of the culture medium that is surrounding the tissue. Proteins and other molecules that are produced upon stimulation may diffuse or be transported into the medium. Cell damage may also facilitate release of proteins that are normally confined to the cytosol. In chapter 5, information on tissue status was obtained by analysis of metabolic and damage markers. Glucose consumption and lactate production, together with medium pH can reveal effects of environmental factors on cells that do not lead to irreversible cell damage. Additionally, MTT conversion was another indicator of cellular metabolism (figure 5.7). Changes in these metabolic determinants, however, may indicate altered metabolic activity but may at the same time display a different number of cells exhibiting an equal metabolic activity. Therefore, complementary online information on cell damage was provided by LDH release from irreversibly damaged cells.

#### **6.4 Imposing experimental compression and ischemia**

The applied compression in the model system was based on a prescribed global displacement rather than a prescribed load acting on the tissue's surface. Application of the latter would result in continuously increasing tissue deformation, or creep response. This is in conflict with the natural situation for a subject whose tissues are loaded with body weight by sitting or lying. In addition, the engineered tissue was not surrounded by epimysium or by other tissues and its mechanical integrity was not of comparable magnitude to obtain a steady deformed state. Therefore, it was assumed that physiologically occurring deformations of muscle tissue should be imposed to mimic the loading condition. The engineered tissue was allowed to deform in an unconfined way, which is clearly not an accurate representation of the physiological loading conditions. However, it was selected because the alternative configuration involving confinement of the muscle tissue model would necessarily complicate the application of mechanical loading and interfere with diffusion between the tissue and medium.

Several models have been applied to study the effect of ischemia or hypoxia in an in vitro setting (Liu et al., 1996; Arthur et al., 1998; Killillea et al., 2000; Louch et al., 2005). All aspects of ischemia can be simulated, namely, hypoxia or anoxia, lactate build-up, glucose depletion, acidification, hypercapnia and hyperkalemia. To simulate oxygen deprivation, the cell or tissue culture is immersed in a medium or buffer solution that is equilibrated with a nitrogenous gas. Glucose deprivation is simulated by culturing the cells in a buffer solution devoid of glucose. Acidification can be obtained by the addition of lactic acid or an equivalent biological acid. Hypercapnia and hyperkalemia may be attained in a comparable way. Only some of these factors were included in the study presented in chapter 5. By contrast, hypercapnia was excluded because its effect would be on the acidity of the medium by acting through the bicarbonate buffer. Hyperkalemia was also excluded as it is thought to mainly affect the excitability and contractility of muscle tissue and therefore be of limited relevance in the present model system (Hansen et al., 2005).

### **6.5 Most important findings and implications**

Chapters 4 and 5 were devoted to studying effects of both deformation and ischemic factors on tissue metabolism and viability. The former focused on whether apoptotic pathways were induced by either 20% or 40% deformation, or by tissue hypoxia, the latter was considered to be the most relevant aspect of ischemia to influence tissue viability. The unpredicted finding indicated that while deformation was able to cause increases in apoptotic and necrotic cell death with increasing magnitudes of deformation, no apparent effect of hypoxia on cell death development was observed within 22 hours (figure 4.7). This observation suggested an important role for deformation in the onset of apoptosis and eventual tissue breakdown. Based on these results, experimental periods were extended and ischemic factors other than hypoxia were examined in chapter 5.

The apparent absence of a response to hypoxia by the cells within 22 hours may be explained by the delayed onset of actual hypoxia in the system. However, hypoxia was obtained within 22 hours. More importantly, it may be caused by the oxygen conformance behavior of the cells. This was described by Arthur et al. (2000) as an adaptive response of cells to decrease their energy demands and hence consume less oxygen under hypoxic conditions, without decreasing their amount of energy present (ATP). The more severe the hypoxic or even anoxic state, the more the cells conform to this by selectively down-regulating cellular processes.

In chapter 5, it was shown that the supposed oxygen conformance behavior is metabolically assisted by a switch to anaerobic metabolism. A direct result of adopting anaerobic metabolism was that lactate started to accumulate in the medium (e.g. figure 5.5b). Besides this, it was found that elevated lactate concentrations further down-regulated metabolism. However, eventually a lactic acid (or pH) threshold was exceeded and further metabolism was arrested. Additionally, once glucose was depleted, cell viability was compromised.

Together, the results obtained in chapters 4 and 5 strongly suggest an early role for deformation in the development of muscle tissue apoptosis and subsequent or direct necrosis. This is comprehensible as ischemic factors appeared to impinge on cellular metabolism first concomitantly with activation of adaptational processes, and once lactic acid or glucose thresholds were exceeded, cell death followed. Based on these results, a sequence of events following tissue compression is proposed in figure 6.1.

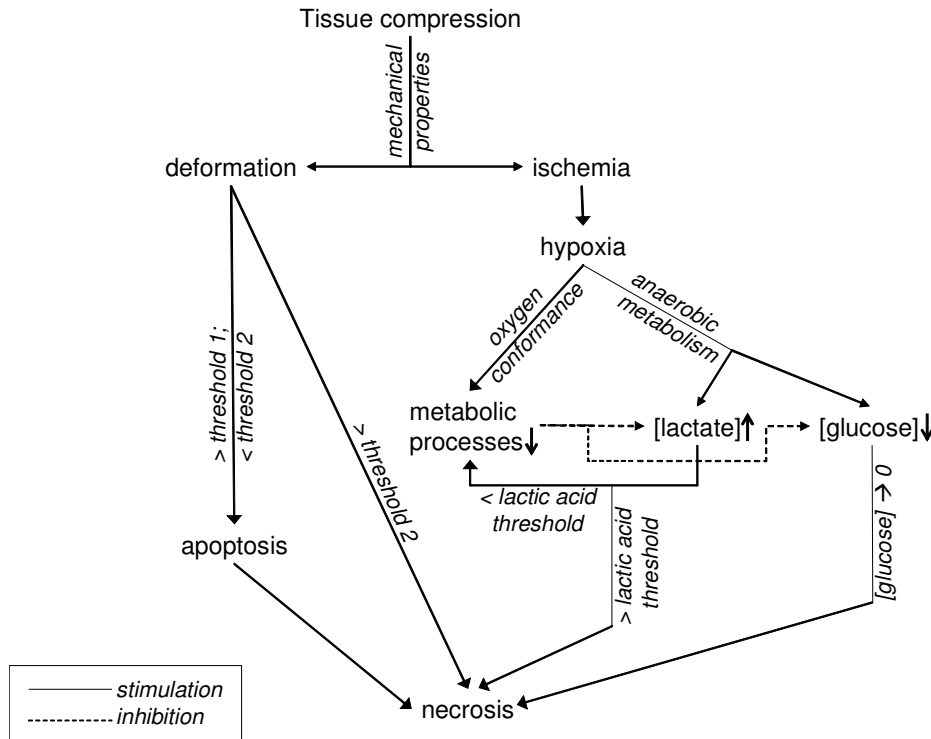


Figure 6.1: Schematic depicting the hypothesized order of events taking place during tissue compression. Tissue compression will act through cellular deformation and ischemia on cell death development and metabolism. Thresholds for deformation, acidification and glucose deprivation dictate the maintenance of tissue viability.

Tissue compression will lead, depending on tissue mechanical properties, to tissue and cellular deformation on the one hand and on the other hand to ischemia by mechanical closure of blood vessels. If deformation exceeds a lower threshold (figure 6.1, (1)), apoptosis may be enhanced in the cells but if a higher threshold (figure 6.1, (2)) is surpassed, cells will enter necrosis. Ischemia compromises hypoxia, which will induce the muscle cells to conform to lower oxygen tensions and thus down-regulate metabolic processes. Additionally, anaerobic metabolism will be adopted leading to increased glucose consumption and increased lactate production. Lactate production will, however, further down-regulate metabolic processes, causing an inhibition of lactate production and glucose consumption (figure 6.1, dashed lines). Once a lactic acid threshold is exceeded, the tissue's cells may become necrotic (possibly through apoptosis). In a comparable fashion, glucose deprivation towards 0 mM will induce necrosis in the tissue.

It would be impudent to translate the current results on muscle models directly towards animal or human situations. Nonetheless comparisons between both ends of the hierarchical spectrum are still appropriate. Indeed following the work of previous investigators (Breuls et al., 2003a; Wang et al., 2005), increased cell death has been associated with both increasing time and deformations. Also, use of an in vivo rodent model in the host lab has shown that deformation combined with ischemia rather than ischemia alone caused muscle damage if loaded for 2 hours (Stekelenburg, 2006). In addition, a strong correlation between highly deformed ischemic regions and damage development was observed. Together with the in vitro findings in the engineered model, this may suggest a more critical role for cellular deformation in the onset of deep tissue damage development than has been previously assumed. It needs to be emphasized that the observed effects of ischemia and deformation were within a relatively short 2-hour period.

Another factor that should not be ignored when considering pressure ulcer etiology is the effect of mechanical loading on tissue diffusion properties. Both, the in vivo and the in vitro presence of collagen fibers in the extracellular environment hinders diffusion (Ramanujan et al., 2002). Its effect on solute diffusion will indeed increase as compression will lead to a decrease in water content and thus a relative increase in collagen concentration and thus the effective density of the fibrillar network (Netti et al., 2000; Ramanujan et al., 2002; Evans and Quinn, 2006). It is proposed that the effects of compression on diffusional properties in the extracellular environment will add to the problem associated with ischemia. Compression will therefore not only limit the supply of blood by closure of the vessels, but, in addition, the transport through the interstitial space from the vessels to the cells is compromised. To the author's knowledge, the effects of compression on transport processes inside single cells are as yet unknown but may, if present, contribute to even more adverse effects of compression on transport phenomena. Indeed, the impairment of transport during compression may explain the apparent absence of enhanced T2 values during compression as obtained by MRI techniques (Stekelenburg, 2005b). A microscopic technique, for example, based on fluorescence recovery after photobleaching (FRAP), may be applied to examine diffusional changes in the cytoplasm upon cellular compression. Furthermore the staining and visualization of intracellular structures, such as the cytoskeletal proteins that are involved in intracellular transport, might increase the overall understanding of the effects of deformation on cellular processes.

## **6.6 Future of pressure ulcer research**

Apart from the aforementioned factors, other issues need to be addressed in the future. As mentioned before, superficial and deep ulcers have different pathogeneses. Detection of the deep ulcers under the intact skin is difficult as mere visual inspection of the skin will not provide full thickness information on tissue status. Though Shea's classification system (Shea, 1975) has been widely used and cited, the description of the closed pressure ulcers, incorporating deep tissue injury (DTI), was not included in current pressure ulcer staging methods. However, the staging determines which clinical



treatment protocol will be adopted. This was recently recognized by the EPUAP and NPUAP (European and National Pressure Ulcer Advisory Panels, respectively) and efforts will be made to include DTI in the staging of pressure ulcers in the future. Development of tools, which would facilitate obtaining objective information on deep tissue layers, also needs to be encouraged. Another issue in ulcer staging that was acknowledged was that once an ulcer has been staged, it may evolve into a different stage, which emphasizes the temporal component of the clinical problem.

Table 6.1: Overview of skeletal muscle markers and their detection times in plasma.

Marker	Detection time after damage in plasma	Reference(s)
FABP	30 min. - <24 hr	Sorichter et al., 1998
Mb	30 min. - <24 hr	Sorichter et al., 1997; 1998
IL-6	<6 hr	MacIntyre et al., 2001
sTnI	6 hr - < 24 hr	Sorichter et al., 1997
CK	2hr – 48 hr	Sorichter et al., 1998
MHC	6 hr – 7 d	Sorichter et al., 1997; 2001

*FABP: fatty acid binding protein; Mb: myoglobin; IL-6: interleukin-6; sTnI: skeletal troponin I; CK: creatine kinase; MHC: myosin heavy chain; min.: minutes; hr: hours; d: days.*

Besides detection methods based on visualization of deep tissues, the presence of a deep ulcer may be revealed by measurement of muscle-specific proteins that are released into the bloodstream upon cell damage or death, as provided as an overview in table 6.1. The standard markers, popularly termed biomarkers, include creatine kinase, myosin heavy chain and myoglobin. These markers, though, are not specific for skeletal muscle damage. More recently, a ratio value of myoglobin to FABP, which is estimated to be between 20 and 70 was proposed as a specific marker for skeletal muscle damage (van Nieuwenhoven et al., 1995). Skeletal muscle damage can, in addition, be assessed from skeletal troponin I (sTnI) elevation in plasma (Takahashi et al., 1996; Sorichter et al., 1997; Simpson et al., 2005; Life Diagnostics, Inc.). Another category of damage indices may be based on the early markers that are up-regulated and released due to an inflammatory response. For example, IL-6 has been shown to be up-regulated in skeletal muscle damaged after intense exercise (MacIntyre et al., 2001; Peake et al., 2005; Gomez-Merino et al., 2006). Interestingly, Bonnefoy and colleagues found significantly elevated levels of IL-6 in blood samples of patients with stage III or IV pressure ulcers compared to blood of control subjects.

In addition to molecular markers, a physical parameter, the transcutaneous oxygen tension, was proposed as a measure, capable of identifying paraplegic patients at risk of developing pressure ulcers (Liu et al., 1999). Another approach utilizes blood flow recovery time after pressure relief as a promising measure for patient susceptibility (Meijer et al., 1989; 1994). However, these techniques are not simple, expensive and in the case of transcutaneous gas tensions, heating to 44°C may be required.

As has been previously proposed (Stekelenburg, 2005b), an intelligent marker system needs to be developed, which should be applicable in particular risk groups, such as immobile elderly and spinal cord injured patients. Early detection of deep tissue injury is essential, to ensure that intervention will prevent progressive damage towards the skin surface. The sensor should be able to identify early damage development in deep tissues. Damage markers may be included in a 'credit card system' similar to the one presented by Chan et al. (2003), which applied H-FABP immuno-detection for early detection of cardiac failure. Daily detection methods in patients at risk of development of deep tissue injury may preferably be based on protein detection in body fluids other than blood, such as the patient's urine or saliva. Myoglobin levels, for example, may be detected in human urine.

Tissue that may be involved in deep tissue injury but has not received much attention is the bursa (Hooker et al., 1988). Bursae produce synovial fluid to reduce friction between muscle, tendon and bone tissue. They also serve to provide tissue cushioning. Bursae may vary in number, position, and histological appearance (Dunn et al., 2003), and some are located in common (deep) pressure ulcer sites, including the trochanteric bursa, gluteofemoral bursa, and the ischial bursa. During pressure ulcer surgery, they are often excised (Dardour et al., 1984) although, more recently, sclerotherapy (treatment based on tissue shrinkage) has been proposed as an alternative treatment method (Hayashi et al., 2004).

The contents of this thesis focused on effects of compression and simulated factors of ischemia on muscle tissue viability. The tissue, however, was a simplified model of living muscular tissue, lacking vasculature and innervation. In addition, not all the stimuli that have been proposed to cause tissue damage in pressure ulcer development were examined. For example, occlusion of lymphatic vessels and reperfusion are both considered to contribute to damage development. The latter factor may be simulated to a certain extent in an *in vitro* cultured model system. Reperfusion experiments in animal models have already provided a considerable amount of data on its effect on tissue viability. It has been shown, for example, that the adverse effect of reperfusion on tissue viability may be diminished by gradually unloading the tissue (Unal et al., 2001; Durrani et al., 2006). Such a clinically relevant result could be implemented in the turning regimen that is applied to regularly relieve the patient's tissue from continuous loading by gradually turning them. An equivalent approach may be necessary during tissue loading at high frequencies, a loading regimen which has been shown to be more damaging to the cells than applying the load at a slow rate to an equivalent tissue deformation (Peeters et al., 2005b).

Pressure ulcers seldom occur in healthy subjects (Bliss, 1998). Obviously, apart from the duration and magnitude of tissue compression and possibly resulting transport impairments, other predisposing factors play a role in the onset of deep pressure ulcers. Illness or trauma can disturb naturally present equilibria to an extent that enables pressure ulcer development (Bliss, 1998). Disturbing factors may include circulatory

disturbances, malnutrition, administration of medication, and dehydration. Other factors such as immobility, age, temperature, sensory deficit, and incontinence may also be involved. In vitro models can contribute to the understanding of the fundamental processes underlying pressure ulcer development. The ability to control most predisposing factors independently of each other in these models can facilitate the quantification of the relative contribution of these factors to the etiology of pressure ulcers. The effects of malnutrition and medication for example, could be simulated by controlling medium composition. In addition, an illness may be simulated by incorporating cells derived from patients into the muscle model or by imitating tissue adaptations caused by a particular disease process.

Ultimately, a full thickness in vitro model consisting of several tissue layers, such as skin, fat, muscle and bone, may be developed not only to study damage development, but also to serve as a model for investigating new prevention and treatment strategies. The applicability of, for example, ischemic preconditioning (Addison et al., 2003), electrical stimulation therapies (Bogie et al., 2000), nutritional supplementation (Houwing et al., 2003) and possibly deformation preconditioning in preventing or treating pressure ulcers could then be examined. Additionally, apoptotic pathways may be explored in a tissue model to identify molecules (e.g. caspases) that are activated in the processes associated with apoptosis, with the potential of developing the successful intervention of therapeutic agents (Denault and Slavesen, 2002).

# References

- Addison, P. D. et al. (2003). Noninvasive remote ischemic preconditioning for global protection of skeletal muscle against infarction. *Am. J. Physiol. Heart Circ. Physiol.*, **285**, H1435-H1443.
- Andres, V. and Walsh, K. (1996). Myogenin expression, cell cycle withdrawal, and phenotypic differentiation are temporally separable events that precede cell fusion upon myogenesis. *J. Cell Biol.*, **132**, 657-666.
- Ankrom, M. A. et al. (2005). Pressure-related deep tissue injury under intact skin and the current pressure ulcer staging systems. *Adv. Skin Wound. Care*, **18**, 35-42.
- Arthur, P. G., Giles, J. J., and Wakeford, C. M. (2000). Protein synthesis during oxygen conformance and severe hypoxia in the mouse muscle cell line C2C12. *Biochim. Biophys. Acta*, **1475**, 83-89.
- Bach, L. A., Salemi, R., and Leeding, K. S. (1995). Roles of insulin-like growth factor (IGF) receptors and IGF-binding proteins in IGF-II-induced proliferation and differentiation of L6A1 rat myoblasts. *Endocrinology*, **136**, 5061-5069.
- Barbenel, J. C. (1991). Pressure management. *Prosthet. Orthot. Int.*, **15**, 225-231.
- Begum, S., Komiyama, M., Toyota, N., Obinata, T., Maruyama, K., and Shimada, Y. (1998). Differentiation of muscle-specific proteins in chicken somites as studied by immunofluorescence microscopy. *Cell Tissue Res.*, **293**, 305-311.
- Benders, A. A., van Kuppevelt, T. H., Oosterhof, A., and Veerkamp, J. H. (1991). The biochemical and structural maturation of human skeletal muscle cells in culture: the effect of the serum substitute Ultrosor G. *Exp. Cell Res.*, **195**, 284-294.
- Benjaminson, M. A., Gilchrist, J. A., and Lorenz, M. (2002). In vitro edible muscle protein production system (MPPS): stage 1, fish. *Acta Astronaut.*, **51**, 879-889.
- Blaisdell, F. W. (2002). The pathophysiology of skeletal muscle ischemia and the reperfusion syndrome: a review. *Cardiovasc. Surg.*, **10**, 620-630.
- Blankenberg, F. G., Tait, J. F., and Strauss, H. W. (2000). Apoptotic cell death: its implications for imaging in the next millennium. *Eur. J. Nucl. Med.*, **27**, 359-367.
- Blau, H. M., Chiu, C. P., and Webster, C. (1983). Cytoplasmic activation of human nuclear genes in stable heterocaryons. *Cell*, **32**, 1171-1180.
- Bliss, M. R. (1998). Pressure injuries: causes and prevention. *Hosp. Med.*, **59**, 841-844.
- Boffa, D. J. et al. (2005). Measurement of apoptosis of intact human islets by confocal optical sectioning and stereologic analysis of YO-PRO-1-stained islets. *Transplantation*, **79**, 842-845.
- Bogie, K. M., Reger, S. I., Levine, S. P., and Sahgal, V. (2000). Electrical stimulation for pressure sore prevention and wound healing. *Assist. Technol.*, **12**, 50-66.
- Bosboom, E. M., Bouten, C. V., Oomens, C. W., van Straaten, H. W., Baaijens, F. P., and Kuipers, H. (2001). Quantification and localisation of damage in rat muscles after controlled loading; a new approach to study the aetiology of pressure sores. *Med. Eng. Phys.*, **23**, 195-200.

## References

- Bours, G. J. J. W., Halfens, R. J. G., Abu-Saad, H. H., and Grol, R. T. P. M. (2002). Prevalence, prevention, and treatment of pressure ulcers: descriptive study in 89 institutions in the Netherlands. *Res. Nurs. Health*, **25**, 99-110.
- Bouten, C. V., Knight, M. M., Lee, D. A., and Bader, D. L. (2001). Compressive deformation and damage of muscle cell subpopulations in a model system. *Ann. Biomed. Eng.*, **29**, 153-163.
- Bouten, C. V., Oomens, C. W., Baaijens, F. P., and Bader, D. L. (2003a). The etiology of pressure ulcers: skin deep or muscle bound? *Arch. Phys. Med. Rehabil.*, **84**, 616-619.
- Bouten, C. V. C., Breuls, R. G. M., Peeters, E. A. G., Oomens, C. W. J., and Baaijens, F. P. T. (2003b). In vitro models to study compressive strain-induced muscle cell damage. *Biorheology*, **40**, 383-388.
- Boutillier, R. G. (2001). Mechanisms of cell survival in hypoxia and hypothermia. *J. Exp. Biol.*, **204**, 3171-3181.
- Braden, B. and Bergstrom, N. (1987). A conceptual schema for the study of the etiology of pressure sores. *Rehabil. Nurs.*, **12**, 8-12.
- Breuls, R. G. M., Bouten, C. V. C., Oomens, C. W. J., Bader, D. L., and Baaijens, F. P. T. (2003a). Compression induced cell damage in engineered muscle tissue: an in vitro model to study pressure ulcer aetiology. *Ann. Biomed. Eng.*, **31**, 1357-1364.
- Breuls, R. G. M., Mol, A., Petterson, R., Oomens, C. W. J., Baaijens, F. P. T., and Bouten, C. V. C. (2003b). Monitoring local cell viability in engineered tissues: a fast, quantitative, and nondestructive approach. *Tissue Eng.*, **9**, 269-281.
- Bronneberg, D., Bouten, C. V. C., Oomens, C. W. J., van Kemenade, P. M., and Baaijens, F. P. T. (2006). An in vitro model system to study the damaging effects of prolonged mechanical loading of the epidermis. *Annals of Biomed. Eng.*, **34**, 506-514.
- Brunelle, J. K. and Chandel, N. S. (2002). Oxygen deprivation induced cell death: an update. *Apoptosis*, **7**, 475-482.
- Burattini, S., Ferri, P., Battistelli, M., Curci, R., Luchetti, F., and Falcieri, E. (2004). C2C12 murine myoblasts as a model of skeletal muscle development: morpho-functional characterization. *Eur. J. Histochem.*, **48**, 223-233.
- Burnell, J. M. (1968). In vivo response of muscle to changes in CO<sub>2</sub> tension or extracellular bicarbonate. *Am. J. Physiol.*, **215**, 1376-1383.
- Byrne, D. W. and Salzberg, C. A. (1996). Major risk factors for pressure ulcers in the spinal cord disabled: a literature review. *Spinal Cord.*, **34**, 255-263.
- Caliri, M. H. L. (2005). Spinal cord injury and pressure ulcers. *Nurs. Clin. North Am.*, **40**, 337-347.
- Castro, M. J., Apple, D. F. J., Staron, R. S., Campos, G. E., and Dudley, G. A. (1999). Influence of complete spinal cord injury on skeletal muscle within 6 mo of injury. *J. Appl. Physiol.*, **86**, 350-358.
- Chan, C. P. Y. et al. (2003). Development of a quantitative lateral-flow assay for rapid detection of fatty acid-binding protein. *J. Immunol. Methods*, **279**, 91-100.
- Cheema, U., Brown, R., Mudera, V., Yang, S. Y., McGrouther, G., and Goldspink, G. (2005). Mechanical signals and IGF-I gene splicing in vitro in relation to development of skeletal muscle. *J. Cell Physiol.*, **202**, 67-75.
- Chen, Y., Devivo, M. J., and Jackson, A. B. (2005). Pressure ulcer prevalence in people with spinal cord injury: age-period-duration effects. *Arch. Phys. Med. Rehabil.*, **86**, 1208-1213.

- Cheng, W. et al. (1995). Stretch-induced programmed myocyte cell death. *J. Clin. Invest.*, **96**, 2247-2259.
- Chung, K. T. (1983). The significance of azo-reduction in the mutagenesis and carcinogenesis of azo dyes. *Mutat. Res.*, **114**, 269-281.
- Conejo, R., Valverde, A. M., Benito, M., and Lorenzo, M. (2001). Insulin produces myogenesis in C2C12 myoblasts by induction of NF-kappaB and downregulation of AP-1 activities. *J. Cell Physiol.*, **186**, 82-94.
- Coolican, S. A., Samuel, D. S., Ewton, D. Z., McWade, F. J., and Florini, J. R. (1997). The mitogenic and myogenic actions of insulin-like growth factors utilize distinct signaling pathways. *J. Biol. Chem.*, **272**, 6653-6662.
- Covington, M. D., Bayless, K. J., Burghardt, R. C., Davis, G. E., and Parrish, A. R. (2005). Ischemia-induced cleavage of cadherins in NRK cells: evidence for a role of metalloproteinases. *Am. J. Physiol. Renal Physiol.*, **289**, F280-F288.
- Daniel, R. K., Priest, D. L., and Wheatley, D. C. (1981). Etiologic factors in pressure sores: an experimental model. *Arch. Phys. Med. Rehabil.*, **62**, 492-498.
- Dardour, J. C., Vilain, R., and Castro, D. (1984). [Evaluation of 10 years of surgical treatment for decubitus ulcer] Bilan de dix ans de traitement chirurgical des escarres. *Sem. Hop.*, **60**, 1051-1056.
- De Coppi, P. et al. (2005). Angiogenic gene-modified muscle cells for enhancement of tissue formation. *Tissue Eng.*, **11**, 1034-1044.
- De Deyne, P. G. (2000). Formation of sarcomeres in developing myotubes: role of mechanical stretch and contractile activation. *Am. J. Physiol. Cell Physiol.*, **279**, C1801-C1811.
- Delgado, I., Huang, X., Jones, S., Zhang, L., Hatcher, R., Gao, B., and Zhang, P. (2003). Dynamic gene expression during the onset of myoblast differentiation in vitro. *Genomics*, **82**, 109-121.
- Denault, J. B. and Salvesen, G. S. (2002). Caspases: keys in the ignition of cell death. *Chem. Rev.*, **102**, 4489-4500.
- Dennis, R. G. and Kosnik, P. E. (2000). Excitability and isometric contractile properties of mammalian skeletal muscle constructs engineered in vitro. *In Vitro Cell. Dev. Biol. Anim.*, **36**, 327-35.
- Dennis, R. G., Kosnik, P. E., Gilbert, M. E., and Faulkner, J. A. (2001). Excitability and contractility of skeletal muscle engineered from primary cultures and cell lines. *Am. J. Physiol. Cell Physiol.*, **280**, C288-C295.
- Dinsdale, S. M. (1974). Decubitus ulcers: role of pressure and friction in causation. *Arch. Phys. Med. Rehabil.*, **55**, 147-152.
- Donnelly, J. and National Pressure Ulcer Advisory Panel (2005). Should we include deep tissue injury in pressure ulcer staging systems? The NPUAP debate. *J. Wound. Care*, **14**, 207-210.
- Dunn, T., Heller, C. A., McCarthy, S. W., and Dos Remedios, C. (2003). Anatomical study of the "trochanteric bursa". *Clin. Anat.*, **16**, 233-240.
- Durrani, N. K., Yavuzer, R., Mittal, V., Bradford, M. M., Loboeki, C., and Silberberg, B. (2006). The effect of gradually increased blood flow on ischemia-reperfusion injury in rat kidney. *Am. J. Surg.*, **191**, 334-337.
- Dusterhoft, S. and Pette, D. (1990). Effects of electrically induced contractile activity on cultured embryonic chick breast muscle cells. *Differentiation*, **44**, 178-184.

## References

- Dusterhoft, S. and Pette, D. (1993). Satellite cells from slow rat muscle express slow myosin under appropriate culture conditions. *Differentiation*, **53**, 25-33.
- Edelman, P. D., McFarland, D. C., Mironov, V. A., and Matheny, J. G. (2005). Commentary: In vitro-cultured meat production. *Tissue Eng.*, **11**, 659-662.
- Engler, A. J., Griffin, M. A., Sen, S., Bonnemann, C. G., Sweeney, H. L., and Discher, D. E. (2004). Myotubes differentiate optimally on substrates with tissue-like stiffness: pathological implications for soft or stiff microenvironments. *J. Cell Biol.*, **166**, 877-887.
- Evans, R. C. and Quinn, T. M. (2006). Solute convection in dynamically compressed cartilage. *J. Biomech.*, **39**, 1048-1055.
- Ewton, D. Z., Roof, S. L., Magri, K. A., McWade, F. J., and Florini, J. R. (1994). IGF-II is more active than IGF-I in stimulating L6A1 myogenesis: greater mitogenic actions of IGF-I delay differentiation. *J. Cell Physiol.*, **161**, 277-284.
- Ferrier, G. R. and Howlett, S. E. (2005). Pretreatment with pinacidil promotes arrhythmias in an isolated tissue model of cardiac ischemia and reperfusion. *J. Pharmacol. Exp. Ther.*, **313**, 823-830.
- Florini, J. R., Ewton, D. Z., and Coolican, S. A. (1996). Growth hormone and the insulin-like growth factor system in myogenesis. *Endocr. Rev.*, **17**, 481-517.
- Fuhrer, M. J., Garber, S. L., Rintala, D. H., Clearman, R., and Hart, K. A. (1993). Pressure ulcers in community-resident persons with spinal cord injury: prevalence and risk factors. *Arch. Phys. Med. Rehabil.*, **74**, 1172-1177.
- Furst, D. O., Osborn, M., and Weber, K. (1989). Myogenesis in the mouse embryo: differential onset of expression of myogenic proteins and the involvement of titin in myofibril assembly. *J. Cell Biol.*, **109**, 517-527.
- Garber, S. L. and Rintala, D. H. (2003). Pressure ulcers in veterans with spinal cord injury: a retrospective study. *J. Rehabil. Res. Dev.*, **40**, 433-441.
- Gawlitta, D., Oomens, C. W. J., Baaijens, F. P. T., and Bouten, C. V. C. (2004). Evaluation of a Continuous Quantification Method of Apoptosis and Necrosis in Tissue Cultures. *Cytotechnology*, **46**, 139-150.
- Gawlitta, D., Li, W., Oomens, C. W., Baaijens, F. P., Bader, D. L., and Bouten, C. V. (2006). The relative contributions of compression and hypoxia to development of muscle tissue damage: an in-vitro study. *Ann. Biomed. Eng.*, accepted.
- Gefen, A., Gefen, N., Linder-Ganz, E., and Margulies, S. S. (2005). In vivo muscle stiffening under bone compression promotes deep pressure sores. *J. Biomech. Eng.*, **127**, 512-524.
- Graham, R. M. et al. (2004). A unique pathway of cardiac myocyte death caused by hypoxia-acidosis. *J. Exp. Biol.*, **207**, 3189-3200.
- Griffin, M. A., Sen, S., Sweeney, H. L., and Discher, D. E. (2004). Adhesion-contractile balance in myocyte differentiation. *J. Cell Sci.*, **117**, 5855-5863.
- Griffith, C. K., Miller, C., Sainson, R. C. A., Calvert, J. W., Jeon, N. L., Hughes, C. C. W., and George, S. C. (2005). Diffusion limits of an in vitro thick prevascularized tissue. *Tissue Eng.*, **11**, 257-266.
- Halfens, R. J. G., Janssen, M. A. P., and Meijers, J. M. M. (2006). Decubitus. *Rapportage resultaten Landelijke Prevalentiemeting Zorgproblemen 2006*, Universiteit Maastricht, sectie Verplegingswetenschap.

- Hansen, A. K., Clausen, T., and Nielsen, O. B. (2005). Effects of lactic acid and catecholamines on contractility in fast-twitch muscles exposed to hyperkalemia. *Am. J. Physiol. Cell Physiol.*, **289**, C104-C112.
- Harker, J. (2000). Pressure ulcer classification: the Torrance system. *J. Wound. Care*, **9**, 275-277.
- Hayashi, T., Honda, K., Kimura, C., Yamamoto, Y., Oyama, A., and Sugihara, T. (2004). Treatment of ischial pressure sores by means of sclerotherapy using absolute ethanol. *Ann. Plast. Surg.*, **53**, 554-559.
- Hill, M. and Goldspink, G. (2003). Expression and splicing of the insulin-like growth factor gene in rodent muscle is associated with muscle satellite (stem) cell activation following local tissue damage. *J. Physiol.*, **549**, 409-418.
- Hochachka, P. W. and Lutz, P. L. (2001). Mechanism, origin, and evolution of anoxia tolerance in animals. *Comp. Biochem. Physiol. B Biochem. Mol. Biol.*, **130**, 435-459.
- Hooker, E. Z., Sibley, P., Nemchausky, B., and Lopez, E. (1988). A method for quantifying the area of closed pressure sores by sinography and digitometry. *J. Neurosci. Nurs.*, **20**, 118-127.
- Houwing, R. H., Rozendaal, M., Wouters-Wesseling, W., Beulens, J. W. J., Buskens, E., and Haalboom, J. R. (2003). A randomised, double-blind assessment of the effect of nutritional supplementation on the prevention of pressure ulcers in hip-fracture patients. *Clin. Nutr.*, **22**, 401-405.
- Husian, T. (1953). An experimental study of some pressure effects on tissues, with reference to the bed-sore problem. *J. Pathol. Bacteriol.*, **66**, 347-358.
- Idziorek, T., Estaquier, J., De Bels, F., and Ameisen, J. C. (1995). YOPRO-1 permits cytofluorometric analysis of programmed cell death (apoptosis) without interfering with cell viability. *J. Immunol. Methods*, **185**, 249-258.
- Jacobs, A. E., Benders, A. A., Oosterhof, A., and Veerkamp, J. H. (1992). Effects of growth medium, electrical stimulation and paralysis on various enzyme activities in cultured rat muscle cells. Comparison with activities in rat muscles in vivo. *Int. J. Biochem.*, **24**, 751-758.
- Jerome, K. R. et al. (2001). HSV and glycoprotein J inhibit caspase activation and apoptosis induced by granzyme B or Fas. *J. Immunol.*, **167**, 3928-3935.
- Jiang, B. H., Semenza, G. L., Bauer, C., and Marti, H. H. (1996). Hypoxia-inducible factor 1 levels vary exponentially over a physiologically relevant range of O<sub>2</sub> tension. *Am. J. Physiol.*, **271**, C1172-C1180.
- Kamochi, H. et al. (2006). Transplantation of myocyte precursors derived from embryonic stem cells transfected with IGFII gene in a mouse model of muscle injury. *Transplantation*, **82**, 516-526.
- Kosiak, M. (1959). Etiology and pathology of ischemic ulcers. *Arch. Phys. Med. Rehabil.*, **40**, 62-69.
- Krouskop, T. A., Reddy, N. P., Spencer, W. A., and Secor, J. W. (1978). Mechanisms of decubitus ulcer formation--an hypothesis. *Med. Hypotheses*, **4**, 37-39.
- Kubasiak, L. A., Hernandez, O. M., Bishopric, N. H., and Webster, K. A. (2002). Hypoxia and acidosis activate cardiac myocyte death through the Bcl-2 family protein BNIP3. *Proc. Natl. Acad. Sci. USA*, **99**, 12825-12830.
- Kubo, Y. (1991). Comparison of initial stages of muscle differentiation in rat and mouse myoblastic and mouse mesodermal stem cell lines. *J. Physiol.*, **442**, 743-759.
- Labbe, R., Lindsay, T., and Walker, P. M. (1987). The extent and distribution of skeletal muscle necrosis after graded periods of complete ischemia. *J. Vasc. Surg.*, **6**, 152-157.



## References

- Landis, E. M. (1930). Micro-injection studies of capillary blood pressure in human skin. *Heart*, **15**, 209-228.
- Landsman, A. S., Meaney, D. F., Cargill, R. S., Macarak, E. J., and Thibault, L. E. (1995). 1995 William J. Stickel Gold Award. High strain rate tissue deformation. A theory on the mechanical etiology of diabetic foot ulcerations. *J. Am. Podiatr. Med. Assoc.*, **85**, 519-527.
- Langen, R. C. J., Schols, A. M. W. J., Kelders, M. C. J. M., Wouters, E. F. M., and Janssen-Heininger, Y. M. W. (2003). Enhanced myogenic differentiation by extracellular matrix is regulated at the early stages of myogenesis. *In Vitro Cell. Dev. Biol. Anim.*, **39**, 163-169.
- Lawson, M. A. and Purslow, P. P. (2000). Differentiation of myoblasts in serum-free media: effects of modified media are cell line-specific. *Cells Tissues Organs*, **167**, 130-137.
- Levenberg, S. et al. (2005). Engineering vascularized skeletal muscle tissue. *Nat. Biotechnol.*, **23**, 879-884.
- Lin, F., Moran, B., Bankard, J., Hendrix, R., and Makhous, M. (2004). A subject-specific FEM model for evaluating buttock tissue response under sitting load. *26th Annual International Conference of IEEE EMBS, San Francisco, CA*.
- Lin, Z. et al. (1994). Sequential appearance of muscle-specific proteins in myoblasts as a function of time after cell division: evidence for a conserved myoblast differentiation program in skeletal muscle. *Cell Motil. Cytoskeleton*, **29**, 1-19.
- Lin, Z. X., Eshelman, J. R., Forry-Schaudies, S., Duran, S., Lessard, J. L., and Holtzer, H. (1987). Sequential disassembly of myofibrils induced by myristate acetate in cultured myotubes. *J. Cell Biol.*, **105**, 1365-1376.
- Liu, M. H., Grimm, D. R., Teodorescu, V., Kronowitz, S. J., and Bauman, W. A. (1999). Transcutaneous oxygen tension in subjects with tetraplegia with and without pressure ulcers: a preliminary report. *J. Rehabil. Res. Dev.*, **36**, 202-206.
- Liu, X., Van Vleet, T., and Schnellmann, R. G. (2004). The role of calpain in oncotic cell death. *Annu. Rev. Pharmacol. Toxicol.*, **44**, 349-370.
- Louch, W. E., Ferrier, G. R., and Howlett, S. E. (2005). Attenuation of cardiac stunning by losartan in a cellular model of ischemia and reperfusion is accompanied by increased sarcoplasmic reticulum Ca<sup>2+</sup> stores and prevention of cytosolic Ca<sup>2+</sup> elevation. *J. Pharmacol. Exp. Ther.*, **312**, 238-247.
- Lu, Q. L., Bou-Gharios, G., and Partridge, T. A. (2003). Non-viral gene delivery in skeletal muscle: a protein factory. *Gene Ther.*, **10**, 131-142.
- Maley, M. A., Davies, M. J., and Grounds, M. D. (1995). Extracellular matrix, growth factors, genetics: their influence on cell proliferation and myotube formation in primary cultures of adult mouse skeletal muscle. *Exp. Cell Res.*, **219**, 169-179.
- Mawson, A. R., Siddiqui, F. H., Connolly, B. J., Sharp, C. J., Summer, W. R., and Biundo, J. J. J. (1993). Sacral transcutaneous oxygen tension levels in the spinal cord injured: risk factors for pressure ulcers? *Arch. Phys. Med. Rehabil.*, **74**, 745-751.
- McArdle, A., Maglara, A., Appleton, P., Watson, A. J., Grierson, I., and Jackson, M. J. (1999). Apoptosis in multinucleated skeletal muscle myotubes. *Lab. Invest.*, **79**, 1069-1076.
- McGuire, T. F., Trump, D. L., and Johnson, C. S. (2001). Vitamin D(3)-induced apoptosis of murine squamous cell carcinoma cells. Selective induction of caspase-dependent MEK cleavage and up-regulation of MEKK-1. *J. Biol. Chem.*, **276**, 26365-26373.

- Meijer, J. H., Schut, G. L., Ribbe, M. W., Goovaerts, H. G., Nieuwenhuys, R., Reulen, J. P., and Schneider, H. (1989). Method for the measurement of susceptibility to decubitus ulcer formation. *Med. Biol. Eng. Comput.*, **27**, 502-506.
- Meijer, J. H., Germs, P. H., Schneider, H., and Ribbe, M. W. (1994). Susceptibility to decubitus ulcer formation. *Arch. Phys. Med. Rehabil.*, **75**, 318-323.
- Meldrum, K. K., Meldrum, D. R., Hile, K. L., Burnett, A. L., and Harken, A. H. (2001). A novel model of ischemia in renal tubular cells which closely parallels in vivo injury. *J. Surg. Res.*, **99**, 288-293.
- Miller, G. E. and Seale, J. (1981). Lymphatic clearance during compressive loading. *Lymphology*, **14**, 161-166.
- Mosmann, T. (1983). Rapid colorimetric assay for cellular growth and survival: application to proliferation and cytotoxicity assays. *J. Immunol. Methods*, **65**, 55-63.
- Musaro, A. et al. (2004). Stem cell-mediated muscle regeneration is enhanced by local isoform of insulin-like growth factor 1. *Proc. Natl. Acad. Sci. USA*, **101**, 1206-1210.
- Netti, P. A., Berk, D. A., Swartz, M. A., Grodzinsky, A. J., and Jain, R. K. (2000). Role of extracellular matrix assembly in interstitial transport in solid tumors. *Cancer Res.*, **60**, 2497-2503.
- New, P. W., Rawicki, H. B., and Bailey, M. J. (2004). Nontraumatic spinal cord injury rehabilitation: pressure ulcer patterns, prediction, and impact. *Arch. Phys. Med. Rehabil.*, **85**, 87-93.
- Nola, G. T. and Vistnes, L. M. (1980). Differential response of skin and muscle in the experimental production of pressure sores. *Plast. Reconstr. Surg.*, **66**, 728-733.
- Okano, T. and Matsuda, T. (1997). Hybrid muscular tissues: preparation of skeletal muscle cell-incorporated collagen gels. *Cell Transplant.*, **6**, 109-118.
- Okano, T. and Matsuda, T. (1998a). Tissue engineered skeletal muscle: preparation of highly dense, highly oriented hybrid muscular tissues. *Cell Transplant.*, **7**, 71-82.
- Okano, T. and Matsuda, T. (1998b). Muscular tissue engineering: capillary-incorporated hybrid muscular tissues in vivo tissue culture. *Cell Transplant.*, **7**, 435-442.
- Oomens, C. W. J., Bressers, O. F. J. T., Bosboom, E. M. H., Bouten, C. V. C., and Bader, D. L. (2003). Can loaded interface characteristics influence strain distributions in muscle adjacent to bony prominences? *Comput. Methods Biomech. Biomed. Engin.*, **6**, 171-180.
- Page, S., Jackson, M. J., Coakley, J., and Edwards, R. H. (1989). Isoforms of creatine kinase: MM in the study of skeletal muscle damage. *Eur. J. Clin. Invest.*, **19**, 185-191.
- Palmer, S. et al. (2001). The small muscle-specific protein Csl modifies cell shape and promotes myocyte fusion in an insulin-like growth factor 1-dependent manner. *J. Cell Biol.*, **153**, 985-998.
- Park, J. C., Hwang, Y. S., and Suh, H. (2000). Viability evaluation of engineered tissues. *Yonsei Med. J.*, **41**, 836-844.
- Payumo, F. C. et al. (2002). Tissue engineering skeletal muscle for orthopaedic applications. *Clin. Orthop. Relat. Res.*, S228-S242.
- Peake, J. M., Suzuki, K., Wilson, G., Hordern, M., Nosaka, K., Mackinnon, L., and Coombes, J. S. (2005). Exercise-induced muscle damage, plasma cytokines, and markers of neutrophil activation. *Med. Sci. Sports Exerc.*, **37**, 737-745.

## References

- Peeters, E. A. G., Bouten, C. V. C., Oomens, C. W. J., and Baaijens, F. P. T. (2003). Monitoring the biomechanical response of individual cells under compression: a new compression device. *Med. Biol. Eng. Comput.*, **41**, 498-503.
- Peeters, E. A. G., Bouten, C. V. C., Oomens, C. W. J., Bader, D. L., Snoeckx, L. H. E. H., and Baaijens, F. P. T. (2004). Anisotropic, three-dimensional deformation of single attached cells under compression. *Ann. Biomed. Eng.*, **32**, 1443-1452.
- Peeters, E. A. G., Oomens, C. W. J., Bouten, C. V. C., Bader, D. L., and Baaijens, F. P. T. (2005a). Mechanical and failure properties of single attached cells under compression. *J. Biomech.*, **38**, 1685-1693.
- Peeters, E. A. G., Oomens, C. W. J., Bouten, C. V. C., Bader, D. L., and Baaijens, F. P. T. (2005b). Viscoelastic properties of single attached cells under compression. *J. Biomech. Eng.*, **127**, 237-243.
- Peirce, S. M., Skalak, T. C., and Rodeheaver, G. T. (2000). Ischemia-reperfusion injury in chronic pressure ulcer formation: a skin model in the rat. *Wound. Repair Regen.*, **8**, 68-76.
- Peng, H. and Huard, J. (2004). Muscle-derived stem cells for musculoskeletal tissue regeneration and repair. *Transpl. Immunol.*, **12**, 311-319.
- Portier, G. L., Benders, A. G., Oosterhof, A., Veerkamp, J. H., and van Kuppevelt, T. H. (1999). Differentiation markers of mouse C2C12 and rat L6 myogenic cell lines and the effect of the differentiation medium. *In Vitro Cell. Dev. Biol. Anim.*, **35**, 219-227.
- Powell, C. et al. (1999). Tissue-engineered human bioartificial muscles expressing a foreign recombinant protein for gene therapy. *Hum. Gene Ther.*, **10**, 565-577.
- Powell, C., Smiley, B. L., Mills, J., and Vandenburg, H. H. (2002). Mechanical stimulation improves tissue-engineered human skeletal muscle. *Am. J. Physiol. Cell Physiol.*, **283**, C1557-C1565.
- Prewitt, R. L. and Johnson, P. C. (1976). The effect of oxygen on arteriolar red cell velocity and capillary density in the rat cremaster muscle. *Microvasc. Res.*, **12**, 59-70.
- Rabinovsky, E. D. et al. (2003). Targeted expression of IGF-1 transgene to skeletal muscle accelerates muscle and motor neuron regeneration. *FASEB J.*, **17**, 53-55.
- Radisic, M., Malda, J., Epping, E., Geng, W., Langer, R., and Vunjak-Novakovic, G. (2006). Oxygen gradients correlate with cell density and cell viability in engineered cardiac tissue. *Biotechnol. Bioeng.*, **93**, 332-343.
- Ramanujan, S., Pluen, A., McKee, T. D., Brown, E. B., Boucher, Y., and Jain, R. K. (2002). Diffusion and convection in collagen gels: implications for transport in the tumor interstitium. *Biophys. J.*, **83**, 1650-1660.
- Reddy, N. P. and Cochran, G. V. (1981). Interstitial fluid flow as a factor in decubitus ulcer formation. *J. Biomech.*, **14**, 879-881.
- Reger, S. I., McGovern, T. F., and Chung, K. C. (1990). Biomechanics of tissue distortion and stiffness by magnetic resonance imaging. *Pressure sores - Clinical practice and scientific approach*, (Bader, D. L. ed.) MacMillan, London, 177-190.
- Reipschläger, A. and Pörtner, H. O. (1996). Metabolic depression during environmental stress: the role of extracellular versus intracellular pH in *Sipunculus nudus*. *J. Exp. Biol.*, **199**, 1801-1807.
- Reswick, J. B. and Rogers, J. E. (1976). Experience at Rancho 10s Amigos with devices and techniques to prevent pressure sores. *Bedsore Biomechanics*, (Kenedi, R. M., and Cowden, J. M. eds.) MacMillan, London, 301-310.

- Richmond, K. N., Shonat, R. D., Lynch, R. M., and Johnson, P. C. (1999). Critical PO(2) of skeletal muscle in vivo. *Am. J. Physiol.*, **277**, H1831-H1840.
- Rieseberg, M., Kasper, C., Reardon, K. F., and Scheper, T. (2001). Flow cytometry in biotechnology. *Appl. Microbiol. Biotechnol.*, **56**, 350-360.
- Rodriguez, G. P. and Garber, S. L. (1994). Prospective study of pressure ulcer risk in spinal cord injury patients. *Paraplegia*, **32**, 150-158.
- Salvioli, S., Ardizzoni, A., Franceschi, C., and Cossarizza, A. (1997). JC-1, but not DiOC6(3) or rhodamine 123, is a reliable fluorescent probe to assess delta psi changes in intact cells: implications for studies on mitochondrial functionality during apoptosis. *FEBS Lett.*, **411**, 77-82.
- Sanger, J. W., Chowrashi, P., Shaner, N. C., Spalthoff, S., Wang, J., Freeman, N. L., and Sanger, J. M. (2002). Myofibrillogenesis in skeletal muscle cells. *Clin. Orthop. Relat Res.*, S153-S162.
- Scelsi, R. (2001). Skeletal muscle pathology after spinal cord injury: our 20 year experience and results on skeletal muscle changes in paraplegics, related to functional rehabilitation. *Basic Appl. Myol.*, **11**, 75-85.
- Semsarian, C., Sutrave, P., Richmond, D. R., and Graham, R. M. (1999). Insulin-like growth factor (IGF-I) induces myotube hypertrophy associated with an increase in anaerobic glycolysis in a clonal skeletal-muscle cell model. *Biochem. J.*, **339**, 443-451.
- Shansky, J., Del Tatto, M., Chromiak, J., and Vandeburgh, H. (1997). A simplified method for tissue engineering skeletal muscle organoids in vitro. *In Vitro Cell. Dev. Biol. Anim.*, **33**, 659-661.
- Shea, J. D. (1975). Pressure sores: classification and management. *Clin. Orthop. Relat. Res.*, 89-100.
- Shen, X., Collier, J. M., Hlaing, M., Zhang, L., Delshad, E. H., Bristow, J., and Bernstein, H. S. (2003). Genome-wide examination of myoblast cell cycle withdrawal during differentiation. *Dev. Dyn.*, **226**, 128-138.
- Shiesh, S. C., Ting, W. K., and Jap, T. S. (1992). Measurement of creatine kinase isoforms by agarose gel electrophoresis in the diagnosis of myocardial infarction. *Clin. Biochem.*, **25**, 293-301.
- Shimokawa, T., Kato, M., Ezaki, O., and Hashimoto, S. (1998). Transcriptional regulation of muscle-specific genes during myoblast differentiation. *Biochem. Biophys. Res. Commun.*, **246**, 287-292.
- Simpson, J. A., Labugger, R., Collier, C., Brison, R. J., Iscoe, S., and Van Eyk, J. E. (2005). Fast and slow skeletal troponin I in serum from patients with various skeletal muscle disorders: a pilot study. *Clin. Chem.*, **51**, 966-972.
- Spangenburg, E. E., Bowles, D. K., and Booth, F. W. (2004). Insulin-like growth factor-induced transcriptional activity of the skeletal alpha-actin gene is regulated by signaling mechanisms linked to voltage-gated calcium channels during myoblast differentiation. *Endocrinology*, **145**, 2054-2063.
- Srikakulam, R. and Winkelmann, D. A. (2004). Chaperone-mediated folding and assembly of myosin in striated muscle. *J. Cell Sci.*, **117**, 641-652.
- Stadelmann, C. and Lassmann, H. (2000). Detection of apoptosis in tissue sections. *Cell Tissue Res.*, **301**, 19-31.
- Stekelenburg, A., Oomens, C. W., Strijkers, G. J., de Graaf, L., Bader, D. L., and Nikolay, K. (2005a). A new MR-compatible loading device to study in vivo muscle damage development in rats due to compressive loading. *Med. Eng. Phys.*, **28**, 331-338.

## References

- Stekelenburg, A. (2005b). The relative contributions of deformation and ischaemia to deep tissue injury. *Mechanisms associated with deep tissue injury induced by sustained compressive loading*, PhD Thesis, Eindhoven University of Technology.
- Stekelenburg, A., Oomens, C. W. J., Strijkers, G. J., Nicolay, K., and Bader, D. L. (2006). Compression-induced deep tissue injury examined with magnetic resonance imaging and histology. *J. Appl. Physiol.*, **100**, 1946-1954.
- Strohman, R. C., Bayne, E., Spector, D., Obinata, T., Micou-Eastwood, J., and Maniotis, A. (1990). Myogenesis and histogenesis of skeletal muscle on flexible membranes in vitro. *In Vitro Cell. Dev. Biol.*, **26**, 201-208.
- Sultan, K. R., Henkel, B., Terlouw, M., and Haagsman, H. P. (2006). Quantification of hormone-induced atrophy of large myotubes from C2C12 and L6 cells: atrophy-inducible and atrophy-resistant C2C12 myotubes. *Am. J. Physiol. Cell Physiol.*, **290**, C650-C659.
- Suzuki, T., Fujikura, K., Higashiyama, T., and Takata, K. (1997). DNA staining for fluorescence and laser confocal microscopy. *J. Histochem. Cytochem.*, **45**, 49-53.
- Swadlow, S. and Mayne, R. (1992). Formation of highly organized skeletal muscle fibers in vitro. Comparison with muscle development in vivo. *J. Cell Sci.*, **102 ( Pt 3)**, 643-652.
- Takahashi, A. et al. (2002). Myogenic Akt signaling regulates blood vessel recruitment during myofiber growth. *Mol. Cell Biol.*, **22**, 4803-4814.
- Tannu, N. S., Rao, V. K., Chaudhary, R. M., Giorgianni, F., Saeed, A. E., Gao, Y., and Raghov, R. (2004). Comparative proteomes of the proliferating C(2)C(12) myoblasts and fully differentiated myotubes reveal the complexity of the skeletal muscle differentiation program. *Mol. Cell Proteomics.*, **3**, 1065-1082.
- Taylor, A. C. (1962). Responses of cells to pH changes in the medium. *J. Cell Biol.*, **15**, 201-209.
- Tsuji, S., Ichioka, S., Sekiya, N., and Nakatsuka, T. (2005). Analysis of ischemia-reperfusion injury in a microcirculatory model of pressure ulcers. *Wound. Repair Regen.*, **13**, 209-215.
- Unal, S., Ozmen, S., Demir, Y., Yavuzer, R., Latifoglu, O., Atabay, K., and Oguz, M. (2001). The effect of gradually increased blood flow on ischemia-reperfusion injury. *Ann. Plast. Surg.*, **47**, 412-416.
- Usher-Smith, J. A., Fraser, J. A., Bailey, P. S. J., Griffin, J. L., and Huang, C. L. H. (2006). The influence of intracellular lactate and H<sup>+</sup> on cell volume in amphibian skeletal muscle. *J. Physiol.*, **573**, 799-818.
- van Kuppevelt, T. H., Benders, A. A., Versteeg, E. M., and Veerkamp, J. H. (1992). Ultrosor G and brain extract induce a continuous basement membrane with specific synaptic elements in aneurally cultured human skeletal muscle cells. *Exp. Cell Res.*, **200**, 306-315.
- van Wachem, P. B., van Luyn, M. J., and da Costa, M. L. (1996). Myoblast seeding in a collagen matrix evaluated in vitro. *J. Biomed. Mater. Res.*, **30**, 353-360.
- Vandenburgh, H. H., Hatfaludy, S., Karlisch, P., and Shansky, J. (1989). Skeletal muscle growth is stimulated by intermittent stretch-relaxation in tissue culture. *Am. J. Physiol.*, **256**, C674-C682.
- Vandenburgh, H. H., Hatfaludy, S., Karlisch, P., and Shansky, J. (1991a). Mechanically induced alterations in cultured skeletal muscle growth. *J. Biomech.*, **24**, 91-99.
- Vandenburgh, H. H., Swadlow, S., and Karlisch, P. (1991b). Computer-aided mechanogenesis of skeletal muscle organs from single cells in vitro. *FASEB J.*, **5**, 2860-2867.

- Vandenburgh, H. H., Karlisch, P., Shansky, J., and Feldstein, R. (1991c). Insulin and IGF-I induce pronounced hypertrophy of skeletal myofibers in tissue culture. *Am. J. Physiol.*, **260**, C475-C484.
- Vandenburgh, H. et al. (1996). Tissue-engineered skeletal muscle organoids for reversible gene therapy. *Hum. Gene Ther.*, **7**, 2195-2200.
- Vandenburgh, H. et al. (1998a). Attenuation of skeletal muscle wasting with recombinant human growth hormone secreted from a tissue-engineered bioartificial muscle. *Hum. Gene Ther.*, **9**, 2555-2564.
- Vandenburgh, H., Shansky, J., Del Tatto, M., and Chromiak, J. (1998b). Organogenesis of Skeletal Muscle in Tissue Culture. *Tissue Engineering*, Humana Press, Inc.
- Vermes, I., Haanen, C., Steffens-Nakken, H., and Reutelingsperger, C. (1995). A novel assay for apoptosis. Flow cytometric detection of phosphatidylserine expression on early apoptotic cells using fluorescein labelled Annexin V. *J. Immunol. Methods*, **184**, 39-51.
- Vezzoli, A., Gussoni, M., Greco, F., Zetta, L., and Cerretelli, P. (2004). Temperature and pH dependence of energy balance by (31)P- and (1)H-MRS in anaerobic frog muscle. *Biochim. Biophys. Acta*, **1608**, 163-170.
- Vidal, J. and Sarrias, M. (1991). An analysis of the diverse factors concerned with the development of pressure sores in spinal cord injured patients. *Paraplegia*, **29**, 261-267.
- Wang, Y. N., Bouten, C. V. C., Lee, D. A., and Bader, D. L. (2005). Compression-induced damage in a muscle cell model in vitro. *Proc. Inst. Mech. Eng. [H. ]*, **219**, 1-12.
- Webster, K. A. and Bishopric, N. H. (1992). Molecular regulation of cardiac myocyte adaptations to chronic hypoxia. *J. Mol. Cell. Cardiol.*, **24**, 741-751.
- Webster, K. A., Discher, D. J., Kaiser, S., Hernandez, O., Sato, B., and Bishopric, N. H. (1999). Hypoxia-activated apoptosis of cardiac myocytes requires reoxygenation or a pH shift and is independent of p53. *J. Clin. Invest.*, **104**, 239-252.
- Webster, K. A., Graham, R. M., and Bishopric, N. H. (2005). BNip3 and signal-specific programmed death in the heart. *J. Mol. Cell. Cardiol.*, **38**, 35-45.
- Wronski, R., Golob, N., Grygar, E., and Windisch, M. (2002). Two-color, fluorescence-based microplate assay for apoptosis detection. *Biotechniques*, **32**, 666-668.
- Yaffe, D. and Saxel, O. (1977). Serial passaging and differentiation of myogenic cells isolated from dystrophic mouse muscle. *Nature*, **270**, 725-727.
- Yang, S. Y. and Goldspink, G. (2002). Different roles of the IGF-I Ec peptide (MGF) and mature IGF-I in myoblast proliferation and differentiation. *FEBS Lett.*, **522**, 156-160.
- Yarkony, G. M. et al. (1990). Classification of pressure ulcers. *Arch. Dermatol.*, **126**, 1218-1219.
- Yotov, W. V. and St Arnaud, R. (1996). Differential splicing-in of a proline-rich exon converts alphaNAC into a muscle-specific transcription factor. *Genes Dev.*, **10**, 1763-1772.
- Ytrehus, K., Reikeras, O., Huseby, N., and Myklebust, R. (1995). Ultrastructure of reperfused skeletal muscle: the effect of oxygen radical scavenger enzymes. *Int. J. Microcirc. Clin. Exp.*, **15**, 155-162.

# Appendix A

Diffusion of markers into and  
out of compressed tissues

## A.1 Background

It is hypothesized that tissue compression influences tissue diffusion properties. The hindering of diffusion by tissue compression may result in a twofold problem: 1) the tissue will not only experience ischemia but also limited diffusion through the extracellular space towards the cells and perhaps inside the cells 2) during deformation, measurement of marker release from damaged cells is impaired. This impediment would interfere with early detection of pressure ulcer development during tissue loading in vivo but also with detection of marker release in an in vitro setting. It may also explain why during tissue compression no increased T2 values were found during the MRI experiments in compressed rat legs (Stekelenburg, 2005b).

## A.2 Approach

In order to obtain more insight in the role of tissue deformation on tissue diffusion properties, a series of pilot experiments was performed in engineered muscle tissue. Diffusion of several molecules of varying size (table A.1) was assessed into as well as out of the tissue. The applied markers were NO (nitric oxide), MTT (metabolic marker), YO-PRO-1 (fluorescent marker of apoptosis), propidium iodide (fluorescent marker of necrosis), CK (creatine kinase), and LDH (lactate dehydrogenase).

*Table A.1: Listing of markers applied to study tissue diffusion properties and their respective weights. Some other molecules are listed as well to indicate their relative sizes.*

Marker	Molecular weight (Da or amu)
Nitric oxide (NO)	30
Lactate	89
Glucose	180
MTT formazan	335
YO-PRO-1 (YP)	376
Propidium iodide (PI)	668
Fatty acid binding protein (H-FABP)	~15,000
Myoglobin (Mb)	~17,000
Creatine kinase (CK)	~82,000
Lactate dehydrogenase (LDH)	~140,000

## A.3 Materials and methods

### NO (30 Da) release from compressed BAMs

Bio-artificial muscle tissues (BAMs, protocol is described in chapter 2) were compressed by load application for 10 minutes. Indenters had 5 mm diameter tips and weighed approximately 4 grams. Controls remained unloaded. Medium samples were removed during and after loading.



Nitric oxide reacts to form nitrite and nitrate. Nitrite was measured applying a fluorescent assay, which is more sensitive than the commonly used Griess assay. NO in medium was allowed to react with 2,3-diaminonaphtalene for 30 minutes at room temperature. Reaction was terminated by addition of NaOH. Fluorescence of the reaction product, 1-(H)-naphotriazole, was measured by exciting at 365 nm and reading emission at 450 nm. Calibration was performed with NaNO<sub>2</sub>.

### **MTT (335 Da) diffusion into deformed BAMs**

BAMs were loaded (by imposing a displacement) with the weights on spacers to 350 µm final height presented in figure 5.1A for 5 or 24 hours. MTT diffusion into the tissue was determined during and after load application by incubation in standard MTT/medium mixture for 30 minutes. Viable cells converted the MTT into purple crystals as a measure for their metabolic activity. A purple color may therefore be caused by either the presence of more cells or by more active cells.

### **Diffusion of YP (376 Da) and PI (668 Da) into a deformed BAM**

A BAM was compressed (by imposing a displacement) with a weight with spacers (figure 5.1A) to 350 µm final height ( $\approx$  34% deformation). After approximately 20 hours, fluorescent probes, propidium iodide and YO-PRO-1, were added to the medium surrounding the compressed tissue. Fluorescence stacked images were obtained every hour on 7 locations in the tissue for 22 hours after addition of the probes. The weight was maintained throughout the entire experimental period.

### **CK (82 kDa) release from compressed blobs**

Disc-shaped engineered muscle tissue (blob) was prepared according to the protocol described by Breuls et al. (2003a). In short,  $0.5 \times 10^6$  C2C12 cells were suspended in a collagen matrigel mixture. The suspension was molded in 6well plates into disc-shaped drops. The discs were allowed to gelate and covered with growth medium. After three days, differentiation was induced by replacing the medium with differentiation medium containing 2% horse serum for another week. The constructs had a diameter of approximately 15-20 mm.

The tissue was compressed by load application with 100 gram weights (diameter 30 mm) that were placed on top of the constructs directly. During and after loading, medium samples were taken for assessing marker release.

Creatine kinase was measured applying a photometric assay (Granutest 2.5 CK NAC DGKCh kit, Merck, Darmstadt, Germany). Activity was determined by measuring the time-dependent change of absorbance at 340 nm of a 40 µl medium sample with 1 ml reagent mixture after 50 minutes of incubation with 10 minute intervals.

### **LDH (140 kDa) release from deformed BAMs**

From the experiments performed for determining diffusion of MTT into BAMs, medium samples were taken after load removal (tissue had been loaded for 24 hours). Medium was analyzed for LDH content by an in vitro toxicology assay kit, LDH based (TOX7, Sigma). Samples were diluted 1.33 times in water to a total volume of 30 µl

before reagent was added. Reaction was terminated at 20 minutes with 10  $\mu$ l 1N HCl. Absorbance was read on a platereader at 490 nm and corrected for background at 650 nm.

### Statistical analysis

Due to the low numbers of samples applied in some of the pilot experiments, no statistics were applied. Where (statistical) significance is mentioned, ANOVA was applied followed by Bonferroni posthoc tests with  $p < 0.05$ . Graphs depict means and their respective standard errors.

## A.4 Results

### NO (30 Da) release from compressed BAMs

Release of nitric oxide by determining nitrite was measured for 120 minutes as shown in figure A.1. In this period, nitrite was determined during and after load application for 10 minutes in the compression group (4 g). Control samples were not compressed. An immediate non-significant increase at 5 and 10 minutes was observed in the compressed group. In addition, the control group as well as the compressed group both exhibited a continuous basal expression of NO.

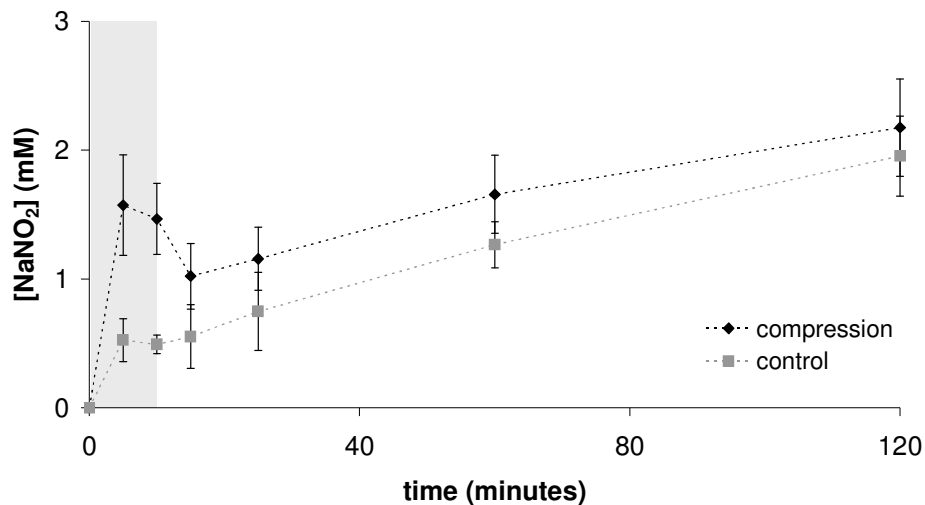


Figure A.1: Difference in NO release between control and compressed samples. No significant differences were present ( $p < 0.05$ ;  $n=4$ ). The grey area shows the period of tissue loading in compressed samples.

**Conclusion:** The response in NO release upon tissue compression appeared to be very early and during load application. However, after only 5 minutes the response was not strong enough (anymore) to result in significant differences from controls.

### MTT (335 Da) diffusion into deformed BAMs

After 5 hours of compression (approximately 34%) the tissue was subjected to an MTT assay. The control tissue stained completely deep purple as evident from figure A.2A. The tissue that had been compressed for 5 hours did seem to stain slightly less intense in the compressed region that was unloaded during MTT incubation (figure A.2B).

However, if the tissue was still loaded during incubation, a clearly delineated unstained region was found where the load had been, as shown in figure A.2C. After 24 hours of loading, control tissue again stained deep purple (figure A.2D). Compressed samples showed reduced staining in the compressed volume after 24 hours of loading but were unloaded during MTT incubation (figure A.2E).

When studying more closely the staining of the tissue in figure A.2C, it may be noted that a line of MTT staining was visible at the sides of the compressed tissue. The width of this line tended not to increase with longer incubation periods (90 minutes compared to 30 minutes). This may imply that diffusion from the top and bottom into the construct was limited by the presence of the stainless steel load and the culture dish, respectively.

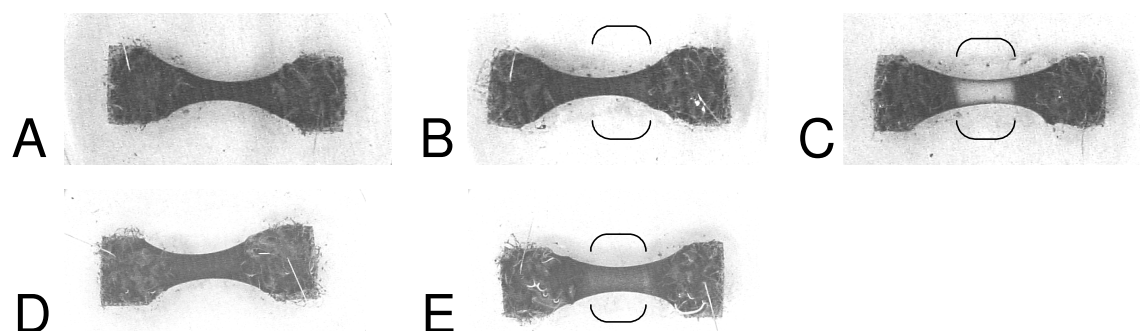


*Figure A.2: Appearance of tissue samples after an MTT assay. (A) Control tissue that was uncompressed for 5 hours, (B) The tissue was subjected to 5 hours of compression and the load was removed during MTT incubation. (C) The tissue was subjected to 5 hours of compression and the load was not removed during MTT incubation. (D) Control tissue that was not compressed for 24 hours. (E) The tissue was subjected to compression for 24 hours and load was removed during MTT incubation. The brackets indicate the compressed regions.*

Diffusion from the tissue's sides was possible, though. The line may represent the lining of dense cell layers at the periphery of the constructs (chapter 4, p. 45). When removing the load after incubation in figure A.2C, the tissue did stain comparable to the BAM in figure A.2B. If less deformation was applied, the 'unstained' area was stained in a light purple shade, which may imply a gradual diffusion limitation with increasing amounts of deformation.

*Conclusion:* MTT diffusion was not hindered from the open sides of compressed tissues. It was inhibited though from the top and bottom of the tissue where the load and dish were located.

### **Diffusion of YP (376 Da) and PI (668) into a deformed BAM**

Figure A.3 shows the average total summed intensities of all pixels in z-projected images from confocal stacks on 7 locations in time. Within the first hour, intensities of both markers increase. YO-PRO-1 intensity reaches already about half the maximum value, whereas propidium iodide showed a slower response, reaching its half-maximum response after 3-4 hours. This was expected as the YO-PRO-1 molecule was smaller than the propidium iodide and they are equally charged.

*Conclusion:* Relatively small charged molecules appeared to exhibit a size-dominated diffusion into a deformed BAM as YO-PRO-1, the smaller molecule, had infiltrated the construct more efficiently on an earlier time point than the larger propidium iodide.

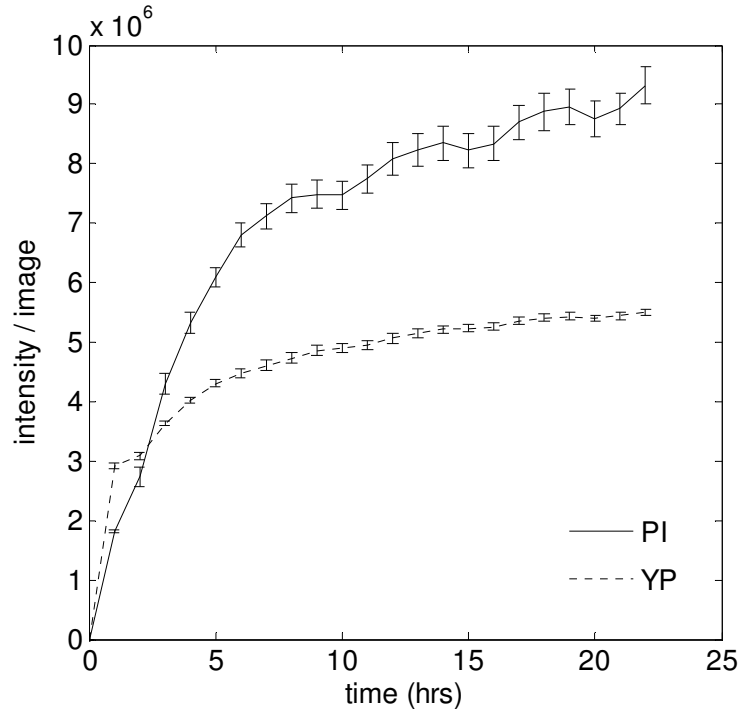


Figure A.3: Means of the summarized pixel intensities for z-projected images obtained from the z-stacks are depicted in time with their respective standard errors. Intensities for both fluorescent probes, YP and PI are shown.

### CK (82 kDa) release from compressed blobs

Tissue samples (blobs) were loaded with 100 grams for 5 or 100 minutes. The influence on the release of a muscle damage marker, creatine kinase, in time is

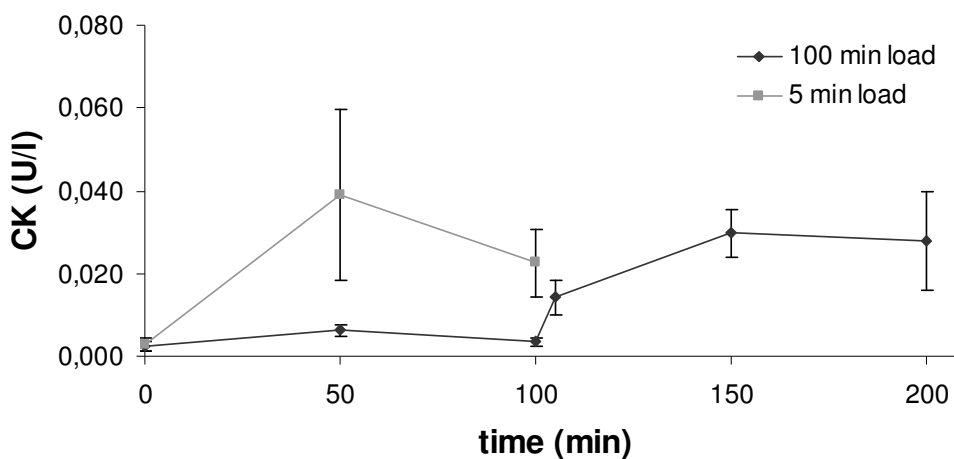


Figure A.4: Release of creatine kinase in time due to compression of engineered muscle with 100 grams. The square graph shows CK release after 5 minutes of loading, while the diamond graph shows CK release during and after 100 minutes of loading ( $n=3$  (square),  $n=5$  (diamond)).

presented in figure A.4. The short, 5 minutes, loading period resulted in increased CK release at the first sampling time point thereafter (50 minutes). If the tissue was loaded longer, for 100 minutes, minimal CK release was observed during this loading period. However, immediately following load removal, CK release was enhanced.

*Conclusion:* CK appeared to be unable to diffuse out of the blobs during compression. This may be due to CK's size but may also be attributed to the extreme deformation of the engineered tissues.

### LDH (140 kDa) release from deformed BAMs

From the BAMs subjected to the MTT experiments mentioned before, medium samples were taken after load removal and analyzed for LDH release. From figure A.5 it is evident that after 24 hours, the levels of LDH in the medium was increased, but

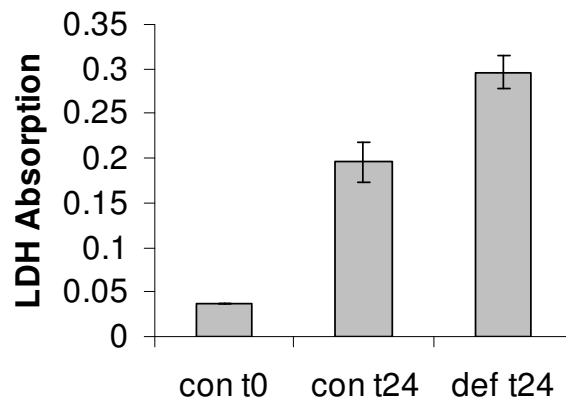


Figure A.5: LDH release in control tissue (con) at time 0, t0, and after 24 hours, t24, is shown. LDH release of the deformed (def) tissue is shown at t24.

also that there was more LDH released from the compressed tissues. This seems contradictory with the findings in chapter 5, where no additional LDH was released by compressed tissues. However, those medium samples were removed without tissue unloading. Together with the data obtained in chapter 5, the data presented in figure A.5 may suggest that during compression, the relatively large LDH molecule was confined within the tissue.

*Conclusion:* There is an indication that LDH can not move freely in compressed tissues.

## A.5 Conclusions

- ❖ From the pilot studies performed in the present appendix, it is concluded that tissue diffusion properties are influenced by tissue deformation. The larger the diffusing molecules, the more they appeared to be hindered by deformation. It is therefore recommended to establish relationships between diffusional properties and amount of tissue deformation in the future. Additionally, the changes in

diffusional properties upon tissue deformation may play a role in pressure ulcer development.

- ❖ Additionally, establishment of a potential threshold size for molecules that are so small that deformation does not influence their movement to a noticeable extent, needs to be investigated for pressure ulcer detection. Moreover, a maximum threshold size for molecules may be defined, beyond which molecules are not able to move.
- ❖ Finally, interpreting the results presented in this appendix, it should be kept in mind that the kind of deformation imposed may influence the outcome of diffusional measures. Tissue compression, based on a constant displacement (in headings referred to as deformation) or on a constant force (in headings referred to as compression), will affect tissue architecture and properties in a different way. A consistent method should be applied regarding how the tissue is deformed.

## **A.6 Acknowledgments**

The culturing and analyses performed by Christa Dam - de Veen were appreciated. Additionally, the author would like to thank the students Petra Dijkman, Kirsten Wishaupt, Cilian White, and Linda Meijer for their efforts.

# Samenvatting

Drukwonden zijn beschadigingen van zachte weefsels veroorzaakt door een aanhoudende drukbelasting. Ze ontwikkelen zich nabij harde objecten, zoals een bot of een prothese. Drukwonden vormen niet alleen een serieus probleem voor de gezondheidszorg, bijvoorbeeld omdat ze het verblijf van een patiënt in een ziekenhuis kunnen verlengen, ze kunnen ook de gezondheid en kwaliteit van het leven van de patiënt in gevaar brengen, meestal bovenop een reeds aanwezige primaire ziekte. Vooral personen met een verlaagde mobiliteit of met verminderde gevoeligheid voor drukbelasting of pijn hebben moeite het samengedrukte weefsel tijdig te ontlasten om schadevorming te voorkomen. De prevalentie van drukwonden is nog steeds te hoog in Nederland. Afhankelijk van de aard van het instituut waar de meting gedaan is, varieert deze tussen 10 en 24%.

In de huidlaag kunnen zich zogenaamde oppervlakkige drukwonden ontwikkelen. Deze oppervlakkige wonden tasten de dermis en/of de epidermis aan en worden geclassificeerd als type I of II. De oppervlakkige wonden kunnen vanaf de huidlaag doordringen in het onderliggende weefsel, zelfs tot aan het bot. Ze zijn dan uitgegroeid tot type III of IV wonden. In tegenstelling tot de oppervlakkig startende wonden, kan een wond ook in het diepere weefsel ontstaan. Van de diepere weefsellagen is vooral het skeletspierweefsel gevoelig voor het ontwikkelen van drukschade. Diepe drukwonden kenmerken zich door zich uit te breiden onder een intacte huid richting het oppervlak. Door deze onderhuidse ontwikkeling zijn ze moeilijk te diagnosticeren en resulteren ze meestal als ze eenmaal de huid perforeren in een ernstige type III of IV wond. Omdat het skeletspierweefsel erg gevoelig is voor drukbelastingen en omdat diepe weefselschade waarschijnlijk in die weefsellaag ontstaat, is dit proefschrift gericht op schadeontwikkeling in skeletspierweefsel.

Ondanks de enorme aandacht voor preventie en behandeling van drukwonden, is de etiologie van de wonden niet volledig bekend. Meer kennis op dit gebied is echter juist van belang om bestaande behandelstrategieën te verbeteren en de wonden in een vroegtijdig stadium te detecteren om zo de juiste individuele zorg te kunnen bieden. Bestaande theorieën omtrent etiologie beschouwen ischemie (onvoldoende doorbloeding), vermindering van lymfetransport, reperfusie en celdeformatie als mogelijke oorzaken voor drukwondontwikkeling. In dit proefschrift is vooral de schadeontwikkeling in skeletspieren als een gevolg van ischemie en/of deformatie tot doel gesteld.

Om de invloed van deze factoren goed te kunnen bestuderen is gekozen voor een *in vitro* benadering waarbij een 'tissue engineered' skeletspiermodel werd gebruikt. Dit model werd verkregen door myoblasten (spiercellen) in kweek in een collageengel te differentiëren tot volwassen spiercellen. Bestaande protocollen voor skeletspierkweek werden hiertoe aangepast en gevarieerd, zodanig dat de meest optimale differentiatie naar volwassen spierweefsel werd verkregen.

Voor de bestudering van celdood als gevolg van deformatie en/of ischemie was het wenselijk zowel apoptose als necrose van de cellen continu te kunnen volgen in tijd en

3D ruimte. Hiertoe werd een vitale detectiemethode ontwikkeld op basis van afzonderlijke fluorescente identificatie van apoptotische en necrotische cellen, waarbij het weefsel intact blijft gedurende tenminste 24 uur.

Daarnaast werden experimentele opstellingen ontworpen om het weefsel bloot te stellen aan deformatie en kenmerken van ischemie, onder fysiologische omstandigheden. De onderzochte ischemische kenmerken waren: hypoxie (gebrek aan zuurstof), glucosedeprievatie en weefselverzuring door vrijkomend melkzuur. De invloed van deformatie en ischemie op schadeontwikkeling in het weefsel werd onderzocht met behulp van verschillende markers voor celdood, maar ook met indicatoren voor metabole veranderingen.

Er werden verschillende series experimenten uitgevoerd, waarbij het weefsel gedurende langere tijd (0 - 5 dagen) blootgesteld werd aan deformatie, ischemie of een combinatie van factoren. In overeenstemming met bestaande gegevens bleek dat bij blootstelling aan deformaties van 20% en 40% de ontwikkeling van weefselschade toenam met de duur en mate van deformatie. Zeer opmerkelijk leverde hypoxie, al dan niet in combinatie met deformatie, gedurende de eerste 24 uur geen extra schade op. Hypoxie veroorzaakte gedurende deze periode wel een verhoogde metabole respons ten opzichte van controle groepen. Na 24 uur had hypoxie geresulteerd in een verhoogd glucosegebruik en een verhoogde melkzuurproductie, hetgeen wijst op een overgang naar anaëroob metabolisme. Er werd echter geen toename in celdood gevonden als gevolg van hypoxie.

De aanwezigheid van melkzuur in het kweekmedium (en daaraan gekoppelde lage pH waarde) bleek het metabolisme negatief te beïnvloeden. Wanneer de melkzuurconcentratie in het medium een grenswaarde van ongeveer 25 mM overschreed, werd het metabolisme als het ware stilgelegd en steeg de hoeveelheid celdood. Dit was vergelijkbaar met de reactie van het weefsel op glucosedeprievatie. Wanneer de glucoseconcentratie gedaald was tot nul, was metabole activiteit afwezig en nam de hoeveelheid celdood toe.

Wanneer de effecten van alle onderzochte factoren afzonderlijk en in verscheidene combinaties beschouwd worden, kan opgemerkt worden dat op een korte termijn (binnen 24 uur) deformatie, extreme verzuring en glucosedeprievatie een toename in celdood veroorzaakten. De niet extreme verzuring en hypoxie hadden na 24 uur alleen een effect op het weefselmetabolisme en niet op de ontwikkeling van celdood. Na 5 dagen hadden echter alleen hypoxie en extreme verzuring volledige celdood tot gevolg terwijl deformatie, glucosedeprievatie en minder extreme verzuring minder celdood veroorzaakt hadden. Hoewel deformatie en minder extreme verzuring niet het gehele weefsel aantastten, was dit wel het geval als het weefsel blootgesteld werd aan een combinatie van deze beide factoren.

Concluderend kan gesteld worden dat een modelsysteem ontwikkeld is waarmee de effecten van deformatie en ischemische factoren op skeletspierweefsel individueel en in onderlinge samenhang nauwkeurig bestudeerd kunnen worden. De gepresenteerde resultaten dragen bij aan verder begrip van de etiologie van drukwonden. Daarnaast kunnen zij uiteindelijk leiden tot een verbetering van klinische richtlijnen en meer gericht onderzoek naar drukwonddetectie en -preventie.



# Dankwoord

Tijdens een promotie krijg je met veel mensen te maken, terwijl je uiteindelijk vooral jezelf tegenkomt. Al die mensen die de afgelopen jaren bijgedragen hebben aan het totstandkomen van dit boekje wil ik hier bedanken en in het bijzonder de mensen die hierna volgen.

Allereerst natuurlijk het begeleidende team. Op de eerste plaats wil ik mijn mental coach, Cees, bedanken omdat zonder hem dit boekje niet zou bestaan. Cees, bedankt dat je deur altijd openstond voor peptalks en voor alle gesprekken over het werk maar ook soms over belangrijkere dingen in het leven. Je enthousiasme voor het decubitusonderzoek heeft altijd aanstekelijk op me gewerkt. Carlijn, bedankt voor je vertrouwen en je kritische blik. Frank, bedankt voor het vertrouwen en de vrijheid die ik kreeg om het onderzoek in te vullen naar eigen inzichten. Here, I'd also like to thank Dan Bader for the inspiring discussions and his many eloquent and elegant contributions.

Ik heb genoten van de geweldige samenwerking en uitvoerige discussies met het 'dream team' bestaande uit Anke, Lisette, Karlien en Debbie. Voldoende borreltjes op zijn tijd hebben ons dichterbij elkaar gebracht. Go team!

Rob, zonder jou was er niet veel terecht gekomen. Bedankt voor al je gezellige praatjes en alle hulp en ideeën bij het bedenken van de opstellingen. Ook Harrie's hulp heb ik zeer gewaardeerd.

Dankzij een schare aan studenten heb ik meer inzicht gekregen in het gedrag van de spiertjes en het vrijkomen van schademarkers: David Hautemann, Kirsten Wishaupt, Cilian White, Linda Meijer, Marloes Langelaan, Petra Dijkman, Marijke van Vlimmeren en Bart van Dijk. Allemaal bedankt voor jullie fijne samenwerking. In het bijzonder wil ik Kristel Boonen bedanken zonder wie hoofdstuk twee er akelig leeg had uitgezien.

Verder wil ik alle collega's van het cellab en daarbuiten bedanken voor de prettige werksfeer en de zinnige en onzinnige gesprekken. Speciale dank aan mijn N<sub>2</sub>-buddy Sjoerd. Christa, bedankt voor alle assays en discussies. Many thanks also to Wei Li for our pleasant collaboration on the oxygen concentrations and for all the fun we had! Marcel Wijlaars wil ik bedanken voor alle hulp met de gasaansluitingen en microscopen. Leo en Patrick, ik ben blij dat jullie veel meer van computers snappen dan ik. Janine, door jouw vrolijkheid werd ik erg blij de laatste tijd.

Ook mag de 'family room' hier niet ontbreken. Leonie bedankt voor alle gesprekken, die ik erg gemist heb toen je bij ASML begon. Roy, je was een gezellige kamergenoot en ik heb altijd erg met je kunnen lachen. Emiel, op die kamer maar vooral in het lab is het allemaal begonnen. Katy, thank you for your gezelligheid en de groetjes! Ook Rudi

en Jeroen, jullie waren fijne kamergenoten. En tsja, Tom, jij zat ook zo af en toe op de kamer...

Geralda en Evelyne, bedankt voor alle 'girly' avondjes en dat ik altijd langs kon lopen als ik mijn hart wilde luchten. Lisette, jouw luisterend oor heeft me vooral in de laatste periode erg geholpen. Bart, bedankt voor alle spelletjes en flauwe humor. Lotte, je bent een top-vriendin met wie ik alles kan delen; bedankt voor je begrip in de laatste fase van de promotie. Tamara, al sinds de brugklas zijn we vriendinnetjes en dat zal altijd zo blijven.

Koffie en Zibby, zonder een woord te hoeven wisselen, toverden jullie altijd weer een lach op mijn gezicht. Els, Wil en Guido, bedankt voor alle gezelligheid en goede gesprekken. Jens en Niels, ik zou geen andere broertjes willen hebben. Papa en mama bedankt voor alles. Jullie steun en interesse waren onvoorwaardelijk en motiverend.

Last and most, lieve Emiel, bedankt voor wie je bent. Zonder jou waren ze allemaal gek geworden van me. Na twee promoties samen overleefd te hebben is het nu tijd voor ons.

# Curriculum Vitae

Debby Gawlitta werd op 31 oktober 1979 geboren in Tegelen. Na het behalen van haar VWO diploma op het 'Collegium Marianum' in 1997, begon ze aan de studie Biomedische Technologie (BMT) aan de Technische Universiteit van Eindhoven (TU/e). Tijdens deze studie voerde zij een stageopdracht uit bij het Georgia Institute of Technology in Atlanta. Door de aldaar opgewekte interessen voor de vakgebieden 'tissue engineering' en mechanica, koos zij voor een afstudeeropdracht met als doel het bepalen van de collageendepositie en -oriëntatie op een 2D gekweekt aortaklepvlies. Na het afronden van deze opdracht in 2002 koos zij ervoor onderzoek te doen naar het ontstaan van drukwonden in skeletspierweefsel in de groep 'Soft tissue Biomechanics and Engineering' van de TU/e in de vorm van een promotieonderzoek, waarvan dit proefschrift het resultaat is. Dit project maakte deel uit van het drukwond-onderzoek dat aan de faculteit BMT uitgevoerd wordt.